A NOVEL FRAMEWORK FOR THE ANALYSIS OF LOW FACTOR OF SAFETY SLOPES IN THE HIGHLY PLASTIC CLAYS OF THE CANADIAN PRAIRIES

A Thesis Submitted to the College of

Graduate Studies and Research

In Partial Fulfillment of the Requirements

For the Degree of Master of Science

In the Department of Civil and Geological Engineering

University of Saskatchewan

Saskatoon, Canada

By

Jasyn Alexander Henry

PERMISSION TO USE

In presenting this thesis in partial fulfilment of the requirements for a Postgraduate degree from the University of Saskatchewan, I agree that the Libraries of this University may make it freely available for inspection. I further agree that permission for copying of this thesis in any manner, in whole or in part, for scholarly purposes may be granted by Professor Jitendra Sharma who supervised my thesis work or, in their absence, by the Head of the Department of Civil and Geological Engineering or the Dean of the College of Engineering. It is understood that any copying or publication or use of this thesis or parts thereof for financial gain shall not be allowed without my written permission. It is also understood that due recognition shall be given to me and to the University of Saskatchewan in any scholarly use which may be made of any material in my thesis.

Requests for permission to copy or to make other use of material in this thesis in whole or part should be addressed to:

Head, Department of Civil and Geological Engineering
57 Campus Drive
University of Saskatchewan
Saskatoon, Saskatchewan S7N 5A9
Canada

ABSTRACT

The most common way to analyze slope stability is to employ limit equilibrium (LE) theory and obtain a factor of safety (FOS). Methods of LE analysis balance the forces, and/or moments that are driving and resisting slope movement. Generally, in geotechnical engineering practice, a slope that plays host to an important structure is designed with a minimum factor of safety (FOS) of 1.5 and slope movement is monitored throughout the structure's serviceable life. No further analysis of slope stability is completed until failure occurs when a back analysis is undertaken for the design of remedial measures. This thesis builds on current methods to demonstrate a framework for analysis that can be followed to analyze the state of a slope throughout its serviceable life.

The two bridges at North Battleford, Saskatchewan (Battlefords bridges) were used as case studies for this work. In 1967, the older of the two bridges experienced a slope failure at its south abutment immediately prior to its opening to the public. The failure was remediated reactively by means of subsurface drainage, a toe berm, and river training that included diversion/spur dikes to reduce scour at the landslide toe. Since remediation, there has been no other catastrophic failure at either bridge but slow movement continues in the south abutment slope. Laboratory data and field observations from the onsite inclinometers were provided by Clifton Associates Ltd. (CAL) and Saskatchewan Ministry of Highways and Infrastructure (SMHI).

The following methodology was followed to develop a framework of analysis for low FOS slopes:

1. Synthesis of data collected during previous investigations at the Battlefords bridges;
2. Detailed site characterization using existing research and terrain analysis;
3. Back analysis of the critical section through original failure using traditional limit equilibrium methods to calibrate the soil strength properties;

4. Application of the calibrated soil strength properties to the original failure after remediation;
5. Estimation of unknown soil properties using instrumentation at the site.
6. Create a model of the new bridge south abutment with the calibrated strength properties from steps 4 & 5 using the finite element method (FEM).
7. Confirmation of the mechanism of failure and assessment of the shear strain and mobilized shear strength; and,
8. Comparison of the results of FEM and LEM models and relationship between factor of safety and mobilized shear strength.

The framework presented in this thesis presents a method of modeling the instability of a slope. In the absence of triaxial testing data, it presents a range of mobilized shear strengths along the shear plane.

ACKNOWLEDGEMENTS

I would like to thank Clifton Associates Ltd. and NSERC (Industry Postgraduate Scholarship Program) for providing the financial support that made this work possible. Special thanks are also due to Harpreet Panesar and Saskatchewan Ministry of Highways and Infrastructure for their support of this research and their cooperation throughout this process.

A great deal of thanks is owed to my supervisor, Prof. Jitendra Sharma, for allowing me to study under him. This would not have been possible without the constant encouragement, reassurance, and meetings at Tim Horton's for coffee and snacks. It is most appreciated.

To my committee members, thank you. Dr. Ian Fleming, Dr. Grant Ferguson and Dr. Mohamed Boulfiza (chair) for your support throughout this process and your positive encouragement.

Special recognition is deserved for Mr. Wayne Clifton. Wayne's encouragement and support made it possible for me to take time away from work and develop my knowledge of geotechnical engineering. Special thanks should also be given to Mr. Allen Kelly who helped in the development of this project and provided advice along the way.

Thanks to Dr. Curtis Kelln of GEO-SLOPE International ltd., Professor Lee Barbour and Laura Smith. You made time for me despite your busy schedules and for that I am most grateful.

To the fellow grad students of 3C54 (Erik Ketilson, Nathan Schartner and Darren Neely), thank you for listening to me rant and sharing some laughs over many coffees, lunches, and Friday evening refreshments. Thanks also to Adam Hammerlindl for leaving his office door open and always being of an open mind for new ideas.

Thanks are owed to my family for their love and support throughout this journey. They were always available to listen to problems and offer words of kindness and encouragement. They

were never too busy to make the trip to Saskatoon to buy me breakfast and provide a break at stressful times.

And lastly thank you to my girlfriend of nine years, Emily. You supported me throughout the entire journey. I would not have been able to move away and complete this thesis without your support. Your love and constant encouragement helped me through the toughest of times. I love you very much and look forward to starting a new chapter of our lives together.

DEDICATION

This work is dedicated to my Grandfather.

TABLE OF CONTENTS

LIST OF TABLES

LIST OF FIGURES

Chapter 1 Statement of Problem

1.1 Introduction

The Merriam-Webster dictionary defines science as, “knowledge or a system of knowledge covering general truths or the operation of general laws especially as obtained and tested through scientific method” (Merriam-Webster, 2005). The Merriam-Webster dictionary defines art as, “skill acquired by experience, study, or observation” (Merriam-Webster, 2005). In the author’s opinion, geotechnical engineering falls in between the definitions of art and science. Since its inception the profession has been relying on empiricism and experience to establish guidelines, methods for design, and design codes of practice. The natural earth materials that geotechnical engineers encounter can be immensely variable within a remarkably small area. In a profession such as this, it is important to continue to further science and advance methods.

New technology has given rise to advances in instrumentation and data collection systems that allow engineers to have greater resolution, and more timely data at their fingertips, which in turn, can facilitate the design of safer, less conservative, and thus, more cost-effective structures. Real–time pore pressure response to barometric loading can yield useful values that assist in the estimation of in-situ modulus of elasticity. With no additional soil sampling, this thesis will build on existing methods, using historical observations, combined with simple field measurements, to allow for more advanced analyses of low factor of safety slopes using the south abutment at the Battlefords bridges as a case study site.

1.2 Case Study

The Battlefords bridges are located approximately 140 km northwest of Saskatoon, SK on Yellowhead Trail (Federal Highway 16) between the city of North Battleford and the town of Battleford, SK (Figure 1.1). The bridges at North Battleford, SK are important infrastructure for commercial transport and recreational travel across the western prairies. They allow the users of highway 16 and the provincial highways 4, 29 and 40 to cross the North Saskatchewan River. A photograph of the bridges from the south valley wall looking northeast can be found in Figure 1.2.

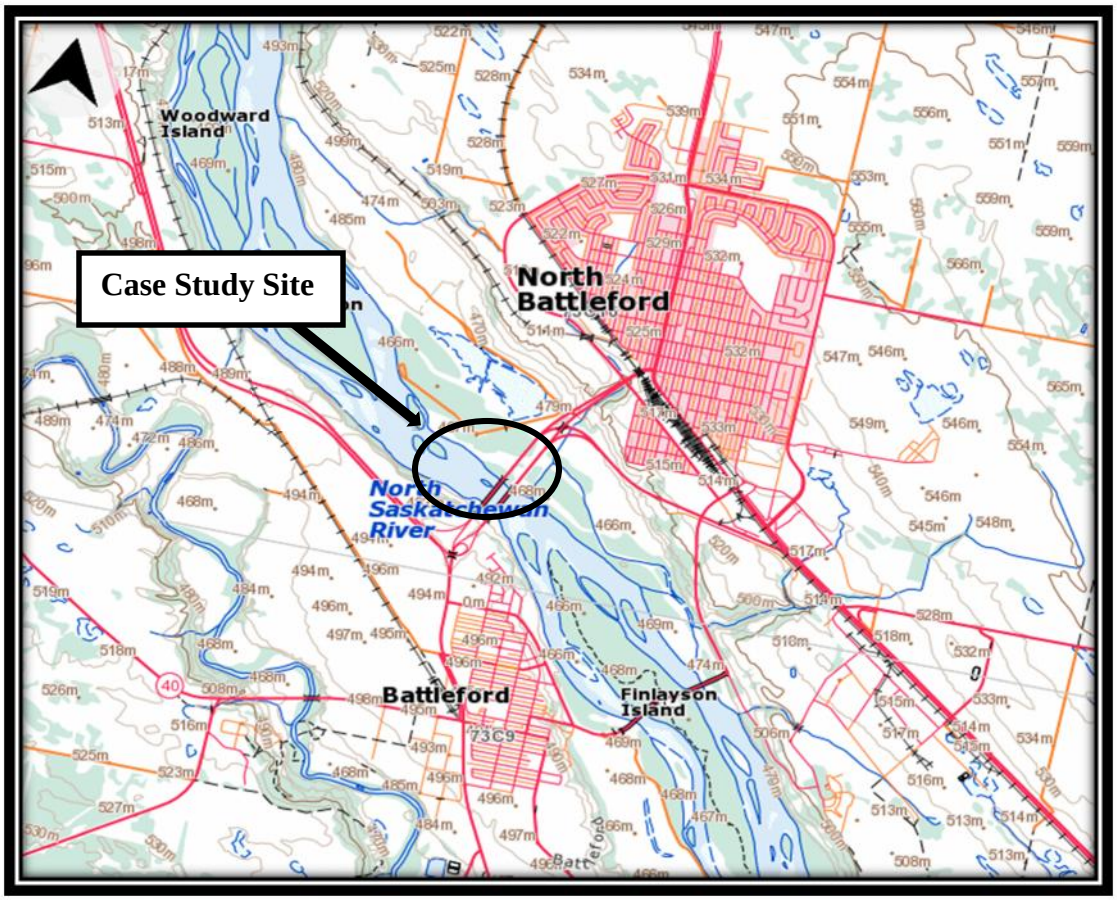

Figure 1.1: Location of the case study site (taken from National Topographic System Map Sheet 73/C)

The North Saskatchewan River valley is plagued with slope with failures (Stauffer et al., 1990). The valley walls near North Battleford, SK are no exception and as such, they have undergone extensive investigation. The stratigraphy at the bridge site generally consists of Quaternary glacial deposits overlying Cretaceous deposits of the Judith River and Lea Park Formations. Empress Group sands and gravels were also observed in boreholes near this site (Clifton et al., 1999).

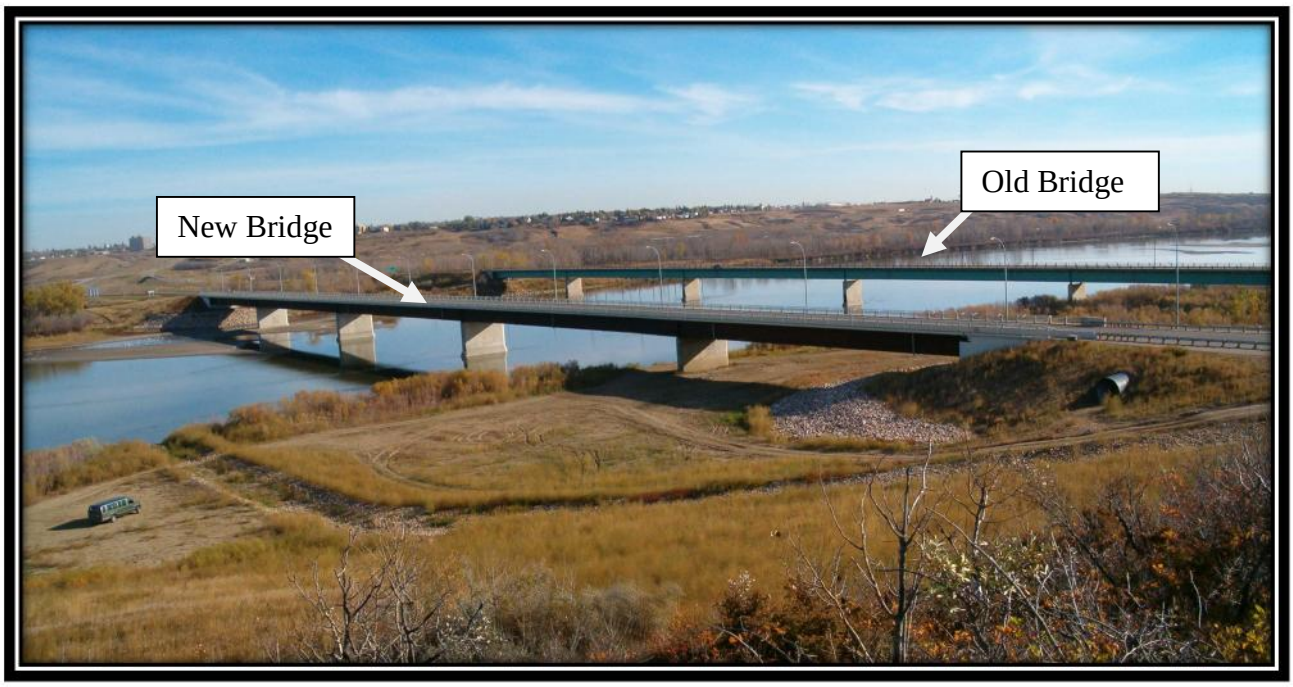

Figure 1.2: Photograph taken from the south valley wall looking northeast over the bridges – photograph courtesy of Saskatchewan Ministry of Highways and Infrastructure

The foundation soils of the Battlefords bridges are bedrock clay shales of the Cretaceous period. Cretaceous clay shales are highly plastic and can be found near surface in the North Saskatchewan River Valley, which served as a melt water channel during glacial retreat. As a result most of the stratified drift and glacial till have been eroded from the valley slopes, leaving highly plastic clay shale near surface. Several structures have been constructed in stratigraphy similar to that of the Battlefords bridges across the Canadian Prairies including, bridges at

Maymont, Deer Creek, Borden, Gronlid, and many more.

Slopes in these clays can be considered “low factor of safety” (FOS) slopes as several of them continue to the exhibit slow movement averaging a few mm/year (Clifton et al., 1999; Sauer, 1984) without experiencing total failure. Such movement is a characteristic of the Late Cretaceous clays (Sauer, 1984). Ancient landslides that have come to rest in these valley slopes are very near of a state of limiting equilibrium and require very little disturbance to be reactivated (Sauer, 1984).

1.2.1 History of Slope Instability at Battlefords Bridges

Historically, slope instability at the Battlefords bridges has been isolated to the south valley wall (Clifton et al., 1999). In October 1967, the older (east) of the two bridges experienced a major slope failure at the south abutment just prior to its being opened to the public. The failure undermined the south abutment and pier 1 and the toe was located between piers 1 and 2 (Clifton et al., 1999).

The landslide was remediated with the construction of a large toe berm and extensive slope flattening and then the bridge was reopened to the public. Since remediation, there has been no other catastrophic failure but slow movements in the south valley wall have continued. The slope movements are slow but continuous as per the monitoring records kept by the Saskatchewan Ministry of Highways and Infrastructure (SMHI).

1.2.2 Summary of Previous Work at the Battlefords Bridges

Previous work at the bridge sites has been extensive. Considerable investigation was undertaken in the 1960s by the Saskatchewan Department of Highways and Transportation. All of the surviving records related to this project have been provided by SMHI. In the late 1990s and early 2000s, Clifton Associates Ltd (CAL) was retained to complete a geotechnical study for a

proposed new bridge to be located immediately to the west of the existing bridge. This work included comprehensive drilling and testing programs and the installation of several piezometers and slope inclinometers.

A three-dimensional (3-D) limit equilibrium model was constructed using CLARA/W by Clifton Associates in 1999. This 3-D model was created to examine the extents of the existing slip surface and to determine a safe spacing for the proposed bridge abutment fill. The CLARA/W model consisted of several two-dimensional (2-D) sections aligned for a 3-D representation of the slip surface. CAL has provided all of the available paper records with regards to the Battlefords bridges for use in this work.

1.2.3 Knowledge Gap

To date, all stability analyses of the south abutment have been completed using the limit equilibrium (LE) method. The concepts of LE analysis are not able to fully describe the slow deformations at this site. Limit equilibrium sums the forces, moments, or both that are driving or stabilizing the slide to determine if it has failed or not by means of a factor of safety. The south abutment slope at the new bridge has a factor of safety that is greater than 1.0 but the slope continues move. More advanced methods must be employed to fully understand mechanism of failure and to estimate how it will impact the bridge in the future. The finite element (FE) method can be used to analyze the stress/deformation characteristics of the system and estimate the distribution of the shear strain at the slip surface. Mobilized strength design (MSD) theory as described by Vardanega and Bolton (2011) could be used to determine how much shear strength is being mobilized at the slip surface and related back to the traditional FOS. This work will be the first to set out a framework for analysis for “low factor of safety” slopes in highly plastic clay shale.

1.3 Project Objectives

The objective of this project is to use FE analyses to analyze the new bridge in order to define a comprehensive method of analysis for low factor of safety slopes in highly plastic clay shales. The developed analyses will contribute to the understanding of the shear strength mobilization in slopes in Cretaceous clay shale by allowing for the estimation of the current factor of safety and mobilized shear strength. Using only historical data complemented by simple field measurements, the case study of the Battlefords bridges will be used to develop a framework for analyses for sites in similar stratigraphy. Every site is unique and caution should be taken when applying this framework to other areas. It is the goal of this work to use MSD to complement traditional methods and relate shear strain and mobilized shear strength to factor of safety.

1.3.1 Scope

This project was limited to analysis of the south abutment. The north valley wall had a different stratigraphy and was therefore not considered for this work.

The cross-sections for this project were constructed using the topographic maps created by CAL while completing investigations for the design of the new bridge. The depth of riverbed alluvium likely varies with seasonal flows and would have an impact on stability. Frequent bathymetric surveys would be required to include these effects. As such, transient depth of alluvium was outside the scope of this project.

The piezometric surface was constructed using data at the time of failure for the back analysis and the most current, available data for the present day models. It was the aim of this thesis work to match the status quo. There is no real-time monitoring at this site and piezometer monitoring occurs on a quarterly basis with the SMHI's instrumentation program. Due to the lack of real-time pore pressure data, transient spring flows were excluded from this project.

A major constraint of this project was that no further field investigation could be completed. In approving and supporting this thesis work, SMHI requested that no field drilling or further fieldwork be carried forth at the Battlefords bridges.

1.4 Methodology

The following steps were used to explore the objectives within the scope of this research:

1. Synthesis of data collected during previous investigations at the Battlefords bridges;
    - All existing data was provided by CAL and SMHI. The data needed to be synthesized into a useful format within the scope of this research.
2. Detailed site characterization using existing research and terrain analysis;
    - A detailed characterization of the physical environment was completed using airphoto interpretation, terrain analysis and data from previous investigations.
3. Back-analysis of the critical section through original failure using limit equilibrium methods to calibrate the original post-failure soil strength properties;
4. Application of the calibrated strength properties to the original failure after remediation;
5. Barometric efficiency testing to estimate the in-situ compressibility of the bedrock clay shale;
6. Finite element model of the new bridge south abutment using the calibrated strength properties.
7. Explanation the mechanism of failure and assessment of the mobilized shear strength; and
8. Comparison of the results of FEM and LEM models and relationship between factor of safety and mobilized shear strength.

1.5 Organization of Thesis Document

This thesis is organized into the following five chapters:

- Chapter 1 (this chapter) introduces the case study of the Battlefords bridges and discusses the gaps in knowledge with respect to slope movements at that site. This chapter also introduces the project objectives, scope and methodology.
- Chapter 2 is a detailed literature review including discussion on landslides in the Late Cretaceous clay shale deposits, the Observational Method, barometric efficiency testing, types of slope stability analyses and Mobilized Strength Design.
- Chapter 3 is a detailed site description including all relevant data from previous site investigations.
- Chapter 4 describes the slope stability models used to develop a framework of analysis.
- Chapter 5 presents the conclusions of this work and recommendations for further research.

Chapter 2 Literature Review

2.1 Landslides in the Late Cretaceous Clay Shale Deposits

Late Cretaceous clay shales are highly plastic clays that can be found near surface in the North Saskatchewan River Valley and many other valleys in the Canadian prairies. These valleys served as meltwater channels during glacial retreat. The meltwater in the Battlefords area was confined between the Eagle Hills Escarpment to the south and the glacier to the north (Christiansen, 1979) causing most of the surficial stratified drift and glacial till to be eroded and leaving the highly plastic clay shale near surface (Christiansen, 1979). The clay shale was left exposed and was subject to disturbance by the shearing forces of the Battleford glacier (Stauffer et al., 1990). This disturbance caused softening of the bedrock clay, which no doubt contributes to the instability of the valley walls (Stauffer et al., 1990).

Mollard (1975) states that the Lea Park shale is highly unstable in areas where it has been disturbed. Many of the existing failures in the walls of the North Saskatchewan River Valley occurred when the river level was approximately 100 ft lower than the present day (Mollard, 1975). Since that time, substantial deposition of river bed alluvium has helped to stabilize the landslides, leaving many ancient landslides near a state of limiting equilibrium (Sauer, 1984; Mollard, 1975). Many areas in the North Saskatchewan River Valley and the Battle River Valley possess slope failures with slow rates of movement in the Lea Park Formation (Mollard, 1975).

According to Christiansen and Sauer (2001) the Late Cretaceous clay shale deposits are members

of the Montana group and are part of the following three formations (from youngest to oldest):

- Bearpaw Formation;
- Judith River Formation; and,
- Lea Park Formation

The Lea Park shale is usually a grey, non-calcareous, highly over consolidated marine silt and clay deposit (Christiansen, 1979). It consists of approximately 2% sand, 48% silt and 50% clay sized particles(Christiansen, 1979). There is an increase in sand content near the contact with the Judith River Formation. Its colour changes to a lighter olive brown in the disturbed areas (Clifton et al., 1999).

The Lea Park clay shales are montmorillonitic and have seams of bentonitic clay that are prone to shearing (Christiansen, 1983; Clifton et al., 1999, 1999; Clifton & Kelly, 2001). The Lea Park Formation has proven to exhibit low shear strength and slow movement in the order of mm/year is common (Clifton et al., 1999; Sauer, 1984). Previous investigations in the North Saskatchewan River Valley show residual angles of shearing resistance (ϕ') to be between 4.8° and 11.6° with cohesion of 0 kPa – 10 kPa (Sauer, 1984; Sauer, 1983; Clifton et al., 1999).

2.2 Observational Method

The observational method was pioneered by Karl Terzaghi while writing his book, *Soil Mechanics in Engineering Practice* (Peck, 1969). Geotechnical design is unique in that there is no “one size fits all” design. At the time, many geotechnical designs fell under the following two general models (Terzaghi et al, 1996):

- Excessive factor of safety; or,

- Relied only on experience.

Designing with an excessive factor of safety is wasteful and expensive while relying only on experience is potentially dangerous.

At its inception, the observational method was called the "experimental method" (Peck, 1969). It involved (Terzaghi et al., 1996):

- Creating a design based on information gathered by investigations;
- Ensuring to note where assumptions were made; and,
- Measuring unknowns and adjusting design based on those field measurements.

This method was introduced for significant time and cost savings during the construction phase of projects. It allowed designers to be less conservative but required them to have better judgment of unknown variables (Powderham, 1994). The method was listed to include the following eight steps (Peck, 1969):

1. Investigation to determine the general properties of the area of interest;
2. Assessment of the status quo and the most significant deviation from it;
3. Design based on the assessment made in step 2;
4. Select variables to be measured and monitored in the field during construction;
5. Determine how the variables from step 4 will impact the design;
6. Run models with the best case and worst case of the variables determined in step 4 to view their impact on design and devise an action plan for any foreseeable changes;
7. Measure the variables in question; and,

8. Modify design based on field measurements during or even after construction.

As noted in step 3, most designs are for the worst-case scenario. With the successful employment of the observational method, it is more likely that the actual design will reside between the status quo and worst-case scenario (Powderham, 1994).

Major flaws in this method include the inability of the designer to properly predict all possible outcomes and courses of action, and incorrect selection of variables for measurement (Peck, 1969). Timing of the readings is of great importance. Monitoring must occur at the appropriate times and be applied to the design immediately (Powderham, 1994).

It is possible to employ a post-construction observational method in order to help examine the effectiveness of design (Powderham, 1994). Powderham (1994) notes that post-construction observations are most suitable for monitoring slope failures and earth fill dams and that applying the method post-construction reduces the benefit of savings and requires long-term communication with the designers/contractors of the project.

2.3 Slope Stability Analyses

The following subsections will be used to discuss slope stability analyses with focus on the current industry standard of practice.

2.3.1 Limit Equilibrium Method

Limit equilibrium (LE) analysis is the most common method used for the determination of factor of safety for slope stability. This method is based on analysis using statics to calculate the driving and resisting moments and/or forces acting on the slices of a specified slip surface within a slope. The ratio of resisting moments and/or forces to driving moments and/or forces provides a factor of safety for that slip surface. A LE model requires the selection of a slip surface type

(circular or non-circular), radius and an orientation. This may be viewed as a drawback as significant experience and knowledge of the failure surface are required to accurately define these parameters.

Two significant assumptions present in the limit equilibrium method (LEM) analyses are that (Griffiths & Lane, 1999):

- The slope can be divided into slices; and,
- There are forces acting between each of those slices.

Practicing engineers use LEM because it does not require complex input parameters. LEM neglects stress/strain behavior and gives no information about deformations (RocScience, 2004); it will simply provide a factor of safety for a specified slip surface.

2.3.2 Finite Element Method

Finite element (FE) analysis has been used in slope stability since 1966 (RocScience, 2004); however it has not gained the same industry respect as LE analyses. Some engineers claim that FE analyses require substantial computing power and complex input parameters. Advanced and accessible technology makes the computing power to run these models available to everyone.

FE analysis has several advantages over the LEM in slope stability analysis, including (Griffiths & Lane, 1999):

- No assumptions about shape or location of the failure surface are needed;
- No assumptions about inter-slice forces are required;
- FE analysis yields deformations if correct compressibility properties are used; and,

- FE analysis can be used to monitor progressive failure.

2.3.2.1 Parameters

One of the reported disadvantages of FE models for slope stability is the requirement for soil deformation parameters. For example, in an effective stress analysis with an elastic-plastic constitutive model, in addition to the standard Mohr-Coulomb parameters (unit weight, angle of shearing resistance and apparent cohesion), the model requires the following deformation properties:

- Young's Modulus (E) and;
- Poisson's Ratio (ν);

Griffiths & Lane (1999) and Hammah et al. (1999) have proven that the sensitivity of the model to these parameters is negligible with respect to the computed factor of safety. If the purpose of the model was to extract deformation data, the values of E, and ν would need to be correct.

Common FE models for slope stability include:

- Shear strength reduction; and,
- FE stresses in LE framework.

2.3.2.2 Shear Strength Reduction

The most common method in the literature for analyzing slope stability using the finite element method (FEM) is the Shear Strength Reduction (SSR) method. SSR allows for the prediction of factor of safety on slopes using FEM. This factor of safety is not a balance of forces and

moments acting on the slope as it is in LEM. It is instead a factor by which the strength of the soil must be reduced to initiate failure of the elements (Abramson, 2002). A failure plane develops progressively and it can be difficult to relate this back to a traditional FOS (Abramson, 2002). SSR can also predict stresses and deformations in support elements (piles, anchors, or geosynthetics) at failure (Hammah et al., 1999).

In SSR the Mohr-Coulomb soil parameters, c' and ϕ', are multiplied by a reduction factor, SR. There is flexibility in varying these parameters; that is c' can be reduced by a different factor than ϕ'. The results of this type of variation may not be realistic and more research needs to be conducted regarding this topic. The value of SR that, if increased by another increment, would cause failure is the critical factor of safety of that slope. FEM-based SSR has advantages to LEM in that the user needs to make no assumptions about the failure location.

2.4 FEM Stresses in LEM Framework

In his 2001 Hardy Lecture, John Krahn presented an improved method of LEM analysis in which the slope geometry is set up in a stress-strain environment (SIGMA/W) allowing for the in-situ stresses of the soil to be determined (Krahn, 2003). These stresses are moved into LEM framework and a better prediction of shear stresses along the failure plane can be found. Instead of using the mass of the slice and statics equations, the analysis begins with the stresses that have been calculated at each node. One advantage to this method is being able to graph how the shear stresses change along the shear plane instead of having a single assumed stress across the entire shear plane. This method can be used to verify the SSR method.

2.4.1 Soil Deformation Properties

One major difference between LE analyses and FE analyses is the introduction of elements. Each element is assigned properties and is allowed to deform. Deformations at the nodes of one element will impact the performance of other elements. In order to describe the deformations of

these elements, soil deformation properties such as Young's modulus (E'), also referred to as elastic modulus or soil stiffness, and Poisson's ratio (ν') are required. These properties can be obtained through laboratory testing; however, there proves to be some discrepancy between lab tested and in-situ values.

Young's modulus is defined as:

$$E' = \frac{d\sigma'_a}{d\varepsilon^e_a} \qquad [2.1]$$

Where σ'_a is the axial effective stress and; ε^e_a is the axial elastic strain. This equation describes how much the soil can strain while still remaining elastic.

Establishing the Young's modulus of a material seems reasonably straightforward with routine laboratory testing; however, Bowles (1997) states that the relationship between the laboratory testing results and in-situ values of elastic modulus can be very difficult to find. There is a large difference between the two values. In-situ values of elastic modulus can be four to five times greater than the values determined in the unconfined test in the laboratory (Bowles, 1997).

2.5 Pore Pressure Response to Barometric Loading

Hydrogeologists have long been interested in the fluctuations of observation well levels due to changes in atmospheric pressure. Until recently, it was difficult to achieve adequate resolution of monitoring data to analyze these fluctuations with any confidence. Vibrating wire piezometers have allowed researchers and practitioners to achieve the resolution necessary to estimate the elastic properties of the soil based on uniform surface loading.

van der Kamp and Gale (1983) review the history of the relationship between stress changes and load carried by the soil skeleton in hydrogeology. Anochikwa, van der Kamp, and Barbour (2012) & van der Kamp and Gale (1983) state that even in fractured porous medium, the elastic

properties can be estimated based on the principle of homogeneity from the initial undrained response of the soil.

2.5.1 Young's Modulus from Skempton's pore pressure coefficient, $\overline{B}$

Skempton (1954) developed the pore pressure coefficient, $\overline{B}$, which relates the change in pore pressure to an applied vertical load by the following equation:

$$\overline{B}=\frac{\Delta u}{\Delta \sigma_1} \qquad [2.2]$$

where Δu is the change in pore pressure and; $\Delta\sigma_1$ is the change in vertical stress.

The coefficient, $\overline{B}$, proves to be very useful when trying to evaluate reasonable values of in-situ Young's modulus. From the theory of elasticity, it is known:

$$K=\frac{E}{3(1-2\upsilon)} \qquad [2.3]$$

where K is the bulk modulus of the soil; E is the Young's (elastic) modulus of the soil and ν is Poisson's ratio for the soil.

From this relationship it can be easily seen that with a Poisson's ratio assumed to be 0.334, as stated above, K=E.

Using the relationship in Equation [2.3] and findings by van der Kamp and Gale (1983), Anochikwa et al. (2012) went on to describe following relationship:

$$\overline{B}=\frac{\frac{1}{E_c}}{\frac{1}{E_c}+\frac{n}{E_w}} \qquad [2.4]$$

where E_c is the confined elastic modulus; n is the soil porosity and; E_w is the elastic modulus of

water.

Porosity values for Cretaceous clay shales range from 0.3-0.45 (Smith et al., 2013). For this work, a porosity value of 0.36 was used as it best correlated with the samples recovered at depths representative of the clay shales at the Battlefords bridges.

Equation [2.4] can be rearranged to show the following:

$$E_c = \frac{E_w(1\text{-}B)}{Bn} \qquad [2.5]$$

From Equation [2.5] it can be seen that, knowing the formation porosity and B values, an estimation of the confined Young's modulus can be made.

van der Kamp and Gale (1983) describe the relationship between confined Young's modulus and drained Young's modulus as:

$$E' = \frac{E_c(1\text{-}\upsilon)(1\text{-}2\upsilon)}{(1\text{-}\upsilon)} \qquad [2.6]$$

where E' is the drained elastic modulus.

Substituting $\nu = 0.334$ into Equation [2.6] yields the following relationship:

$$E' = \frac{2}{3}E_c \qquad [2.7]$$

2.6 Mobilization Factor and Mobilized Strength Design (MSD)

According to British Standard Code of Practice 8002 (British Standards Institution, 1994) mobilization factor (M) is defined as the ratio of the proportion of shear strength of soil that is mobilized during the serviceable life of a structure over available shear strength of soil. M is a factor of safety (FOS) of shear strength and is calculated as follows:

$$M = \frac{Cu}{\tau_{mob}} \quad [2.8]$$

where M is the mobilization factor; C_u is the undrained shear strength of the soil, and; τ_{mob} is the mobilized shear strength.

Mobilized strength design (MSD) offers an alternative method of assessing factor of safety (FOS) (Vardanega & Bolton, 2011). This method provides the link between FOS, mobilized strength, and shear strain. Traditional limit equilibrium methods give no reference to the amount of strain that takes place at a certain FOS. MSD allows an engineer to predict moderate strains and displacements and thus to assess the serviceability of the proposed structure (Vardanega & Bolton, 2011). Vardanega & Bolton (2011) published a database of more than 100 triaxial tests on various clay samples from around the world. They found that normalizing stress-strain data with the shear strain at M=2 ($\gamma_{M=2}$) produced a power law relationship as follows:

$$\frac{\tau_{mob}}{Cu} = 0.49 \left(\frac{\gamma}{\gamma_{M=2}}\right)^{0.6} \quad [2.9]$$

where C_u is the undrained shear strength of the soil; τ_{mob} is the mobilized shear strength; γ is the shear strain, and; $\gamma_{M=2}$ is the shear strain at half of the peak undrained shear strength.

The database with Lea Park shale unconfined compressive strength results can be found in Appendix B. From this database, multiple linear regression was performed and the following relationship to find shear strain at half of the undrained shear strength ($\gamma_{M=2}$) was developed

(Vardanega, 2011):

$$\gamma_{M=2} = C[I_p]^{0.45}\left[\frac{C_u}{P'_o}\right]^{0.59}\left[\frac{P'_o}{P'_{atm}}\right]^{0.28} \quad [2.10]$$

where C_u is the undrained shear strength of the clay (kPa); P'_o is the initial mean effective stress (kPa); I_P is plasticity index; P'_{atm} is atmospheric pressure (101.3 kPa), and; C is the regression constant = 0.0109.

Vardanega (2011) notes that using this equation in the absense of triaxial test data could create a factor of error as great as 2.0. To reduce the error, at least one triaxial test should be completed. Triaxial testing was not an option for this work so all results should be accepted with full knowledge of this possible error.

In order to calculate P'_o the following equation was used:

$$P'_o = \frac{1+2K_o}{3}\ \sigma'_v \quad [2.11]$$

where P'_o is the initial mean effective stress (kPa); K_o is the coefficient of earth pressure – at rest determined using the Jaky formulation, and; σ'_v is the vertical effective stress.

Using this framework, an undrained triaxial test in which $\gamma_{M=2}$ is determined, allows for the calculation of the stress-strain relationship. Vardanega and Bolton (2011) state that this relationship was developed for moderate strain region ($1.25 \leq M \leq 5$). They also state that the relationship would still be valid in the small strain region ($M > 5$) but this region is limited by the types of instrumentation used to measure them.

MSD has been proven with several published works. Bolton and Take (2011) were the first to apply MSD to slope stability analysis using centrifuge tests and Particle Image Velocimetry (PIV). The study focused on first time failures in slopes in London Clay. Bolton and Take

(2011) were able to show that shear strain accumulates at the toe of the slope due to a "ratcheting" effect caused by wet and dry periods. From their analysis, they were able to determine how much of the angle of shearing resistance ($\phi^{'}$) and apparent cohesion (c') were mobilized, and compare that to the soil's critical state. For design purposes, the critical state angle of shearing resistance (ϕ'_{crit}) should be the maximum amount of mobilized ϕ' for the wettest year.

2.7 Summary

The current state of practice in slope stability is limit equilibrium analyses. The stability of a slope is typically analyzed early in the design phase and monitored using slope inclinometers. Observations obtained from site instrumentation are used to determine if the slope is moving, or not, and how much movement is taking place at the slip surface. In many cases, this framework is adequate and successful. For cases such as that found at the Battlefords bridges, the aforementioned framework may not be sufficient. The highly plastic clay shale bedrock deforms slowly along preferential paths. The slow reduction of the FOS is important and needs to be monitored. Using field observations from inclinometers and piezometers, combined with finite element methods allows for the analysis of factor of safety throughout the serviceable life of a structure. It also allows for the determination of mobilized shear strength at the slip surface. These analyses could be used to better understand how the slow movement of the Cretaceous clay shale bedrock impacts the serviceability limits of a structure.

Chapter 3 Site Description

This chapter describes the physical setting, history of fieldwork, and history of slope instability at the Battlefords bridges. Significant work has been completed at the site and these resources were reviewed and their key points highlighted. The resources used to synthesize this information include:

- Project paper files, borehole logs and monitoring data from Saskatchewan Ministry of Highways and Infrastructure (SMHI);
- Consultant reports for geotechnical services of the New Battleford bridge from Clifton Associates Ltd. (CAL);
- Airphoto study completed by J.D. Mollard and Associates Limited (provided by SMHI);
- Various technical papers with a focus on the Battlefords area and glacial geology of the prairie region; and,
- Maps available from NRC Atlas of Canada.

3.1 Physical Environment

3.1.1 Site Location

The Battlefords bridges are located at the North Saskatchewan River crossing between the city of North Battleford, SK and the town of Battleford, SK. The legal land location of the bridges is

the southwest quarter of section 6, township 44 and range 16 west of the third meridian. A map and airphoto showing the location of the bridges can be found in Figure 1.1 and Figure 3.1 respectively. The North Battleford area is located in the Prairie Ecozone of Canada and within the Aspen Parkland Ecoregion (Environment Canada, 1995). The Aspen Parkland is a transition zone between the Boreal Forest to the north and the Northern Grasslands to the south (Environment Canada, 1995). This area is characterized as an undulating, fluted till plain with areas of glaciofluvial deposits (Environment Canada, 1995).

3.1.2 Land Use

The dominant land use immediately surrounding the bridge sites is residential development. The city of North Battleford and the town of Battleford are within a 5 km radius of the Battlefords bridges. The area outside of the residential development is dominated by agricultural land and pasture.

3.1.3 Climate

The typical seasons associated with the climate of the Aspen Parkland are characteristically short, hot summers and long, cold winters (Environment Canada, 1995). The city of North Battleford has an average annual temperature of 1.9°C (Government of Canda, 2012). Its hottest month, on average, is July with its coldest month being January. Annual precipitation in the area is approximately 375 mm with rainfall accounting for approximately 280 mm of that (Government of Canada, 2012). The remaining 95 mm comes from annual snowfall. Rainfall is concentrated in the warm months of the region's spring and summer seasons. The month of July accounts for the highest average rainfall with 71 mm/yr. (Government of Canda, 2012).

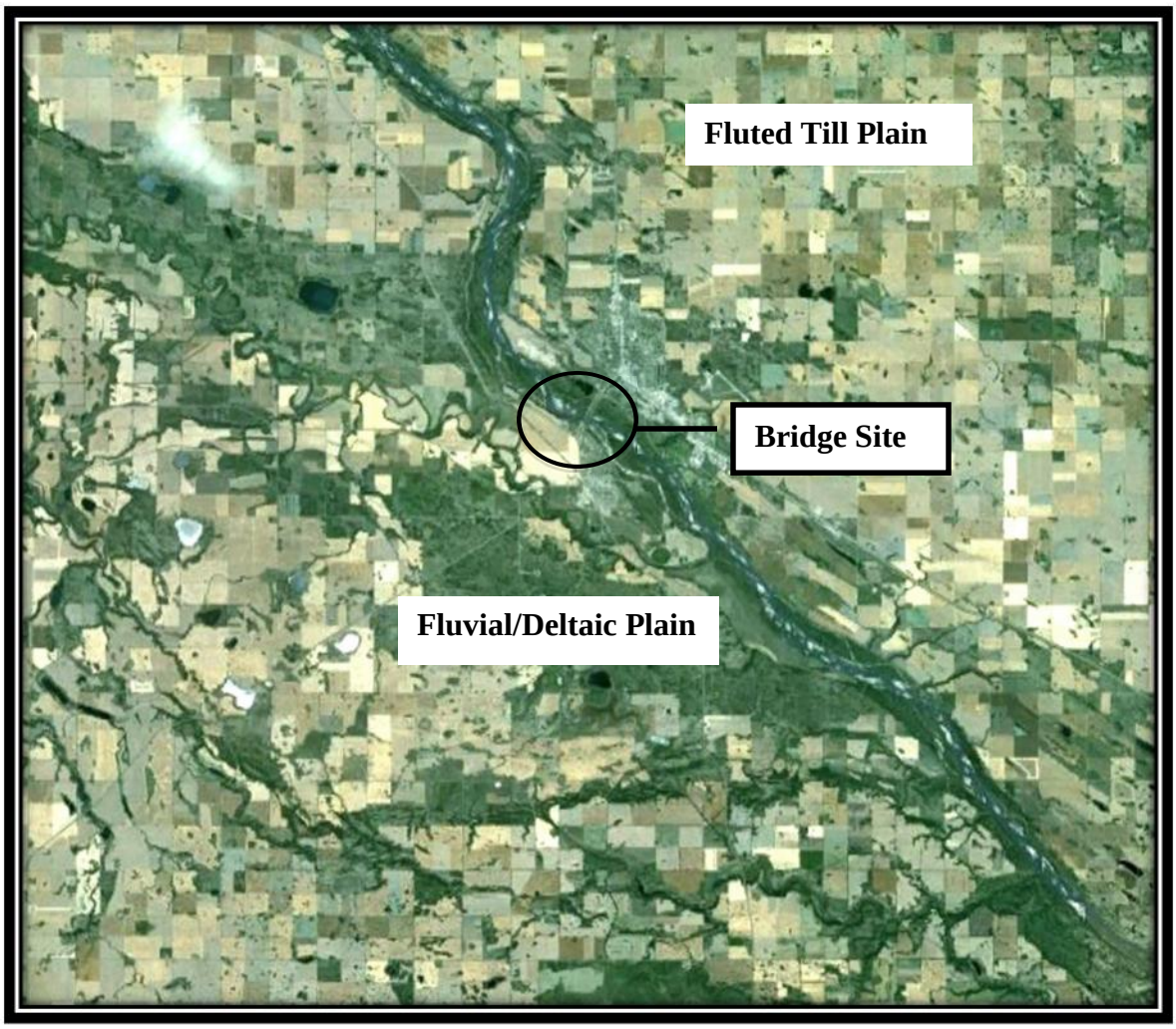

Figure 3.1: Airphoto of the Battlefords area (taken from Google Earth, 2012)

3.1.4 Regional Geomorphology

The Canadian Prairies are part of the Interior Plains physiographic region. North Battleford is located in the Saskatchewan Plains division of this region (NRC Atlas of Canada - 4th Edition, 1974). Figure 3.2 shows the physiographic regions of the Canadian Prairies.

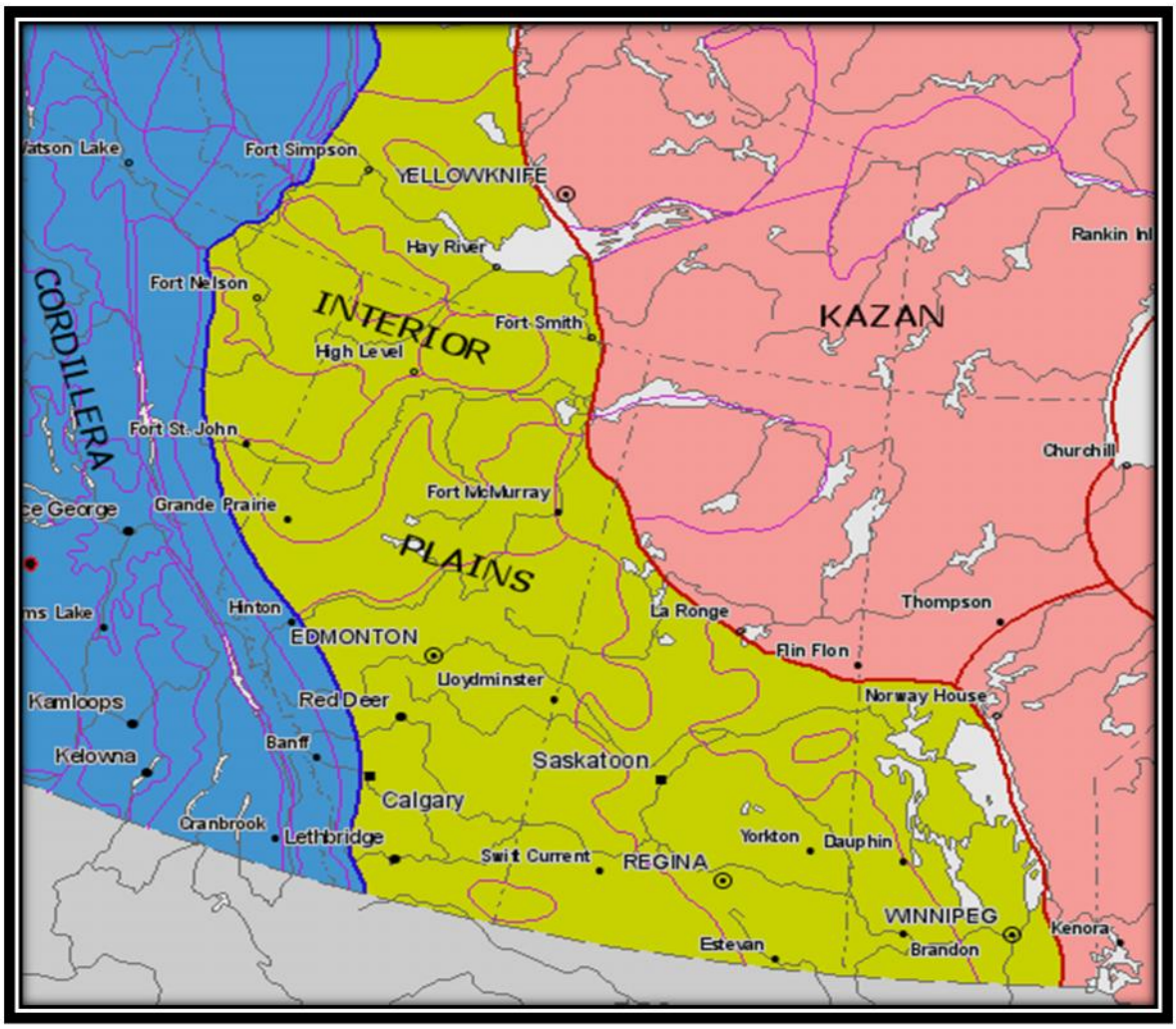

Figure 3.2: Physiographic regions of the Canadian Prairies (taken from NRC Atlas of Canada, 1974)

The Saskatchewan Plains have a surficial geology that is a product of glaciation and was most recently affected by the Wisconsin deglaciation approximately 12,000 years ago (Christiansen, 1979). The city of North Battleford and the town of Battleford are built near the banks of the North Saskatchewan River Valley, which served as a melt water channel during glacial retreat. Glacial melt water in this area was bound by the Eagle Hills Escarpment on the south and the by the glacier to the north (Christiansen, 1983) causing the erosion of the valley. As a result, most

of the stratified drift and glacial till were eroded from the valley slopes, leaving highly plastic clay shale near surface.

The area to the south of the bridge site is a Deltaic/Fluvial plain (See Figure 3.1). Mollard (1975) reports that this plain consists of fine to medium grained sand with silt and clay pockets. The area to the north of the bridge site is a fluted till plain. Nearing the north valley wall, alluvial and fluvial deposits overly the glacial drift (Clifton et al., 1999)

3.1.5 Regional Geology

The regional geology of the area generally consists of Cretaceous bedrock deposits underlying Tertiary, Empress Group sand and gravel underlying Quaternary glacial deposits and post-glacial alluvium (Clifton et al., 1999). Figure 3.3 after Christiansen (1983), Christiansen (1992) and Christiansen & Sauer, (2001) shows a visualization of the regional geology of the North Battleford area. This cross-section was initially developed for a typical section in the Saskatoon area but Christiansen (1983) was able to extrapolate the geology to the Denholm, SK area, which is geographically near to North Battleford, SK.

Age	Group	Formation	Material
Quaternary	Saskatoon Group	Surficial Stratified Drift	Clay, Silt, Sand
		Battleford Formation	Glacial Till
		Upper Floral Formation	Glacial Till
		Floral Inter-Till Sand	Sand - fossilized bone, wood, and shells.
		Lower Floral Formation	Glacial Till
	Sutherland Group	Warman Formation	Glacial Till
		Dundurn Formation	Glacial Till
		Mennon Formation	Glacial Till
Tertiary	Empress Group		Sand and Gravel
Late Cretaceous	Montana Group	Bearpaw Formation	Bedrock - Silt, Clay and Shale
		Judith River Formation	Silt and Sand
		Lea Park Formation	Bedrock - Silt, Clay and Shale

Figure 3.3: Generalized stratigraphy of the Battleford area (after Christiansen, 1983, Christiansen, 1992 & Christiansen and Sauer, 2001)

3.1.6 Bedrock Geology

The lowermost stratigraphic unit of interest is the Lea Park Formation. This formation is the oldest formation of the late Cretaceous deposits found in this area and is described as a dark grey, unoxidized, highly plastic clay that is non-calcareous and is massive to laminated (Clifton et al., 1999). The uppermost portion of the Lea Park Formation has been disturbed by glaciation and has alternating layers of hard and soft consistency. The disturbed zone is characterized as a dark olive brown and grey oxidized clay that ranges is consistency from soft to very stiff (Clifton et al., 1999). The oxidized portion of this formation has been documented to have zones of breccia, fissures and slickensides. At the south abutment, the thickness of the oxidized zone ranges from 3 m to 5 m (Clifton et al., 1999).

Overlying the Lea Park Formation is the silt and sand of the Judith River Formation. The Judith River Formation is present in the North Battleford area but is absent locally at the bridge site (Clifton et al., 1999) due to erosion of the valley and glacial action on the valley walls. The Bearpaw Formation, regionally, overlies the Judith River Formation but is also absent on this site.

3.1.7 Local Geology

The stratigraphy at the bridge site is very similar to the regional geology. The most significant difference at the bridge is the absence of the Judith River, Bear Paw, and Empress Group Formations. The Geology at the bridge site consists of the following strata, in ascending order (Clifton et al., 1999):

- Undisturbed Lea Park bedrock clay shale;
- Disturbed/weathered Lea Park bedrock clay shale;
- Quaternary glacial deposits; and,

- Post-glacial, alluvial, stratified deposits.

3.1.8 Hydrogeology

Many local aquifers, including the Floral inter-till aquifer and the Empress Group sands and gravels drain into the North Saskatchewan River Valley (Clifton et al., 1999). These aquifers are not present at the site; however, the local hydrogeology still must be described. This was accomplished using piezometric data collected between 1967 and 1999. The piezometric conditions will be discussed further in Section 3.3.1.

3.2 Overview of Previous Fieldwork

SMHI and CAL have provided the available records of fieldwork at the Battlefords bridges. Records with dates as early as 1963 have been provided and reviewed. The provided documentation shows that over 100 boreholes have been drilled, with instrumentation completions in many of them, in the south valley wall and south uplands area. Approximately 82 piezometers and 12 slope inclinometers (SI) have been installed on the south side of the river since 1963. Only data since 1967 has been digitized and will be used for this research. The available data will be summarized in this section

3.2.1 Drilling Programs

Drilling at the south abutment of the Battlefords bridges started in 1963 for the investigation of the old bridge. The majority of the documented drilling programs took place between 1967 and 1998. Table 3.1 shows a compilation of the drilling that has taken place in the aforementioned time period.

Samples were taken at varying intervals depending on the hole and the type of sampling tool

being used. Representative soil samples were taken using:

- Thin walled tube samplers;
- Split spoon samplers; and,
- Denison core barrels.

Resistivity and Spontaneous Potential electrical logs were conducted in each hole before completion. All soil samples were tested by SMHI's and CAL's geotechnical laboratories. The testing programs included tests for water content, Atterberg limits, Unified Soil Classification, unconfined compressive strength, unit weight, undrained shear strength via pocket penetrometer, and wet and dry densities.

Table 3.1: Compilation of geotechnical boreholes at the Battlefords Bridges - after Kelly et al. (1995)

Borehole Numbers	Year Drilled	Piezometers	Stratigraphic Holes
63	1967	1	1
100 Series	1967	23	24
300 Series	1967	0	1
400 Series	1967-1968	15	26
500 Series	1968	5	5
600 Series	1968	4	4
700 Series	1967-1968	9	9
800 Series	1967	6	6
900 Series	1968	4	5
1400 Series	1968	6	6
1500 Series	1997	23	23
1700 Series	2000	9	3
SI1 – SI3 & SI6-SI7	1968	-	5
SI8-SI9 & SI172	1997	-	3
SI10-SI12	2000	-	3
Test Shaft	1968		1

3.3 Monitoring Data

3.3.1 Piezometric Data

Approximately 82 piezometers have been installed at this site. Of these, only seven piezometers were installed prior to the 1967 failure at the south abutment (Clifton et al., 1999). These piezometers were numbered 66-3 to 66-9. In 1998, a number of piezometers were installed in

the south approach cut and South uplands to characterize the hydrogeology in these areas.

During the construction of the old bridge, the pore water pressures proved to be problematic in the south approach cut. Contractors reported of "quicking" conditions during construction (Clifton et al., 1999). A subsurface drainage system and cutoff wall were installed to control the groundwater levels at the south abutment. According to Clifton et al. (1999) the water table in the south uplands ranged from 2.4 m to 4.4 m below ground surface (bgs) but dropped substantially to between 7.8 m and 8.1 m bgs near the edge of the valley. In general, the piezometric surface was located near the till/shale contact (Clifton et al., 1999).

Nested piezometers were installed in the south abutment during the drilling program of 1999 in order to characterize the hydraulic gradient. Three piezometers were installed in each nest. One in the glacial deposits, one in the disturbed Lea Park shale, and one in the intact Lea Park shale.

The 1700 series of piezometers were installed for monitoring of pore pressures in the south slope during placement of the abutment fill. A total of three nests were installed, each equipped with 3 pneumatic piezometers. Borehole 1701 is located at the at the top (upslope) of the south abutment, borehole 1702 is located at the midpoint of the south abutment and borehole 1703 is located at the toe of the south abutment. Figure 3.4 shows a Google Earth photo with the 1700 series piezometer locations overlain. This photo was taken from the SMHI Geohazards Risk Management Program for this site. Table 3.2 shows the tip elevation and soil type at the tip of each of the 1700 series boreholes.

Figure 3.5 shows the hydraulic gradients at the south abutment in the spring (April, 2009) and fall (August, 2011). From this figure, it becomes clear that the lower piezometers are impacted by seasonal variations in the river level. The lower most piezometers in the nests showed an increase of approximately 0.56 m to 1.23 m in total head during the spring season. The middle piezometers showed an increase of approximately -0.14 m to 0.35 m in total head during the spring season. The piezometers closest to the surface showed an increase of approximately

0.07 m to 0.14 m in total head during the spring season.

Figure 3.4: 1700 series piezometer locations - Google Earth photo with locations overlain taken from SMHI Geohazards Risk Management Program

Table 3.2: 1700 series piezometers in the new bridge south abutment

Piezometer No.	Tip Elevation	Soil Type at Tip
1701	450.89	Undisturbed shale
1701A	455.9	Disturbed, unoxidized shale
1701B	463.76	Disturbed, oxidized shale
1702	450.18	Undisturbed shale
1702A	455.21	Disturbed, unoxidized shale
1702B	461.71	Disturbed, oxidized shale
1703	447.68	Undisturbed shale
1703A	452.8	Disturbed, unoxidized shale
1703B	460.62	Disturbed, oxidized shale

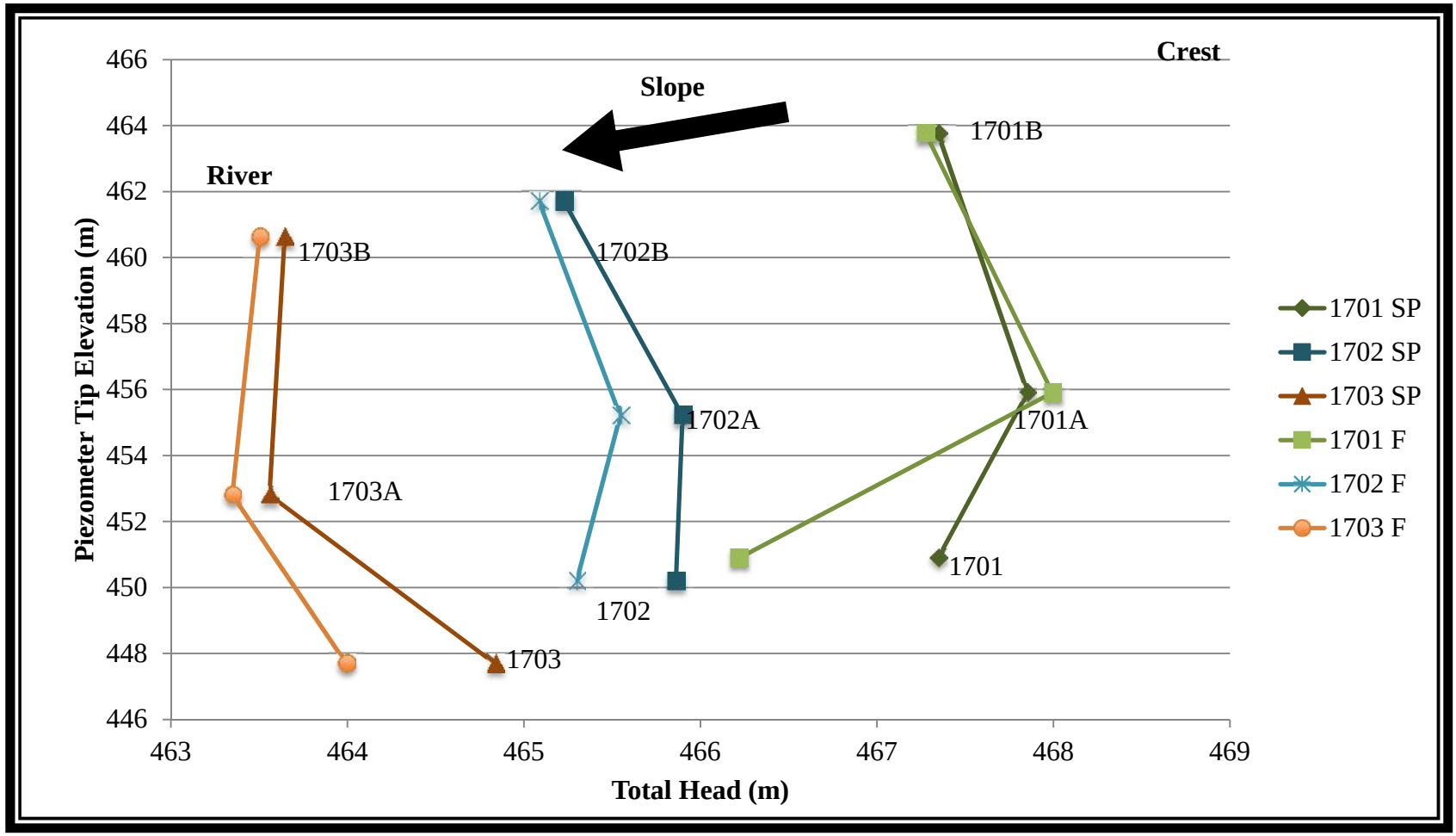

Figure 3.5: Comparison of Hydraulic Gradient (New Bridge)- Spring 2009 to Fall 2011

3.3.2 Slope Inclinometers

There have been 12 slope inclinometers (SI) present at the south abutment of the Battlefords bridges since 1968. All inclinometers at this site were installed with their A-axis aligned parallel the bridge such that positive A-direction movement is in the north direction and positive B-direction movement is in the east direction.

SMHI switched to metric measurements in 1985 and also switched SI probes in 1998. For each of these two situations, the SI must be re-initialized and the data cannot be combined. As such, a separate plot was created for each situation. Table 3.3 shows a summary of inclinometer movements since 1972.

Figure 3.6 shows a Google Earth photo with the instrumentation locations that are relevant to the new bridge overlain on a Google Earth image. This photo was taken from SMHI's Geohazards Risk Management Program. A legend for interpreting the figure is as follows:

- 004-14 – highway 4, control section 14
- SP – standpipe piezometer
- PZ – pneumatic piezometer
- SI – slope inclinometer

Table 3.3: Summary of inclinometer movements since 1972 - after Clifton et al. (1999)

Inclinometer Number	Monitoring Date	A-Axis Cumulative Movement (mm)	B-Axis Cumulative Movement (mm)	Elevation of Movement (m)
SI1	July 72/Aug 85	18.1	-2.9	455.8
SI71 (Replaced SI1)	Aug 85/Mar 98	9	-1.7	455.8
	Dec 00/Apr 12	4.9	1.4	455.8
SI2	July 72/Sept 77	No Movement	No Movement	-
SI172 (Replaced SI2)	Aug 97/Mar 98	No Movement	No Movement	-
	Dec 00/Apr 12	2.9	Erratic Data	453.3
SI3	Aug 72/July 85	No Movement	No Movement	-
SI73 (Replaced SI3)	Sept 85/Mar 98	2.1	0	452.2
	Apr 01/Jul 07	1.8	0	452.2
SI4	July 72/Sept 77	No Movement	No Movement	-
SI74 (Replaced SI4)	July 86/Mar 98	No Movement	No Movement	-
	Not monitored Since 1998	-	-	-
SI5	Aug 72/Aug 81	No Movement	No Movement	-
SI6	Aug 72/Aug 85	No Movement	No Movement	-
SI76 (Replaced SI6)	Aug 85/Mar 98	0	2.9	457.3
	Dec 00/Apr 12	No Movement	No Movement	
SI7	July 72/Aug 85	3.4	0	451.8
SI77 (Replaced SI7)	Aug 85/Mar 98	3.7	0	451.8
	Dec 00/Apr 12	4.2	0.5	451.8
SI8	Aug 97/Mar 98	No Movement	No Movement	-
	Nov 00/Apr 12	3.5	-2.4	458.3
SI9	Aug 97/Mar 98	No Movement	No Movement	-
	Not monitored Since 1998	-	-	-
SI10	Oct 01/Apr 12	3.8	3.3	453
SI11	Jul 01/Apr 12	No Movement	No Movement	-
SI12	Jul 01/Apr 12	20.5	37.5	481

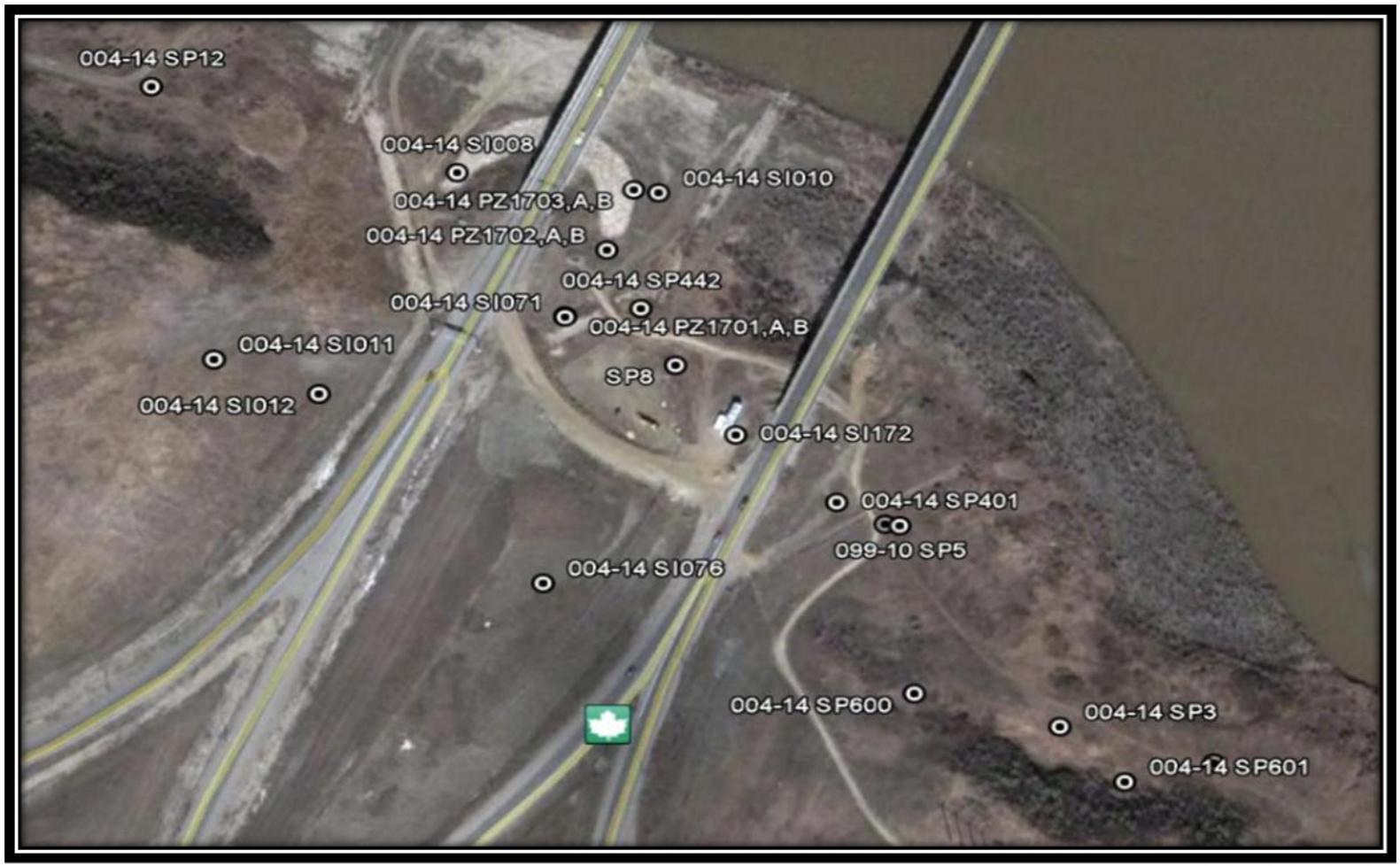

Figure 3.6: Google Earth photo with instrumentation overlay - used by SMHI in their Geohazards Risk Management Program

3.3.3 SI Monitoring Data

The two most significant inclinometers for this research were SI8 and SI10. Both are located in the south abutment fill and provide critical information about the historical movements. Many other SIs were installed at the bridge site but are not critical for scope of this work. The inclinometer measurements for SI8 and SI10 will be described in the following subsections. All other inclinometer measurements can be found in Appendix A.

3.3.3.1 SI8

SI8 was installed in July 1997 west of the new bridge South abutment. The first monitoring of this SI was in August 1997. No movement was observed in this SI until November 2000.

Between November 2000 and April 2012, 3.5 mm of cumulative displacement was observed in the A-axis and -2.4 mm in the B-Axis. Throughout this time period the SI has been showing average movements ranging from 0.2 mm/yr to 0.6 mm/yr.

Movement appears to be taking place along a slip surface located at an elevation of approximately 458.3 m or a depth of 10 m bgs as shown on the SI plots. The stratum at this location is oxidized shale that is described to be heavily jointed. A plot showing cumulative displacement in the A and B axis for this time period is found in Figure 3.7.

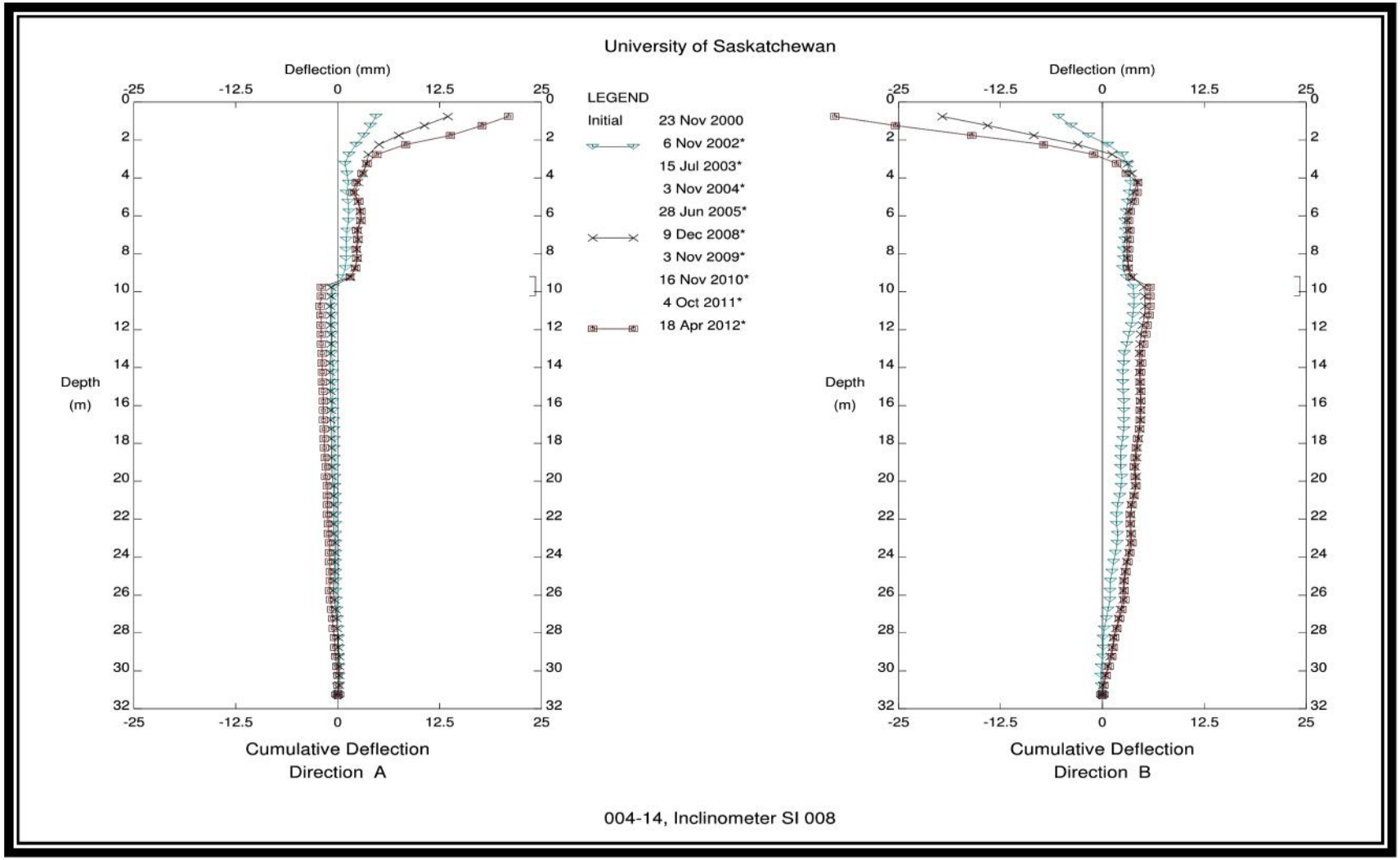

Figure 3.7: SI8 cumulative displacement - A & B axis (2000-2012)

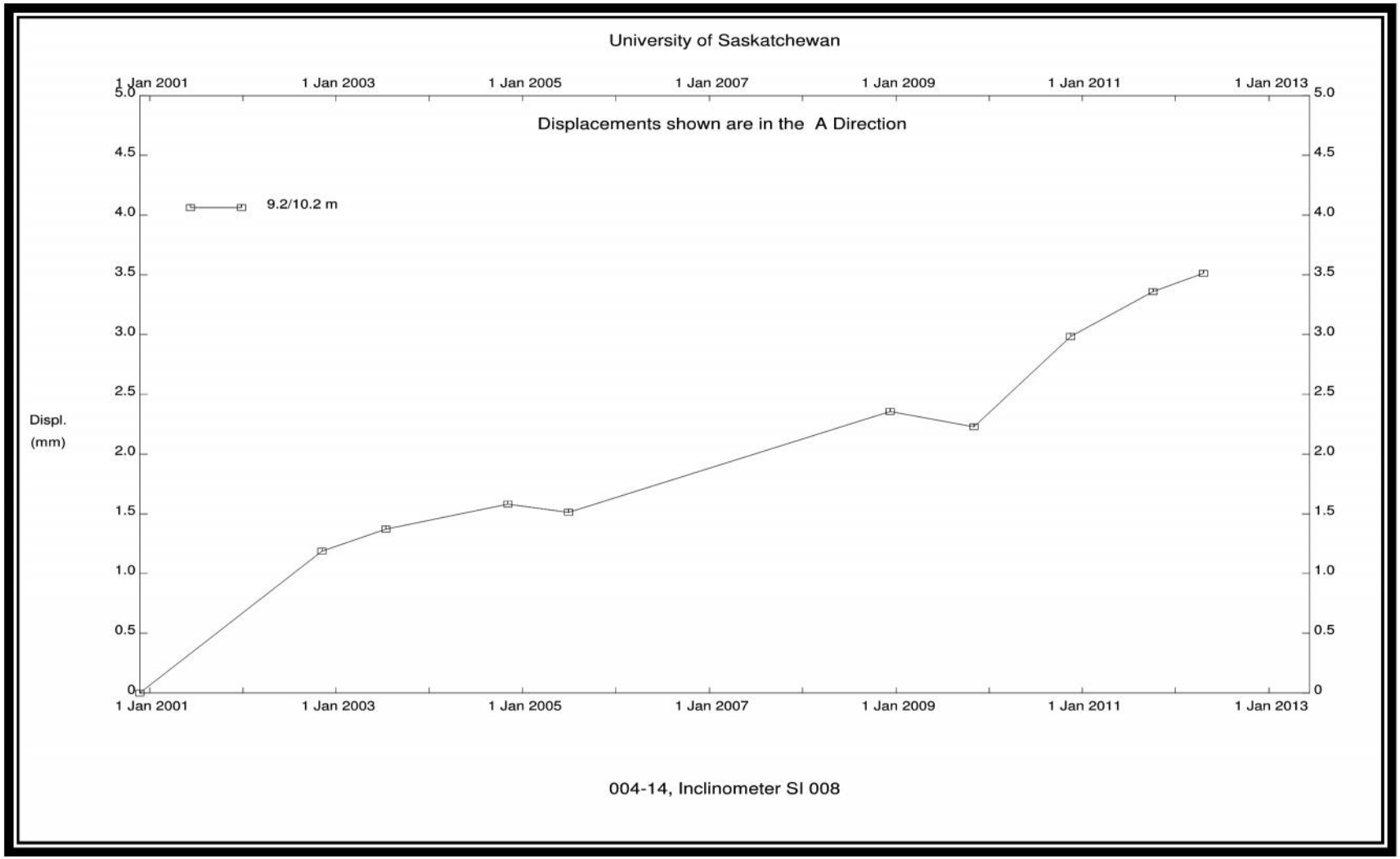

Figure 3.8: SI8 displacement at 10 m bgs vs. time – A axis (2000-2012)

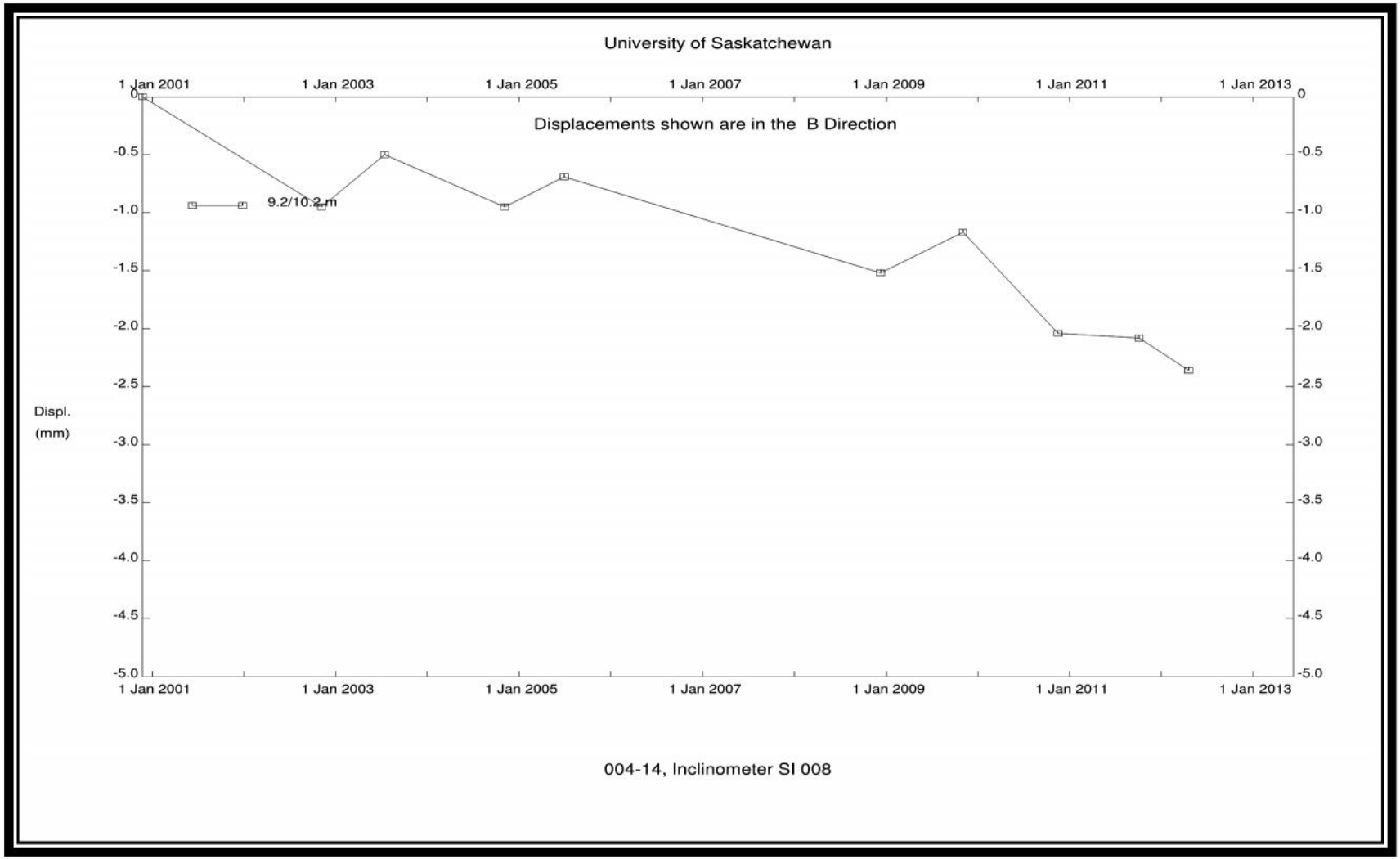

Figure 3.9: SI8 displacement vs. time – B axis (2000-2012)

3.3.3.2 SI10

SI10 was installed sometime in year 2000 to the east of the new bridge South abutment. The first monitoring of this SI was in January 2001. Between January 2001 and April 2012, 3.8 mm of cumulative displacement was observed in the A-axis and 3.3 mm in the B-Axis. Throughout this time period the SI has been showing average movements ranging from 0.1 mm/yr to 1.2 mm/yr.

Movement appears to be taking place along a slip surface located at an elevation of approximately 453 m. The stratum at this location is unoxidized shale. A plot showing cumulative displacement in the A and B axis for this time period is found in Figure 3.10.

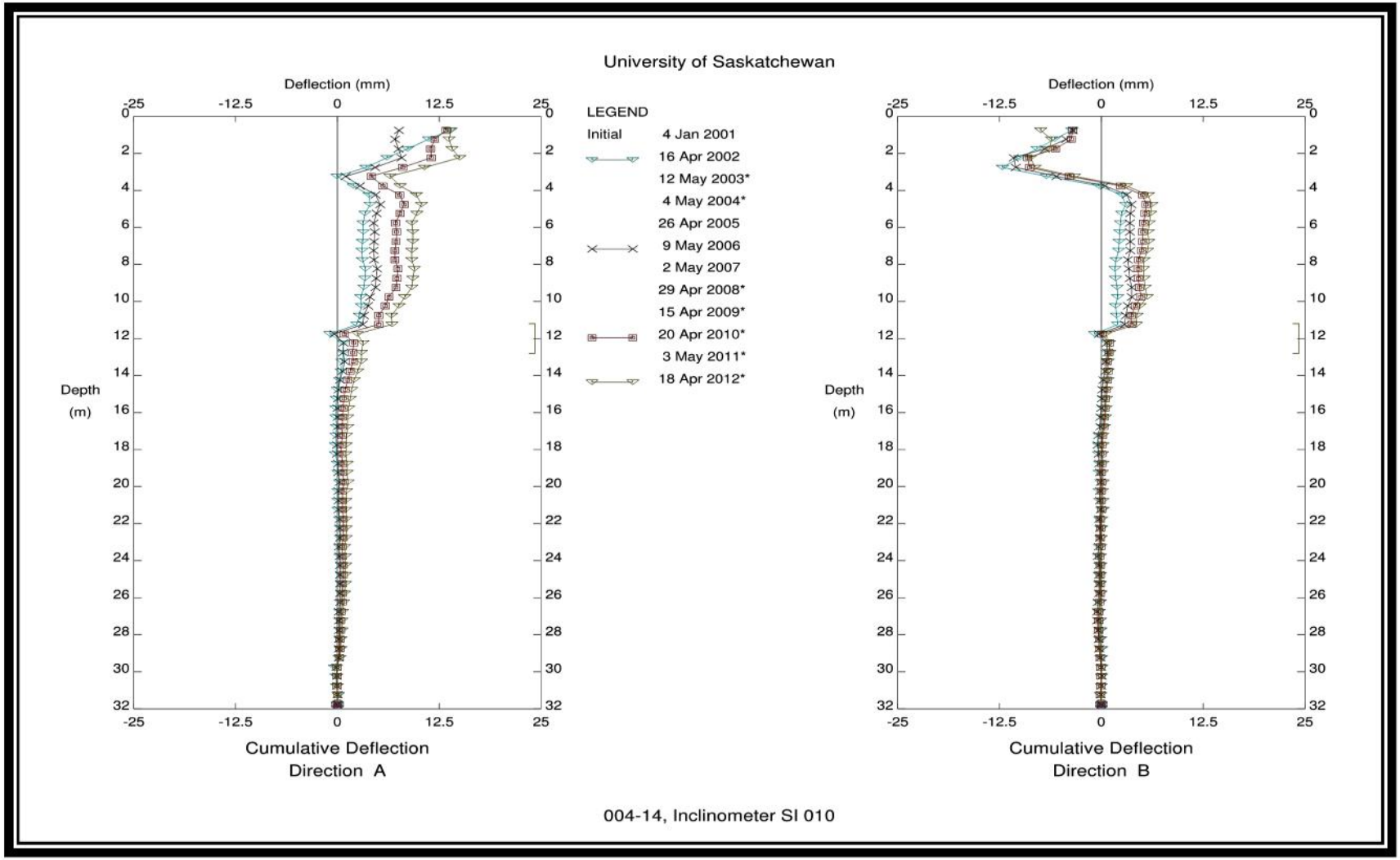

Figure 3.10: SI10 cumulative displacement - A & B axis (2001-2012)

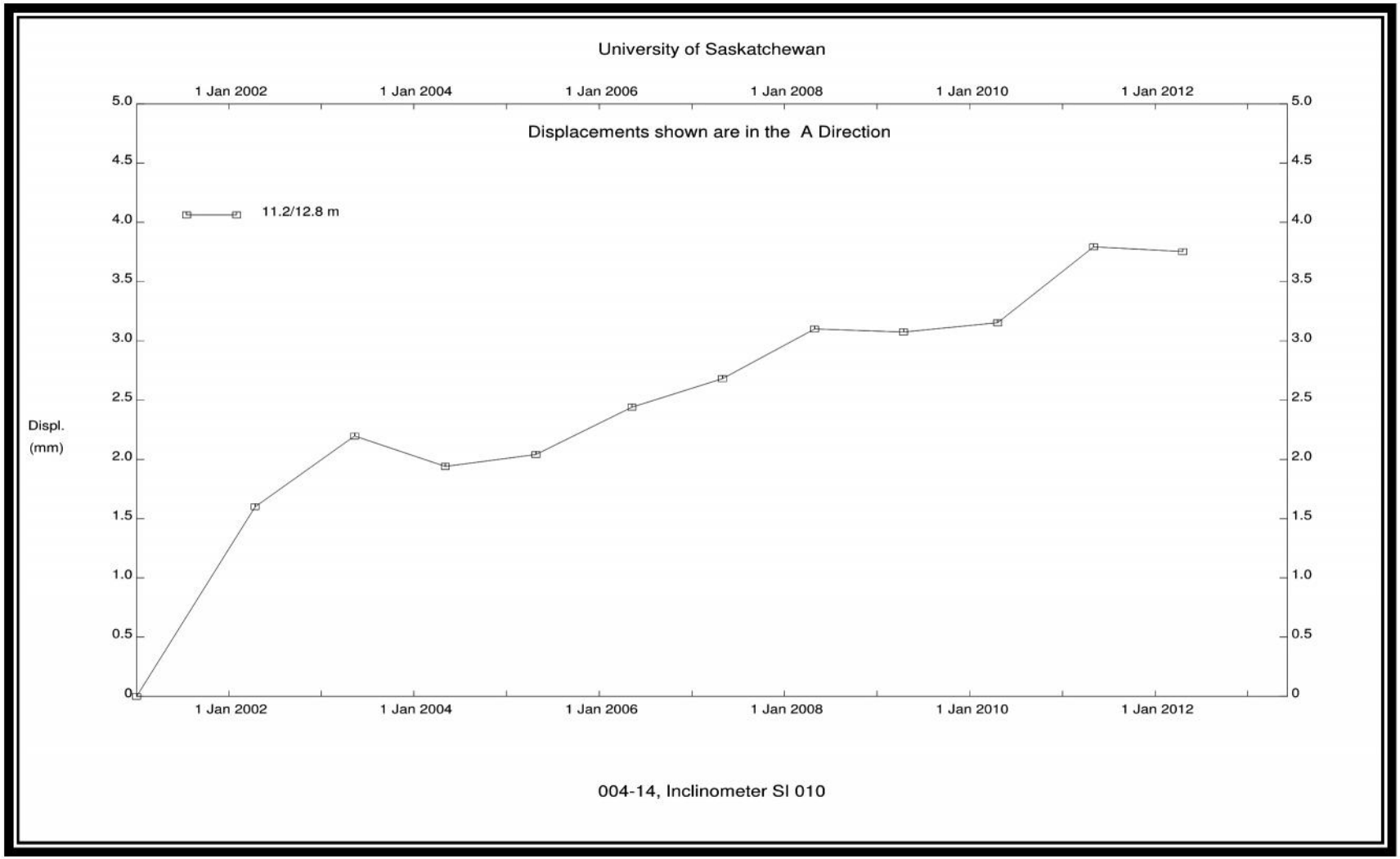

Figure 3.11: SI10 displacement vs. times - A axis (2001-2012)

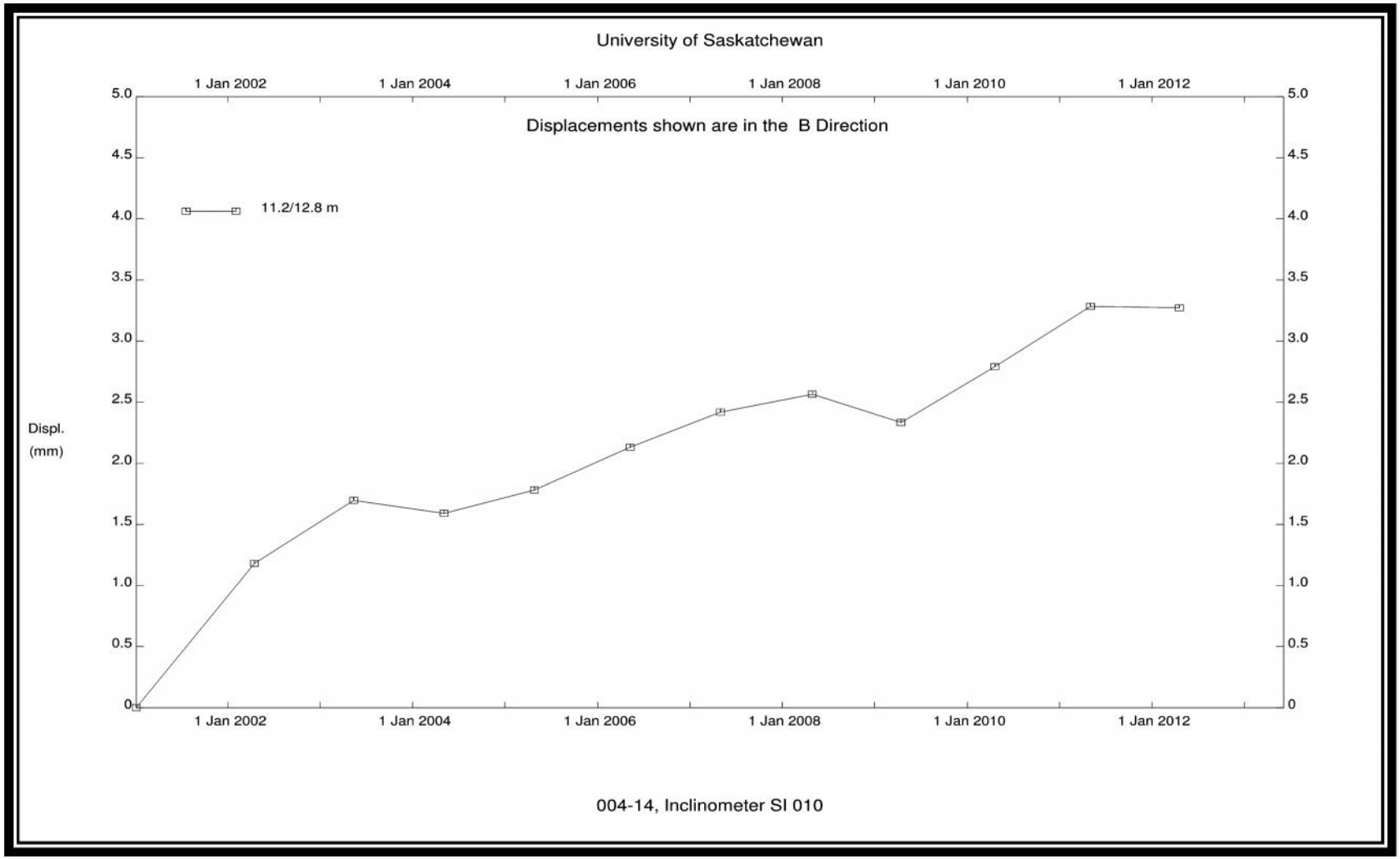

Figure 3.12: SI10 displacement vs. times - B axis (2001-2012)

3.4 Documented History of Slope Instability at the South Abutment

Slope instability at the Battlefords bridges is most recognized for one major event that occurred in 1967. The old bridge's south abutment experienced failure shortly after it was opened to the public. Since that time, no further major failures have occurred however, slow movements associated with the failure planes in the Lea Park clay shale have continued. A detailed history of the October 1967 failure at the old bridge was documented by SMHI personnel in field logs and daily diaries and was summarized by Clifton et al. (1999). Clifton et al. (1999) was used to highlight the important events below:

November 1966

The first signs of groundwater problems occurred in November 1966. The contractor that was working on the south underpass reported having trouble with "quicking" conditions during construction (Clifton et al., 1999). This was an intensive cut operation and the contractor was experiencing blow out conditions associated with the high pore water pressures in that area.

July 1967

Construction continued as planned until the bridge was opened in 1967. The grand opening was in July 12, 1967 however, at this time, the bridge was not yet opened to the public (Clifton et al., 1999).

September 1967

Pavement cracking showed the first signs of slope instability south of the south grade separation (Clifton et al., 1999). SMHI began coring the area to better understand the bedrock influence (Clifton et al., 1999). In the meantime, there was a 3-car collision, potentially due to the road

deformations, that resulted in one fatality.

October 1967

October 11, 1967 more signs of slope failure appeared at the south abutment. There was a reported 50 mm to 75 mm of vertical displacement at the time (Clifton et al., 1999). Immediately, a contractor was retained to construct spur dikes to divert water flow from the south abutment (Clifton et al., 1999). At this time, it was assumed that riverbank scour was the cause of the failure. On October 20, 1967 the bridge engineer determined that scour did not appear to be the cause of the movement and work on the spur dikes was halted.

November 1967

The beginning of November brought the commencement of a geotechnical drilling and instrumentation program. Inclinometers were installed at the south abutment and in piers 1 & 2 (Clifton et al., 1999). The test shaft was also drilled and founded 21 m. into shale. At this time, the rockers on the old bridge were leaning approximately 50 mm to the north (Clifton et al., 1999).

On November 16, 1967 the remediation plan was handed down from the chief engineer. It involved the following (Clifton et al., 1999):

- Remove remnants of coffer dams to divert flow away from south abutment;
- Install a grout cutoff wall near the gore point south of the bridge;
    - The wall will prevent groundwater from the uplands from entering the abutment area;
- Backfill all cracks at the south abutment;

- Create granular fill, interceptor ditches both upstream and downstream;
- Flatten the valley wall to 9:1;
- Cut a strip out of the bridge deck to re-establish the expansion gap; and,
- Construct a diked enclosure to that stretches to pier 2 and carries on both upstream and downstream.

Work began on this plan by November 18, 1967.

February 1968

Most of the remedial work had been completed and the bridge was re-opened to the public. The remaining work could take place with the bridge open to traffic.

June 1968

Reports reached the Chief Engineer that pier 2 was tilting towards the north (Clifton et al., 1999). An action plan was to be drafted immediately. The bridge design engineer sent out a memo stating the limits that the bridge can handle and stated the importance of monitoring the piers, rockers and bearings on a regular basis (Clifton et al., 1999).

There were a series of memos that were sent with each person's opinion on what may be causing the tilting. New tension cracks had also shown up on the east side of the south abutment. Some believed these advancements in the failure were due to scour and some believed they were due to pressure caused by the previous remedial berm (Clifton et al., 1999). It was decided that it would be unwise to reduce the size of the berm as it was providing weight to the toe of the landslide. If any changes were made, they should be to flatten the slope on the east side, lengthen the berm towards pier 3, and reduce the water level in the uplands' unconfined aquifer

with some sort of pumping system (Clifton et al., 1999).

July 1968

The memos state that the berm was not to be extended or lowered unless significant further movement occurred (Clifton et al., 1999). The east slope was to be flattened to 9:1 and any new crack should be filled as they are discovered. The consultant on site was to continue to assess the draining the uplands and extending the berm (Clifton et al., 1999).

The remaining memos address the maintenance of the drainage systems and fill slopes but do not address the main slope failures anymore. As such they were excluded from this work.

Chapter 4 Slope Stability Modeling

Barbour and Krahn (2004), reference the 1987 Nash Lecture, given by Professor John Burland, in which the famous "Burland Triangle" (Figure 4.1), an idealization of geotechnical engineering, was presented. A quick glance at Figure 4.1 shows that modeling is only a small part in a larger cycle that also includes site investigations and laboratory testing. All of these processes are based around precedence and experience. A model without a detailed site investigation and testing program is merely a guess. A model should be a verification of process based on sound engineering judgment but never a guess.

Chapter 3 of this thesis has described, in detail, the site investigation and laboratory testing history of the Battlefords bridges as undertaken by the SMHI and CAL. This data will be called upon when discussing the modeling results.

Chapter 4 will discuss the historical models completed at this site, as well as the modeling that was carried out for this thesis work. The following methods of analysis were employed to analyze the slope stability of the south abutment at the Battlefords bridges:

- Limit equilibrium method;
- Finite element stresses in limit equilibrium framework, and;
- Finite element analysis.

The results of these models will be presented and discussed in the following sections.

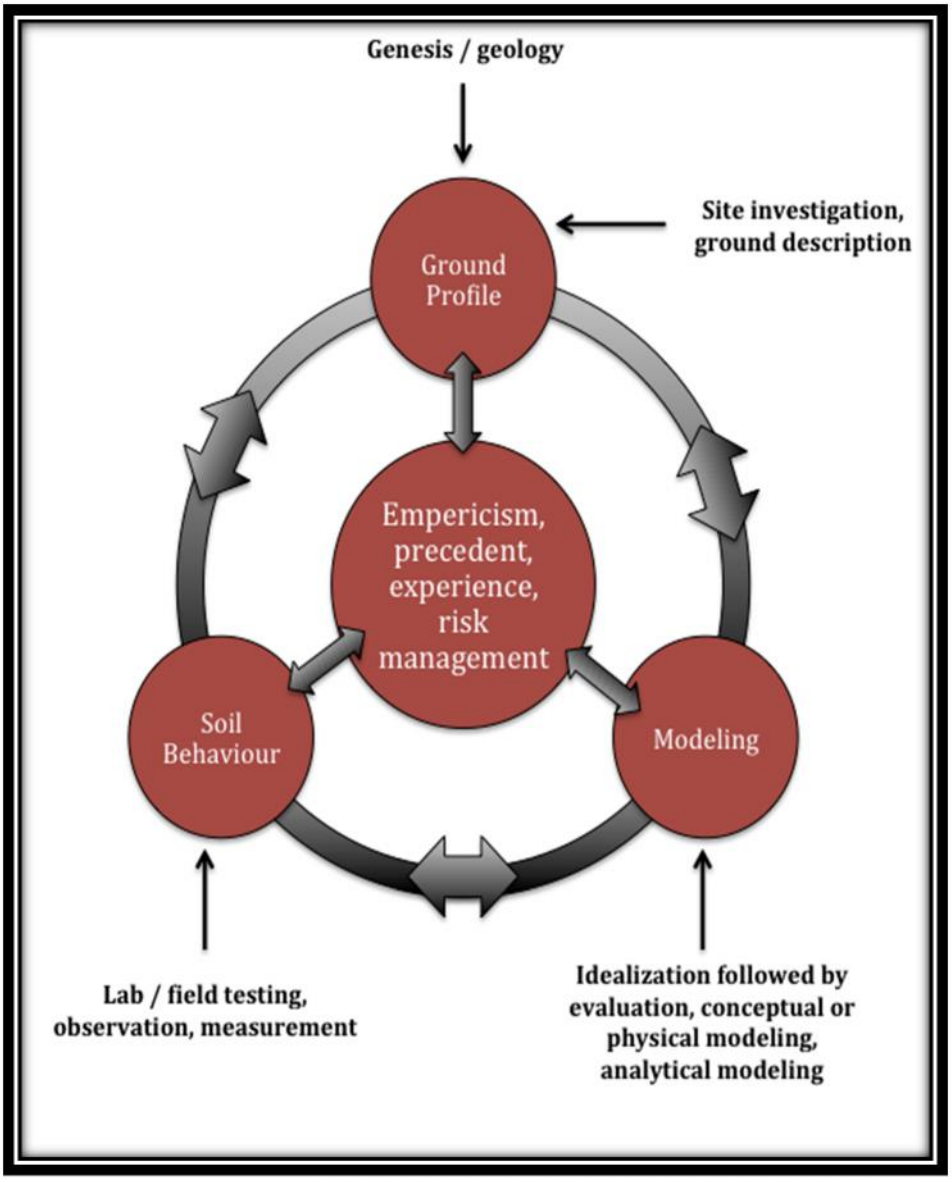

Figure 4.1: Expanded Burland Triangle - After Barbour and Krahn (2004)

4.1 Historical Models – Completed by Clifton Associates Ltd.

The initial slope stability analyses for the old bridge and new bridge are outlined in the report titled *Compilation and Preliminary Geotechnical – Battleford Bridge*. Clifton et al. (1999) analyzed the stability of both bridges using the software SLOPE/W by GEO-SLOPE International Ltd. The lateral extent of the old bridge's failure surface was then examined using 3-D limit equilibrium software, CLARA/W by O. Hungr Geotechnical Research, Inc. The results of the 3-D analysis were used to determine appropriate bridge spacing such that the new bridge abutment fill would not accelerate or contribute to the existing failure. Table 4.1 shows the various factors of safety for the analyses performed by Clifton et al. (1999).

Table 4.1: Summary of results from Clifton et al. (1999)

Type of Analysis	Factor of Safety
Old Bridge - At time of failure	1.00
Old Bridge - After Remediation	1.14
New Bridge – Before Construction	1.13
New Bridge - Approach cut	1.52-1.76

A variety of sensitivity cases involving river scour and construction pore water pressures were completed by Clifton et al. (1999). Within the sensitivity analyses, the factor of safety at the new bridge varied.

4.2 Models Completed for this Thesis

All modeling for this research was completed using SLOPE/W and SIGMA/W software from GeoStudio 2012 by GEO-SLOPE International Ltd. The models were completed in both limit equilibrium (SLOPE/W) and finite element (SIGMA/W) environments. The following steps were required in the modeling for this work:

- SLOPE/W – Back analysis of the old bridge at the time of failure for calibration of soil

strength parameters;

- SLOPE/W – Application of the calibrated, post failure, strength parameters to the old bridge after remediation;
- SLOPE/W - Application of the calibrated strength parameters to the new bridge to analyze the factor of safety;
- SIGMA/W – Strength reduction analysis to match inclinometer performance to date, and;
- SIGMA/W + SLOPE/W – Verification of reduction in factor of safety using both finite element and limit equilibrium methods.

4.2.1 Slope Geometry and Site Stratigraphy

The geometric and cross-section data for the Battlefords Bridges was taken from topographic survey data provided by the Central Survey and Mapping Agency of Saskatchewan, City of North Battleford and Saskatchewan Ministry of Highways and Infrastructure. A borehole location plan with surface elevation contours was created by CAL during their preliminary work in 1999. AutoCAD Civil 3-D software was used to manage the survey data for this work.

Borehole data was summarized using printed copies of the drilling logs and digitized versions of the laboratory testing results. This summary included marking the major stratigraphic members and their associated properties as confirmed by laboratory testing results. The stratigraphy was divided into the following major groups:

- Alluvium/Fill;
- Oxidized till;
- Oxidized shale;

- Disturbed, unoxidized shale, and;
- Undisturbed unoxidized shale.

Using the (x, y) coordinates of the borehole surface location and the elevation (z coordinates) of the top of each stratigraphic unit, the changes in stratigraphy at each borehole could be assigned to a point in 3-D Space (x, y, z). Each of these (x, y, z) points was assigned to a "point group" named after one of the five stratigraphic units listed above. These point groups were used to create 3-D surfaces that contour the top of each stratigraphic unit. This 3-D, spatial distribution of properties allowed for cross-sections to be taken anywhere within the investigation area. The cross-sections for this project were taken along the bridge alignments at the south abutment. Figure 4.2 shows a topographic map with the cross-sections A-A' and B-B' and the borehole locations marked.

The survey data that was used to create the surface elevation contours dates to 1996 and the new bridge abutment geometry, as proposed by CAL, had to be superimposed on the undisturbed slope after cutting the cross-section for the models (Figure 4.5). Figure 4.3 through Figure 4.6 show the cross-sections that were used for this work.

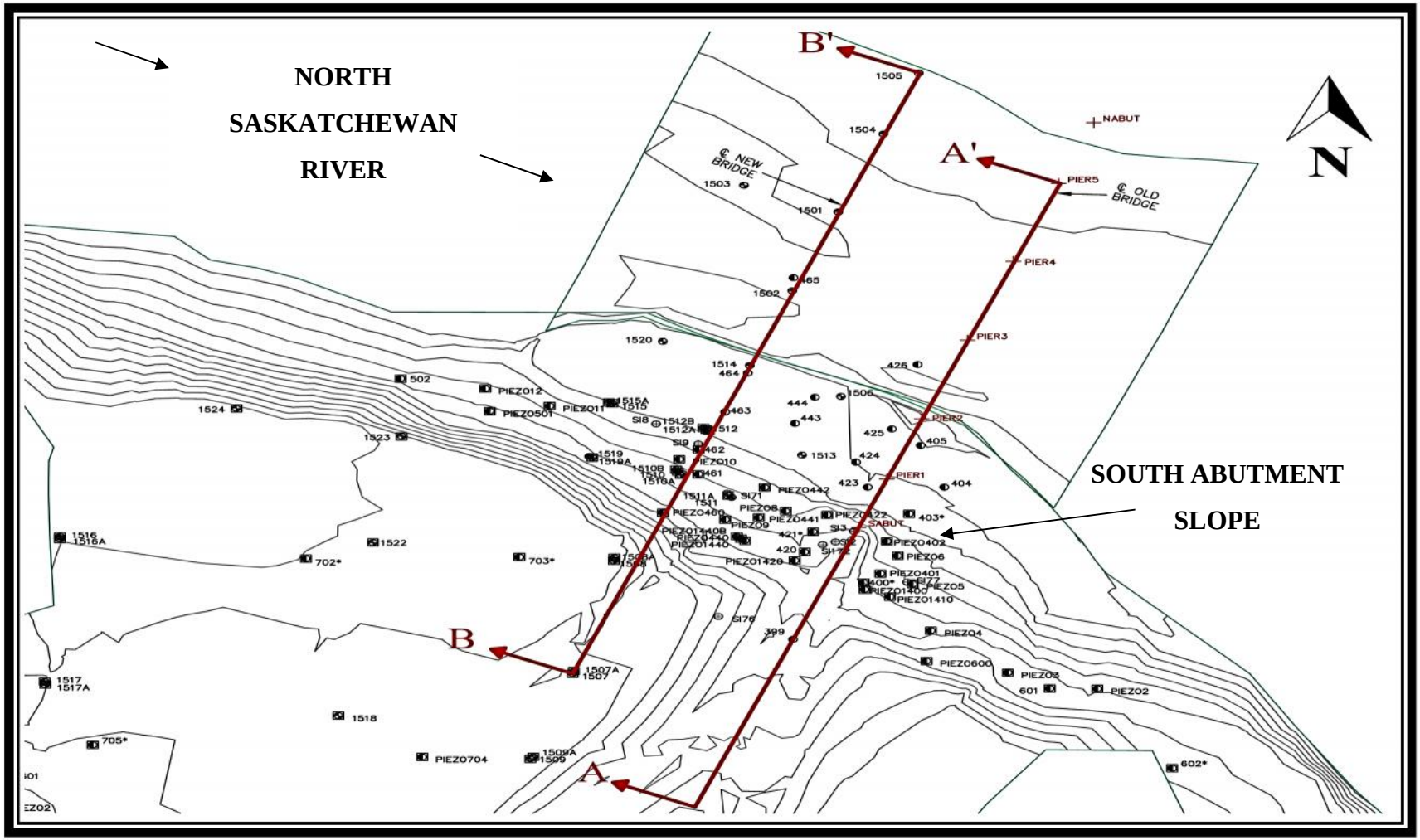

Figure 4.2: Topographic map of the south abutment at the Battlefords Bridges - after Clifton et al. (1999)

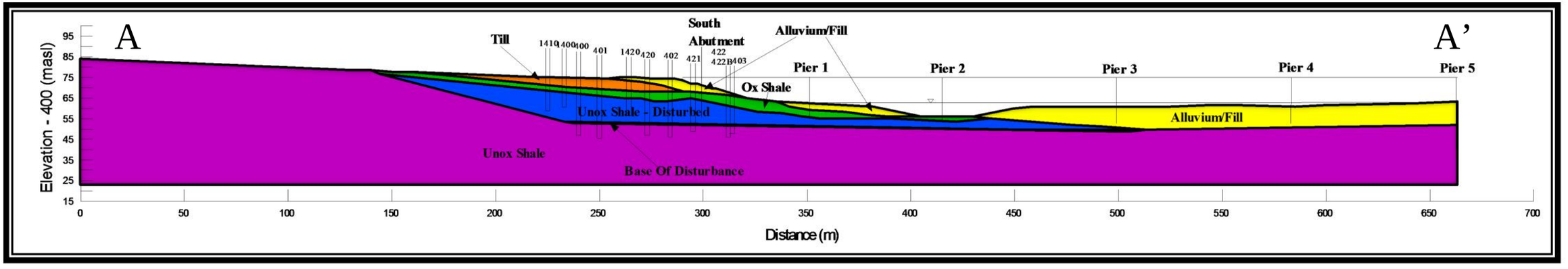

Figure 4.3: Cross-section geometry - old bridge before remediation

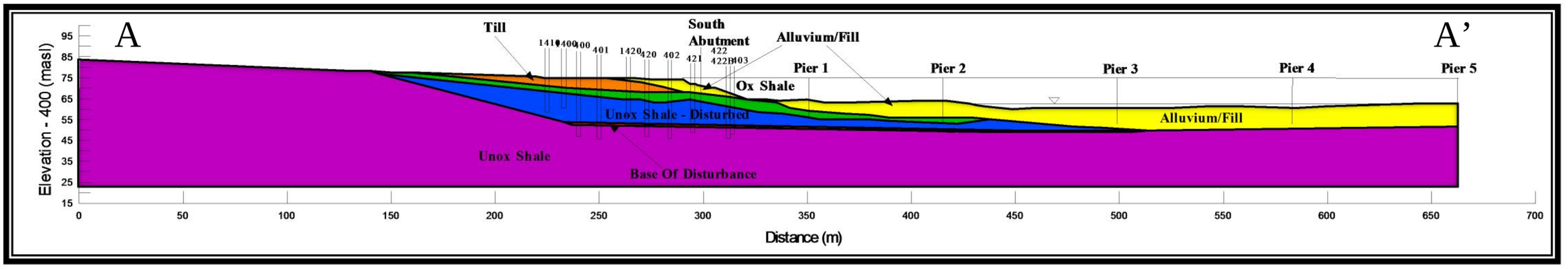

Figure 4.4: Cross-section geometry - old bridge after remediation

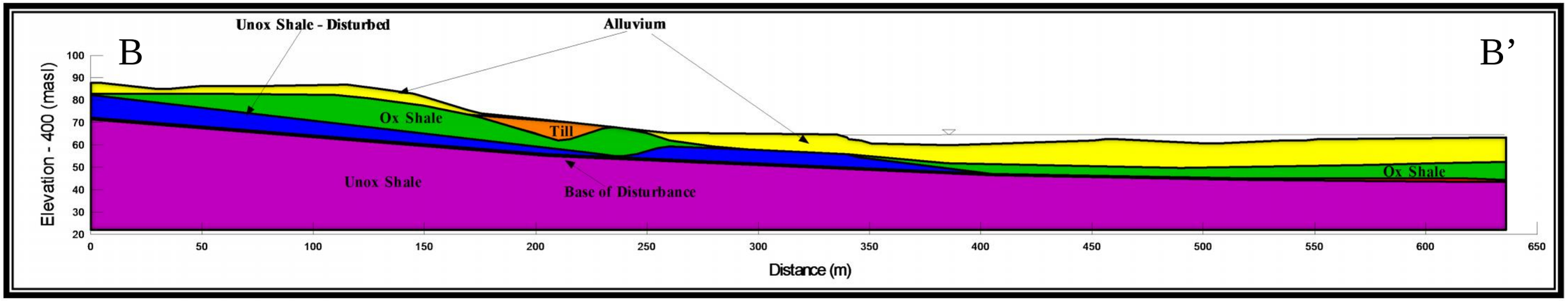

58

Figure 4.5: Cross-section geometry - new bridge pre-construction

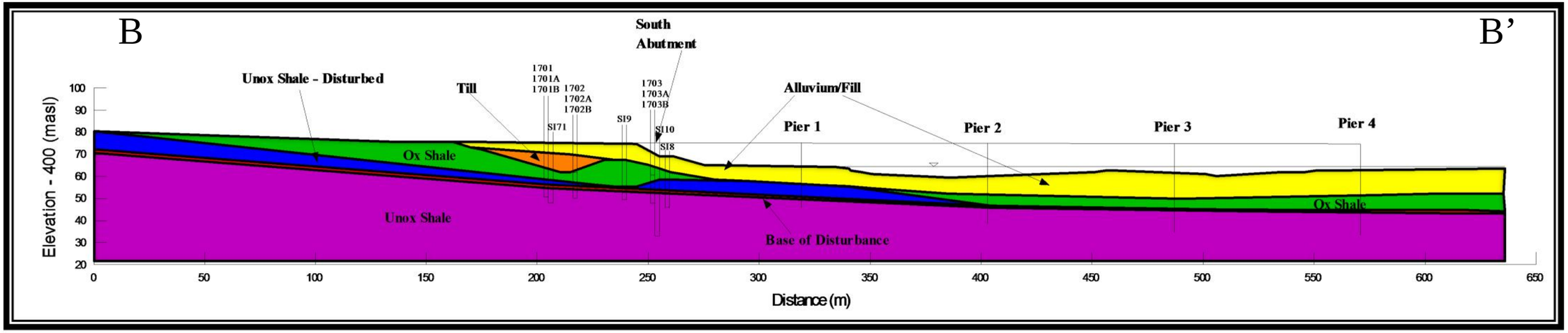

Figure 4.6: Cross-section geometry - new bridge post construction

4.2.2 Limit Equilibrium Analyses

The first stage of modeling was completed using limit equilibrium analysis. The concepts of limit equilibrium are discussed in Section 2.3.1. All of the limit equilibrium analyses were completed using effective strength parameters. The Morgenstern and Price method of analysis was used with a half sine side force function.

4.2.2.1 Back Analysis of the 1967 Failure at the Old Bridge

The old Bridge was back analyzed in order to try and match conditions from the time of failure in 1967. A piezometric surface very similar to that established by Clifton et al. (1999) was used for this model. The site geometry was constructed using cross-section A-A' found in Figure 4.3. A shear plane of residual material strength, as tested by CAL, was added to the top of the undisturbed shale layer. In analyzing the instrumentation plots (Section 3.3.3) and by the presence of bentonitic layers within the shale, it becomes clear that there are preferential paths of weakness within the Lea Park clay shale (Christiansen, 1983; Clifton et al., 1999; Clifton & Kelly, 2001). By adding this layer of residual strength material at the identified shear zone a composite type failure can be created. Table 4.2 shows various ranges of material properties, for the soils at the south abutment and used in previous research within similar areas in the North Saskatchewan River Valley. These values provide a range in which the back-analyzed properties should fall.

Table 4.2: Material properties determined by previous research – after Clifton et al. (1999) and Kelly et al. (1995)

Soil Stratum	Unit Weight, γ (kN/m^3)	Angle of Shearing Resistance, Φ' (degrees)	Apparent Cohesion, c' (kPa)	Source
Undisturbed Lea Park shale	19.8-21	19.5-28	10-30	SMHI; Clifton Associates Ltd., 1995
Disturbed Lea Park shale	19.8-21	7.5-20	8-16	Clifton Associates Ltd, 1995
Residual Lea Park shale	19.8-21	5-11.5	0-10	SMHI, Kelly et al., 1995; Clifton Associates Ltd., 1995; Insley et al., 1977
Glacial Till	20-21.8	25-29	7-72	Lindgren and Sauer, 1982; Richardson, 1984; Wilson and Clifton, 1983
Alluvium	19-20	25-39	0	Lindgren and Sauer, 1982; Richardson, 1984; Wilson and Clifton, 1983

Figure 4.7 shows the SLOPE/W analysis that was used to confirm the material properties. Using the material properties found in Table 4.3 the back analysis shows a FOS of 1.01.

The critical slip surface is highlighted in green with its associated factor of safety listed on the figure. This failure surface is consistent with the findings by Clifton et al. (1999). The slip surface was expected to undermine pier 1 and exit to surface before pier 2. The material strengths were all within the ranges that have been identified in previous research (Table 4.2). Of note, greater stregth was used for the undisturbed lea park shale to keep the slip surface from penetrating it, similar to an impenatrable material. The back analyzed strength parameters in Table 4.3 will be used for further analyses within the scope of this work.

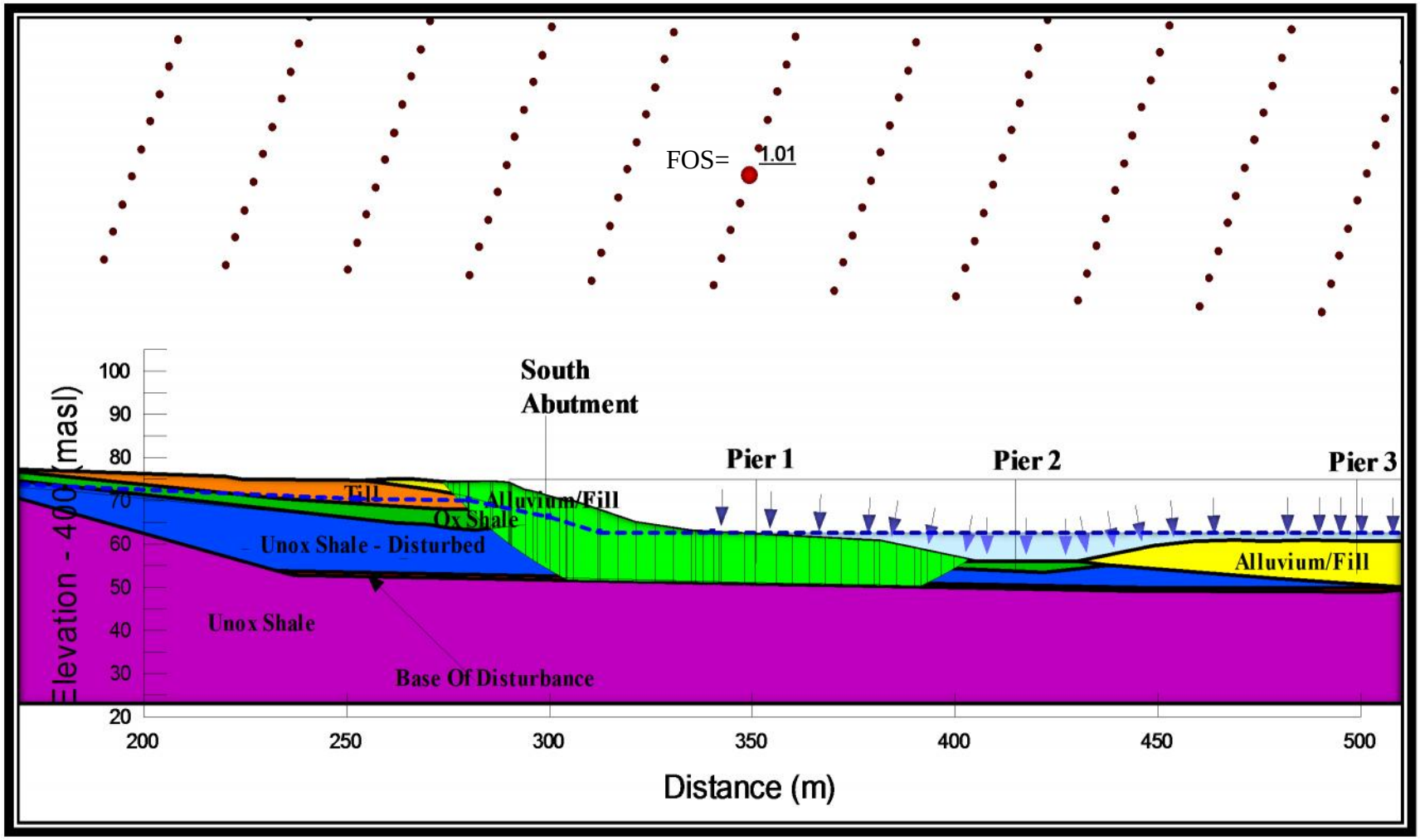

Figure 4.7: Back-analysis of old bridge at time of failure - October 1967

Table 4.3: Summary of material properties used for back analysis of the Old Bridge

Soil Stratum	Unit Weight, γ (kN/m^3)	Angle of Shearing Resistance, Φ' (degrees)	Apparent Cohesion, c' (kPa)
Undisturbed Lea Park shale	20.9	28	10
Disturbed, unoxidized Lea Park shale	20.9	16	8
Residual Lea Park shale	20	6.5	2.5
Disturbed, oxidized Lea Park clay shale	20.9	16	8
Glacial Till	20.7	25	7
Alluvium/Fill	19	25	7

4.2.2.2 Old Bridge – After Remediation

After the slope failure in 1967, emergency measures were taken to stabilize the south abutment slope. A detailed log of these events can be found in section 3.4. The main stabilizing measure used was a toe berm stretching out to pier 2. The analysis was carried out using the post-remediation cross-section through A-A', shown in Figure 4.4, and the material properties from the back analysis, presented in Table 4.3. It was found that the factor of safety immediately after the completion of the remedial work was 1.27. The results of this analysis are shown in Figure 4.8. The critical slip surface is highlighted in green with its associated factor of safety listed on the figure. The critical slip surface is different than the initial failure, which is expected when remedial measures such as a large stabilization berm are added.

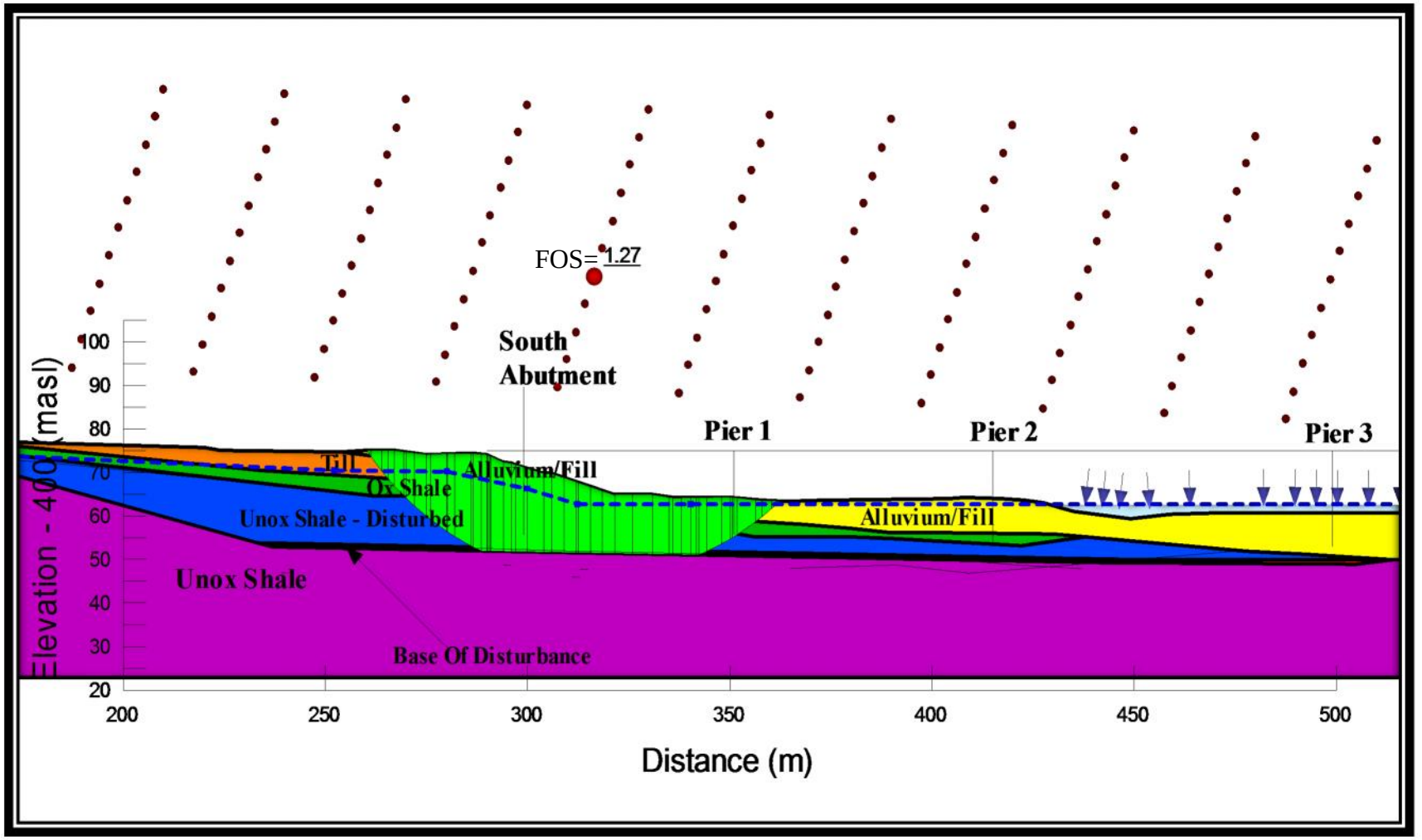

Figure 4.8: Old bridge analysis using back-analyzed properties - after the addition of a stabilizing berm

4.2.2.3 New Bridge

The new Bridge was analyzed using piezometric conditions from 2012 and the back analyzed soil strength parameters from Table 4.3. The site geometry was constructed using the section B-B' found in Figure 4.6. A 1-m-thick shear band of residual material strength was again added to the top of the undisturbed shale layer. It is understood that this was likely not the case at the time of construction, however, due to the movements observed in the site instrumentation, it provides an accurate estimation of current conditions.

The new bridge LE analysis can be found in Figure 4.9. The factor of safety of the slope using this method was found to be 1.33. It should be noted that, as seen in Table 4.1, the factor of safety of the south approach was higher after construction. This could be attributed to slightly different geometry and the changed location of the water table. The conditions at the time of construction will not be assessed in this work as they are considered outside the scope of this project.

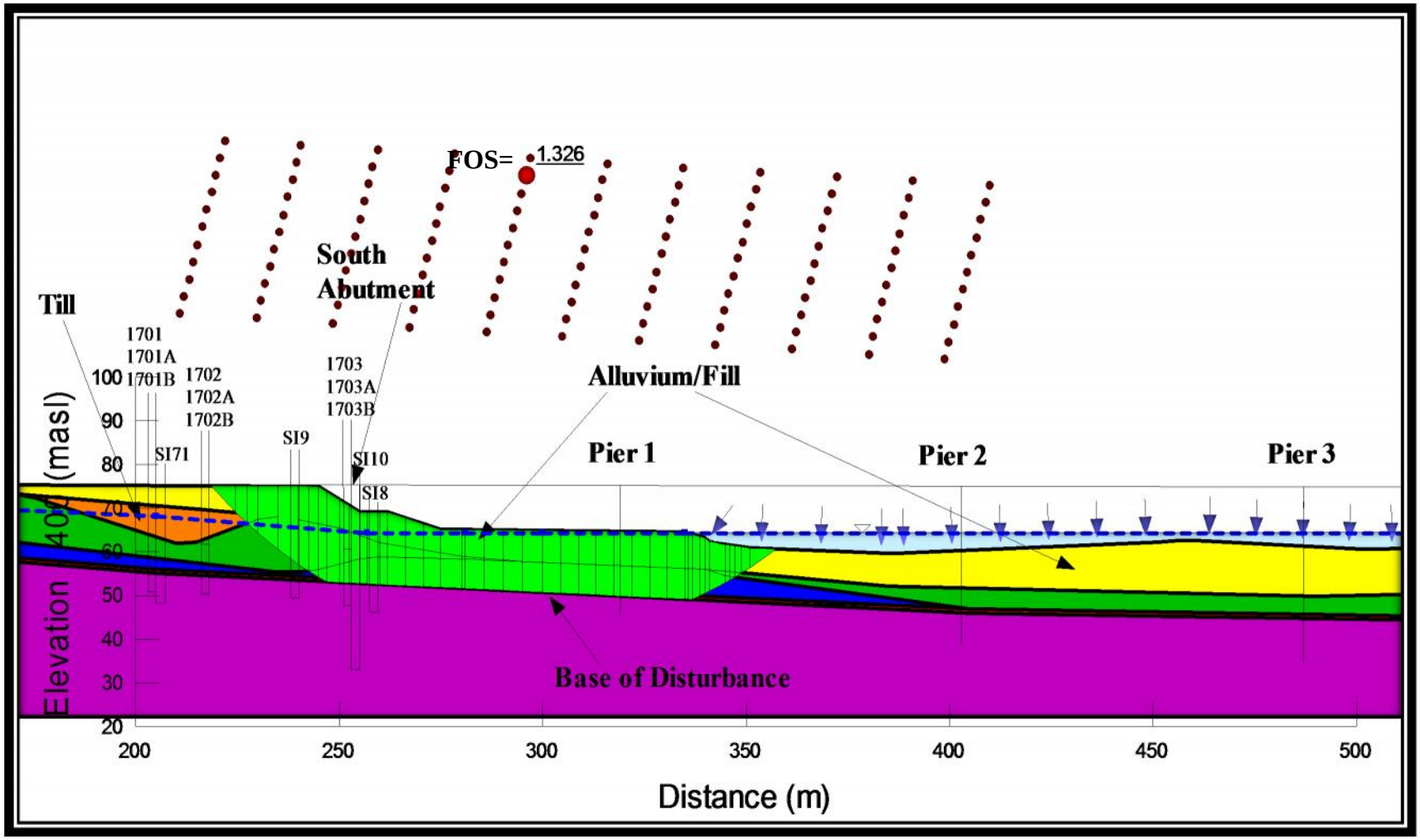

Figure 4.9: New bridge analysis using back analyzed properties and 2012 water table

4.3 Finite Element Analyses – New Bridge

Limit equilibrium analyses are unable to fully account for the behavior of this slope. The slope has a FOS that is greater than 1.00 but yet the slope exhibits monitored movement and deformation. As such, FE analyses will be used to help describe the behavior of the slope. The details of finite element analyses can be found in Section 2.3.2.

The ideal approach to this problem would be to complete a new field investigation with hopes of capturing undisturbed samples from the shear plane, and the disturbed and undisturbed shale layers. An additional field investigation would be quite costly and unnecessary, as the bridges have not shown any major serviceability issues since the failure in 1967. Also, a constraint of this thesis work was that no additional drilling could be completed; as such additional field borings and sampling were not a possibility.

It should be noted that, the geometric regions were simplified for the finite element analyses. This is to say that since the disturbed unoxidized shale and the disturbed oxidized shale were modeled with the same material properties, they were combined into one region called disturbed shale for the purposes of simplifying the finite element mesh. The small pocket of glacial till was also excluded from the finite element analyses and was modeled as alluvium/fill. The number of points in the analysis was reduced to the minimum while still maintaining the general cross-section geometry.

The FE models were discretized using a six-noded triangular mesh. The global mesh size was set to 5 m. Sensitivity analyses were completed using larger and smaller mesh with minimal variation in the results. In order to keep analysis times practical, the mesh size was kept at 5 m. The left and right boundaries were fixed in the x-direction. The bottom boundary was fixed in both the x and y-directions.

4.3.1 Soil Constitutive Model

The analyses were carried out using effective stress parameters in an elastic-plastic (EP) soil constitutive model. An EP model suffers from the generality that yield = failure. Other models such as the hyperbolic model presented by Duncan and Chang (1970) and Modified Cam Clay provide better non-linear stress-strain relationships. Due to the soil properties, and convergence issues faced with the hyperbolic model, they were excluded from this work.

4.3.2 Barometric Efficiency Testing

Ideally, barometric efficiency testing would be undertaken on the bridge site to develop values of the in-situ Young's Modulus; however, no vibrating wire (VW) piezometers have been installed on this site and due to public access to the site, it would not be safe to leave packer-testing equipment at any of the standpipe piezometer locations.

Alternatively, a series of three boreholes were completed with VW piezometers in the north valley wall, approximately 2.5 km west the bridge site, for a feasibility study of an overpass at the intersection of Poundmaker Trail and Highway 16. A summary of the VW completion depths is presented in Table 4.4. The sensors in BH101 were destroyed and could not be used in any analysis. Barometric efficiency testing was completed at the remaining boreholes. For the analysis, it was assumed that the properties of the Lea Park Formation would not vary considerably over that distance.

Table 4.4: Boreholes used in barometric efficiency analysis

Borehole No.	VW Tip Elevation (masl)	Soil Type at Tip
101	469.31	Till / Disturbed, Oxidized Shale Contact
101	440.86	Undisturbed, Unoxidized Shale
102	459.36	Sand / Undisturbed, Unoxidized Shale Contact
102	424.96	Undisturbed, Unoxidized Shale
103	495.1	Glacial Till
103	467.7	Undisturbed, Unoxidized Shale

Vibrating wire sensors and data loggers were manufactured by RST Instruments Inc. The vibrating wire sensors were Model # VW2100 and the data loggers were Model # DT2011B. A 5 m level logger was used to record the barometric pressure at the ground surface. Figure 4.10 presents photographs of the equipment used in the collection of data.

Figure 4.10: Photographs of the equipment used for barometric response testing

The data loggers recorded readings from the VW sensors at 15-minute intervals over the period of one month. Figure 4.11 shows the barometric efficiency data for Borehole 102 at a depth of 39.3 m. The effects of barometric loading were best minimized by applying a loading efficiency (B) of 0.9. Figure 4.12 is a second visualization of the data, plotting the change in barometric pressure with its corresponding change in pore pressure to estimate the trend in the data. The slope of the linear best-fit line is the B value. The trend in the data shows the slope to be approximately 0.95; however, by visual inspection the 0.95 slope is slightly steep and 0.9 was used.

Knowing the in-situ value of B, Equations [2.2] – [2.9] were used to estimate the value of the small strain, in-situ value of Young's Modulus of 450,000 kPa. A Poisson's ratio of 0.334 was used for this research.

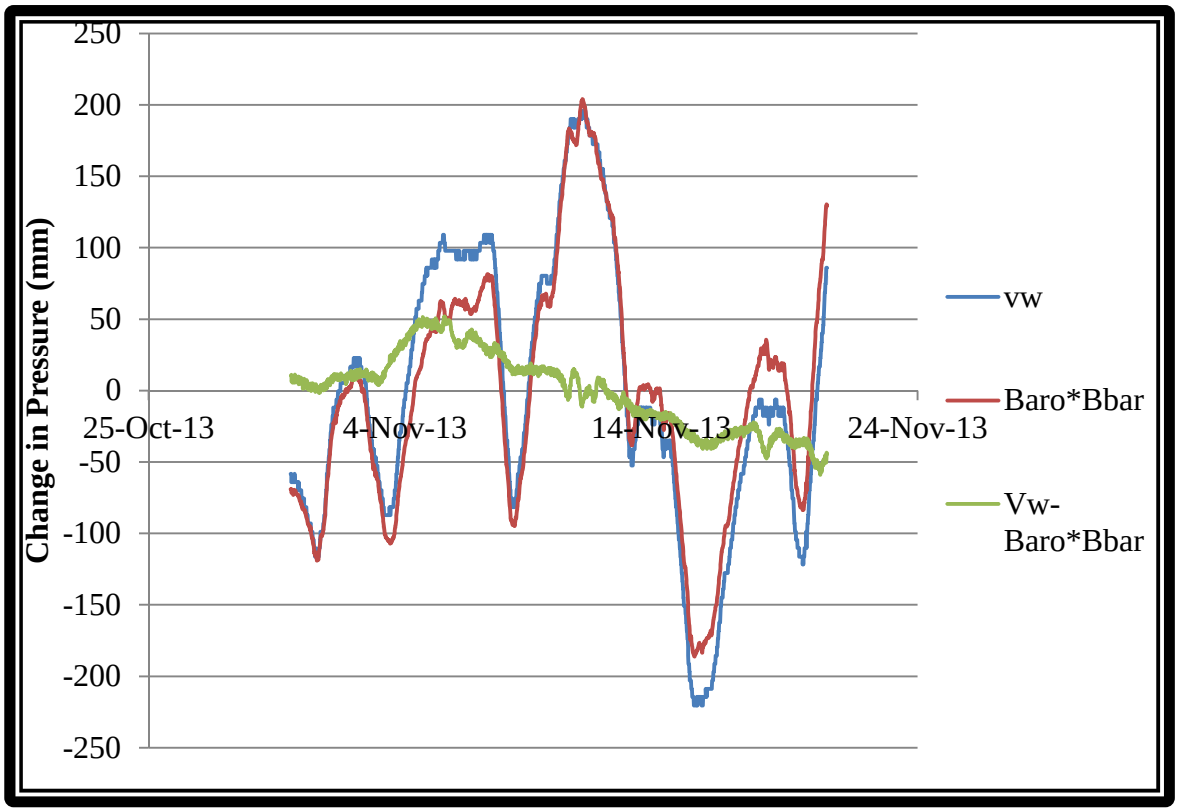

Figure 4.11: Barometric efficiency - BH102 @39.31m

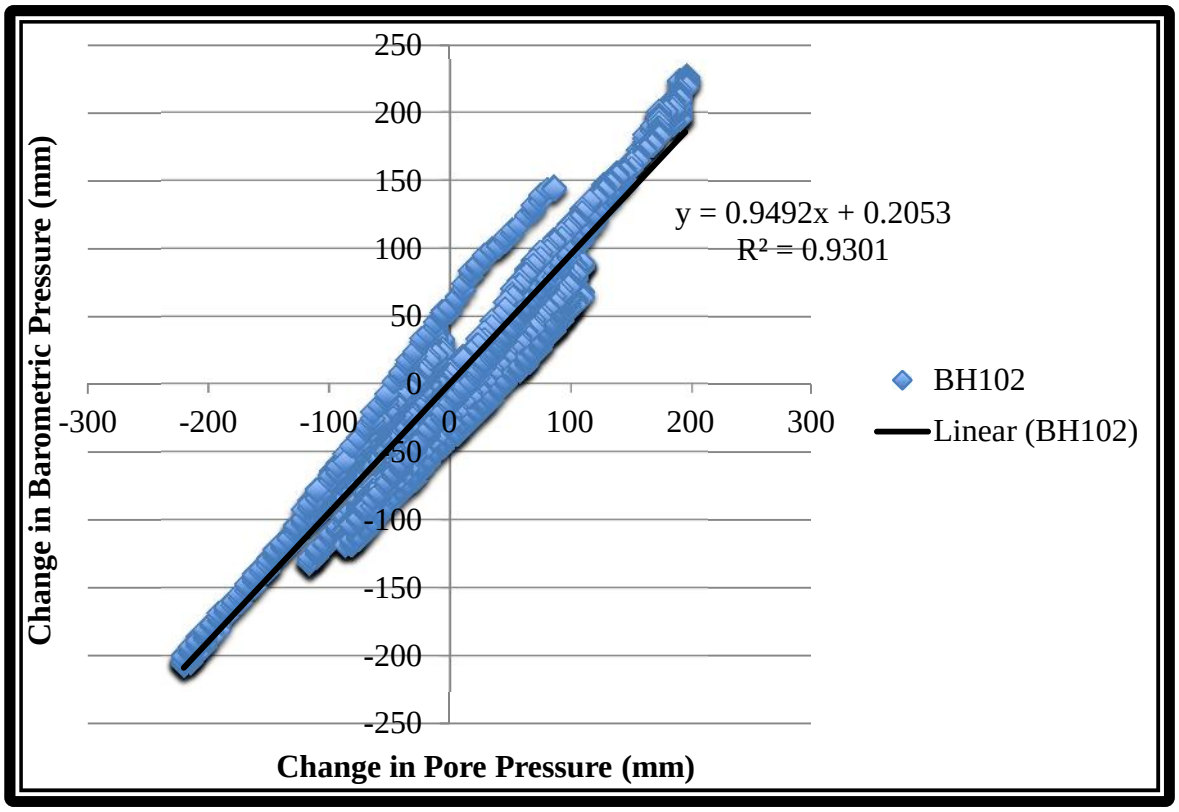

Figure 4.12: Change in barometric pressure vs. change in pore pressure – BH102 @ 39.31m

Smith et al. (2013) conducted a series of $\overline{B}$ tests on Pierre shale at varying depths. With a series of vibrating wire piezometers, they were able to determine the formation's pore pressure response to barometric loading. That is, how the formation responded to barometric highs and lows over a period of time. The values of E' for Pierre shale at 25 m and 49 m depth were 455,000 kPa and 417,000 kPa respectively.

Whitaker et al. (1987) states that there is remarkable similarity between the Pierre shale and the Lea Park shale Formations. Shultz (1978) states that the mineralogical composition of the Lea Park shale is very similar to that of the Pierre shale.

Analyses were completed with a Young's modulus value of 450,000 kPa for the Lea Park clay shale.

4.3.3 In-situ Stresses

The first stage of the FE modeling associated with this thesis work involved establishing a realistic profile of in-situ stresses. Initially, an unrealistic distribution of in-situ effective stresses was produced when complex slope geometry was used; therefore, a simplification was required. SIGMA/W is reliable when creating a realistic stress distribution on a horizontal ground surface. With this in mind, the following steps were taken:

- Start with a horizontal ground surface and establish in-situ stresses for that geometry;
- Using multiple load steps, simulate the erosion of the valley by removing material in each step to create the slope, and;
- Apply the weight of water to simulate the North Saskatchewan River.

Regional topographic maps were used to select the elevation of the ground surface before the valley was eroded. This elevation was chosen to be 490 masl and was used as the horizontal surface elevation for the in-situ analysis. The starting point for this analysis can be found in Figure 4.13.

The next step was to simulate the erosion of the valley using multiple load steps as to maintain the distribution of effective stresses. The valley was eroded in six load steps using a load-deformation type of analysis. It is of great importance to make changes to the value of Poisson's ratio at this stage. The Poisson's ratio was reduced to 0.15 for the valley erosion process (C. Kelln, personal communication, March 8, 2013). This value is quite low and requires explanation. As the valley is eroded, the goal is to effectively "lock in" the stresses in the slope. With each unloading, more of the slope is exposed and it naturally wants to expand laterally.

Setting the Poisson's ratio to a low value limits the soils lateral expansion with the changes in vertical stress. Once the stresses are established, the Poisson's ratio can be returned to a more conventional value for the remainder of the analyses.

At the end of the analyses, the weight of water was added to simulate the North Saskatchewan River. The final stage of this process can be found in Figure 4.14. After eroding the valley, all cumulative values and displacements were ignored and this was considered a starting point for the bridge. The in-situ vertical and horizontal effective stress contours, after the valley erosion, can be found in Figure 4.15 and Figure 4.16 respectively. The values in the figures are not important for the purposes of this report; however, it is important to how the distribution of stresses follows the slope and does not stay horizontal as would be expected with such geometry.

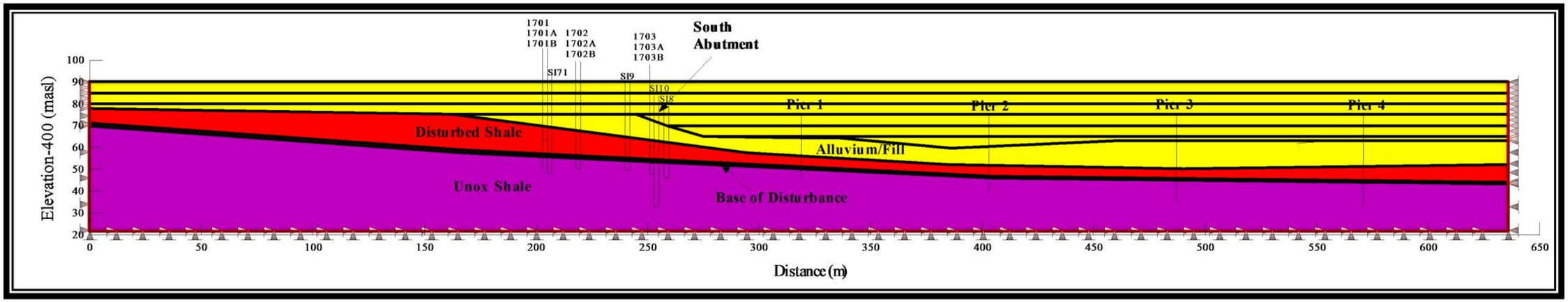

Figure 4.13: New bridge in-situ stresses – horizontal surface for gravity turn-on

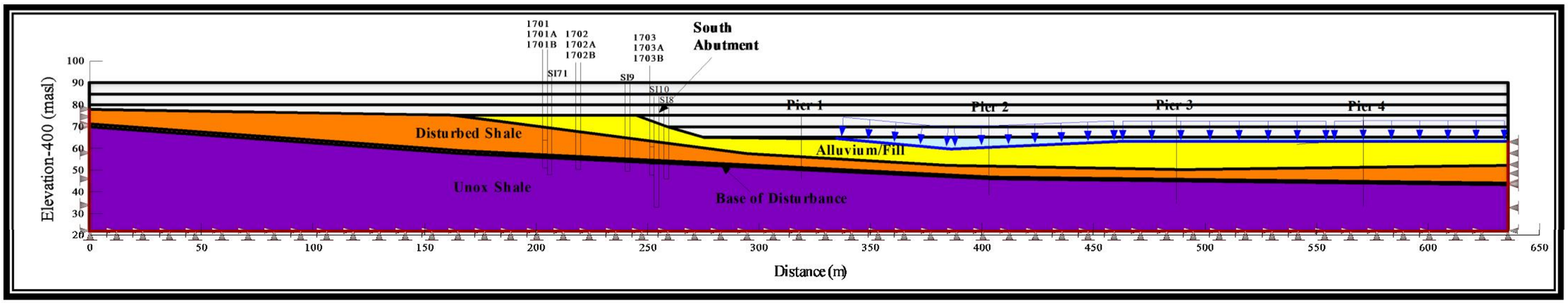

Figure 4.14: New bridge in-situ stresses - after valley erosion and application of water load

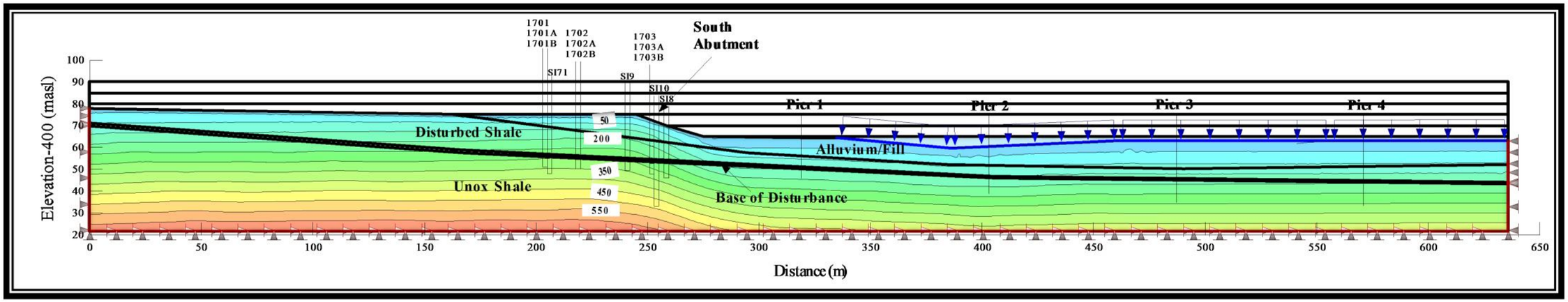

Figure 4.15: New bridge in-situ stresses - contours of vertical effective stress

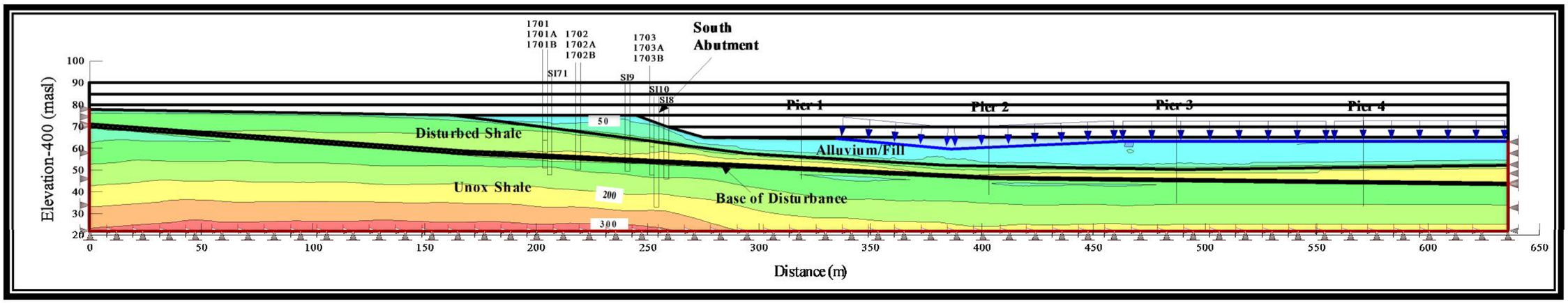

Figure 4.16: New bridge in-situ stresses - contours of horizontal effective stress

4.3.4 Shear Strength Reduction for SI Calibration and Correlation

Since the time of bridge construction, there have been observed movements in the instrumentation at the south abutment. Strength reduction analysis was completed in attempt to match the observed displacements with a model. The three strength reduction scenarios that were analyzed were:

- One material;
- Reduced shear plane (RSP), and;
- Residual shear plane with reduced disturbed shale (RP-RS).

The "one material" scenario considered the disturbed shale as one material without the presence of a 1-m-thick residual strength layer along the shear plane. The strength was reduced evenly throughout the disturbed shale layer.

The "reduced shear plane" scenario considered shear plane starting at the same strength as the disturbed shale above it. The strength was reduced only along the shear plane to simulate the failure propagating through the zones of preferential weakness within the shale.

The "residual shear plane with reduced disturbed shale" scenario considered the presence of a residual strength shear plane from the start. The strength of the disturbed shale was reduced to simulate the failure propagation through that layer.

Strength reduction factors were selected in intervals of 0.2, starting at 1.0 and increasing to 2.2. Reduction factors were applied to the disturbed shale only. The reduced material properties for the disturbed shale can be found in Table 4.5. Each shear strength reduction was modeled as a stress redistribution type of analysis.

Table 4.5: Reduced material properties for disturbed shale

Reduction Factor	ϕ’	c'
1	16.00	8.00
1.2	13.33	6.67
1.4	11.43	5.71
1.6	10.00	5.00
1.8	8.89	4.44
2	8.00	4.00
2.2	7.27	3.64

The “residual shear plane with reduced disturbed shale” (RP-RS) scenario is hypothesized to be the most realistic for this site. From the previous movement in SI71, it is likely that the shear plane had developed near the new bridge. Also, since the failure surface will eventually propagate to surface, the RSP scenario is less realistic. It considers only reducing the strength in shear plane. The one material case is the least realistic of the three scenarios.

Reduction factors were applied to each of the scenarios. In each analysis, the mechanism of failure was verified. Figure 4.17 shows contours of x and y displacement after a strength reduction of 2.2 for the RP-RS scenario. When this figure is compared to Figure 4.9 it can be seen that the mechanism and extents of the failure are similar. Small differences in the extents of the failure can be attributed to the simplified geometry used in the FE analyses.

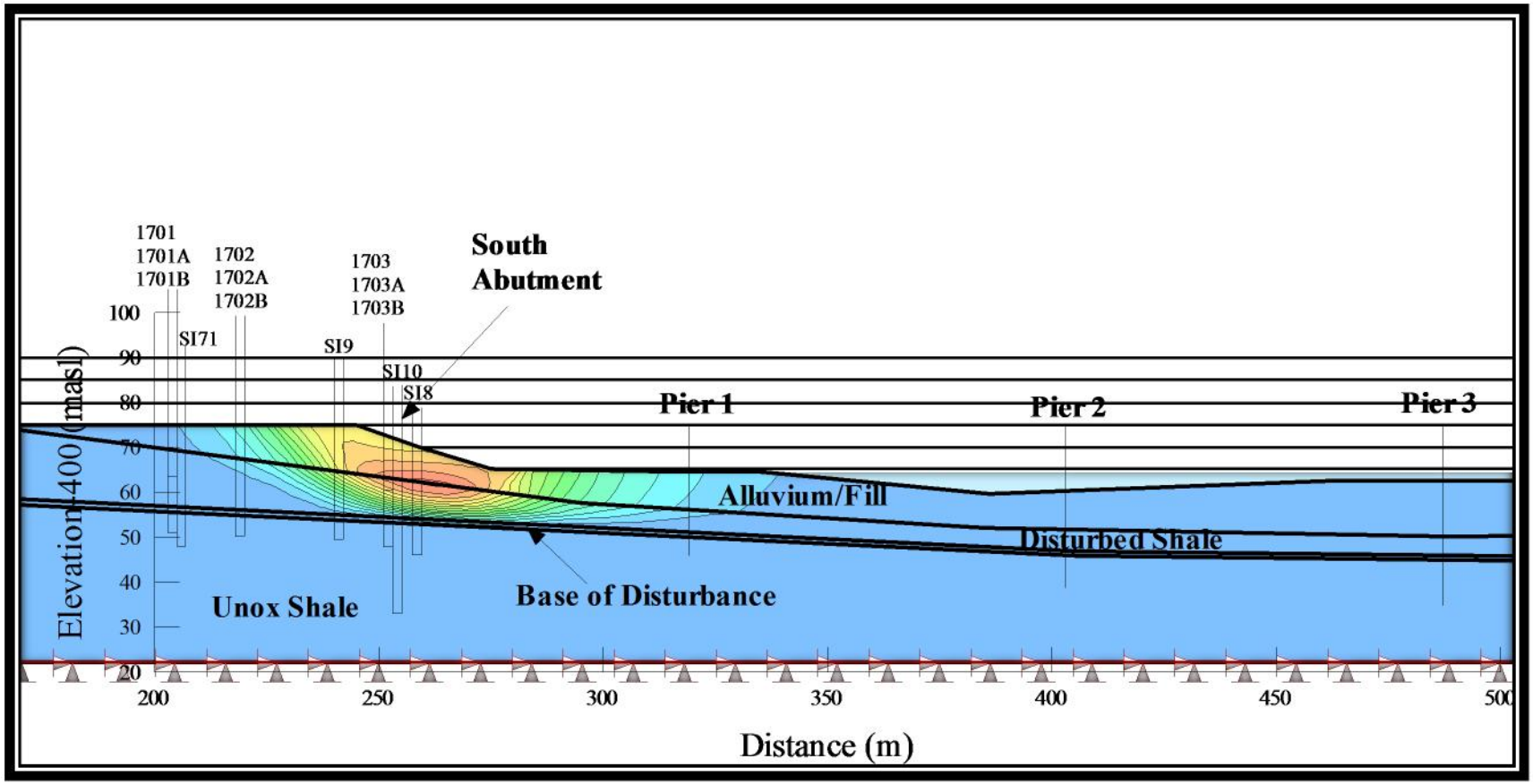

Figure 4.17: Contours of X and Y displacement - SR=2.2, RP-RS scenario, E'=450,000 kPa

Once the failure mechanism was confirmed to be realistic, SI10, and SI8 were added to the model in their approximate locations. SI 9 and SI71 are also in close proximity to the cross-section however, SI9 was destroyed during construction of the bridge and was not monitored and SI71 proved to be too far from the cross-section of the bridge to be of use for this work. As such, the monitoring data from SI10 and SI8 were used for calibration. SI10 was deemed to be nearest to the cross-section and it was therefore most important to match displacements to SI10.

Table 4.6 shows the SI response to the strength reduction analyses. From this data, the reduction factor that provided the closest displacement to those observed in the field (highlighted in bright green) was considered "critical" and was selected for further analysis.

Simulated SI plots were created for each of the "critical" analyses. Plots for RP-RS can be found in Figure 4.18 and Figure 4.19. From these plots, it becomes clear that the "one material" scenario does not create the correct SI response and that both the RP-RS and RSP scenarios are quite similar. Both of the aforementioned scenarios show the majority of their displacement along the defined slip surface and create a plausible SI response.

Table 4.6: Maximum horizontal displacement for strength reduction analyses

			1 material scenario		RSP scenario		RP-RS scenario	
Reduction Factor	**ϕ'**	**c'**	**SI8 (m)**	**SI10 (m)**	**SI8 (m)**	**SI10 (m)**	**SI8 (m)**	**SI10 (m)**
1	16.00	8.00	-2.73E-07	-2.70E-07	-5.47E-11	-3.64E-10	2.43E-04	2.14E-04
1.2	13.33	6.67	3.61E-04	2.77E-04	1.63E-05	1.40E-05	9.32E-04	7.71E-04
1.4	11.43	5.71	1.34E-03	9.77E-04	7.80E-05	7.32E-05	1.93E-03	1.55E-03
1.5	10.67	5.33	3.42E-03	2.73E-03	2.19E-04	2.04E-04	4.18E-03	3.46E-03
1.6	10.00	5.00	7.01E-03	6.03E-03	8.48E-04	7.00E-04	7.53E-03	6.52E-03
1.8	8.89	4.44	1.29E-02	1.16E-02	1.82E-03	1.57E-03	1.29E-02	1.16E-02
2	8.00	4.00	2.15E-02	1.99E-02	2.72E-03	2.42E-03	2.08E-02	1.92E-02
2.2	7.27	3.64	3.18E-02	3.01E-02	3.53E-03	3.21E-03	3.01E-02	2.83E-02

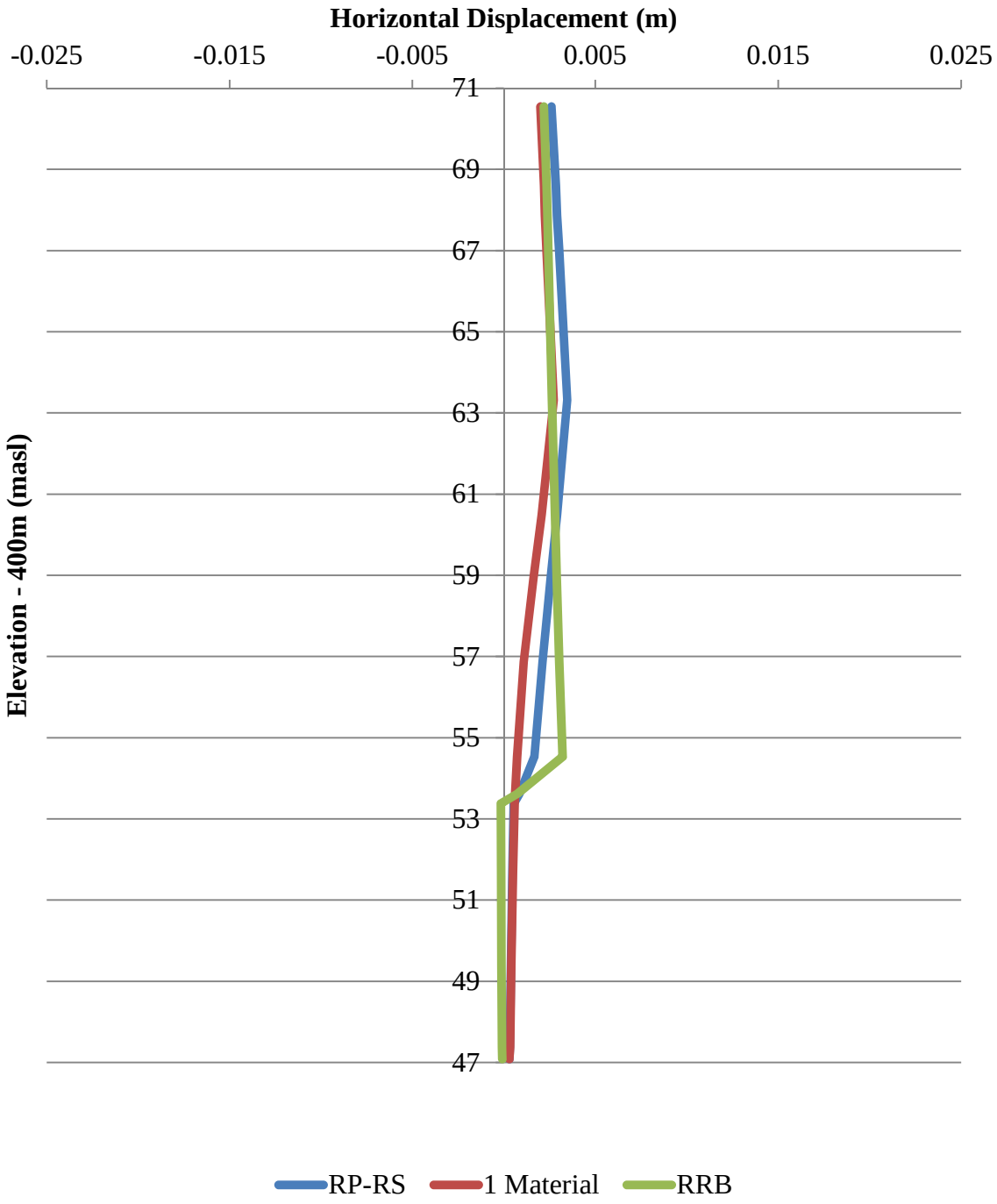

Figure 4.18: Simulated horizontal displacement - SI10

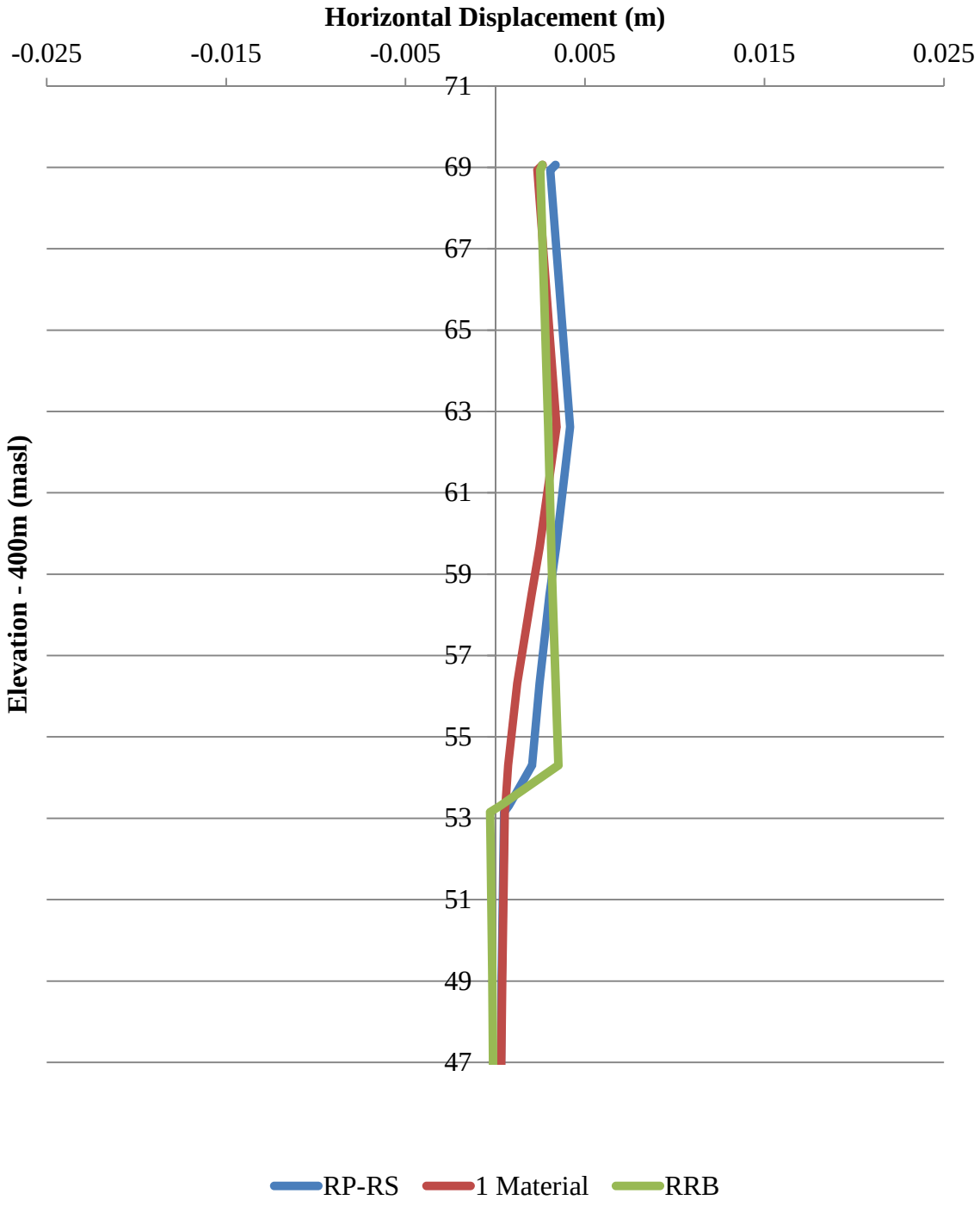

Figure 4.19: Simulated horizontal displacement - SI8

As the shear strength of the soil degrades (reduction factor increases) the displacement rate vs. reduction factor increases non-linearly as shown in Figure 4.20. Fitting a third order polynomial equation to this data gives R^2=0.999. This relationship would be important if your cross-sections were directly through the SI locations. Owners could use this relationship to show how the shear strength in the soil has degraded with observed SI movements. It is not recommended that this be the only tool used to make decisions, however it could be very useful in setting triggers for further analyses and additional monitoring. A new relationship would need to be developed for each site-specific analysis.

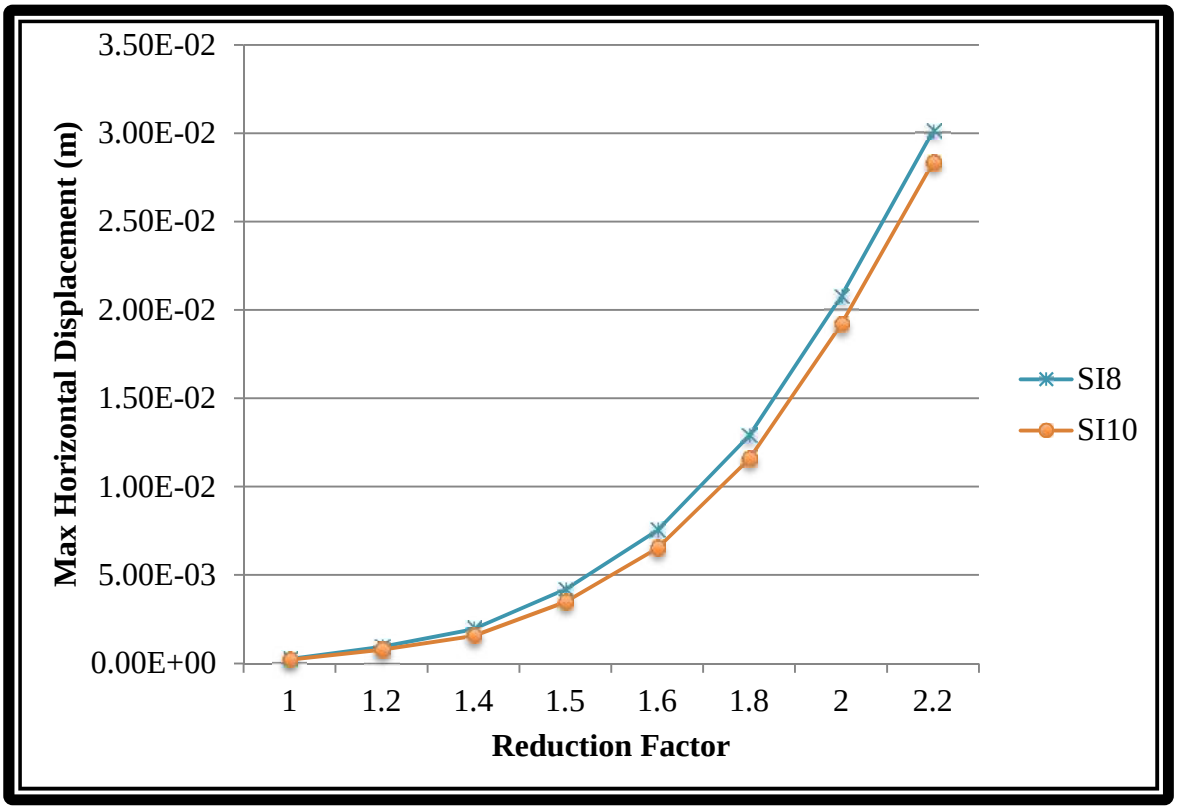

Figure 4.20: Maximum horizontal displacement vs. reduction factor for the RP-RS scenario

4.3.5 Mobilized Strength Design

After simulating SI responses that are similar to those observed in the field, the next phase of this work involves incorporation of this data into the Mobilized Strength Design framework to analyze how much shear strength is being mobilized at the slip surface. MSD framework is explained in Section 2.6. The equation for mobilization factor (M) can be found in Equation [2.8].

Since the critical slip surface is a composite slip surface, σ'_v was calculated for a point along the flat portion slip plane. For this work, P'_o was found to be approximately 310 kPa.

From equation [2.10] and the database of laboratory testing for this site, values of $\gamma_{M=2}$ were found to range between approximately 2% and 0.7%. This is a large range and as such, values of mobilized strength were calculated for the upper and lower bounds.

The results of the MSD analysis can be found in Table 4.7. The difference between the min and max percent of shear strength mobilized (1/M) was 5% to 13%. This range could be significantly reduced with even one triaxial test. The "one material" scenario results were ignored because the mechanism of failure is not realistic.

Table 4.7: Mobilized shear strength - E'=450,000 kPa

Analysis	SI	SR	γ@ Shear Plane	1/M (min)	1/M (max)	M (min)	M (max)
RP-RS	10	1.5	7.83E-04	12.63%	6.68%	7.92	14.97
RP-RS	8	1.5	1.06E-03	15.12%	7.99%	6.61	12.51
RSP	10	2.2	2.59E-03	25.91%	13.70%	3.86	7.30
RSP	8	2.2	2.53E-03	25.52%	13.49%	3.92	7.41

From the results shown in the table above, it can be seen that, for the most realistic (RP-RS) scenario the mobilized shear strength in the south abutment at the Battlefords bridges ranges from approximately 7 % - 15 % for E`=450,000 kPa.

4.3.6 Comparison to Limit Equilibrium

As is common to most fields of practice, when a new method or framework is presented, it must be presented with a comparison to the status quo, which in the field of slope stability, is limit equilibrium analysis. The comparisons made in this section will compare the current FOS at the Battlefords bridges using standard LE analyses, LE analyses with FE stresses and MSD. Table 4.8 presents the results of this comparison.

The results in the Table 4.8 show that the FOS for the RP-RS scenario had a value between 1.21-1.32. These findings in the table agree with hypothesis made by CAL stating that the FOS for slowly moving slopes should be around 1.2 (Clifton et al., 1999). A significant finding in this research is that the FOS of the slope in all analyses remained greater than 1 but the slope shows significant displacement. Without further case studies, no significant correlations can be made between FOS and M.

It may also be noted that the LE analyses had a higher FOS than the LE with FE stresses. For most cases this was due to the fact that the critical slip surface in the LE analysis was circular (Figure 4.21) and the slip surface in the LE with FE stresses was more composite in nature (Figure 4.22). The failure is believed to be a composite failure and as such, the LE with FE stresses is believed to be a more realistic analysis.

Table 4.8: MSD and FOS comparison - E'=450,000

	Mobilized Strength Design		Factor of Safety	
Method	**1/M (SI10)**	**M (SI10)**	**LE**	**LE with FE Stresses**
RP- RS	7%-13%	8-15	1.322	1.211
RSP	14%-26%	4-7	1.448	1.335
One Material	4%-7%	14-26	1.322	1.2

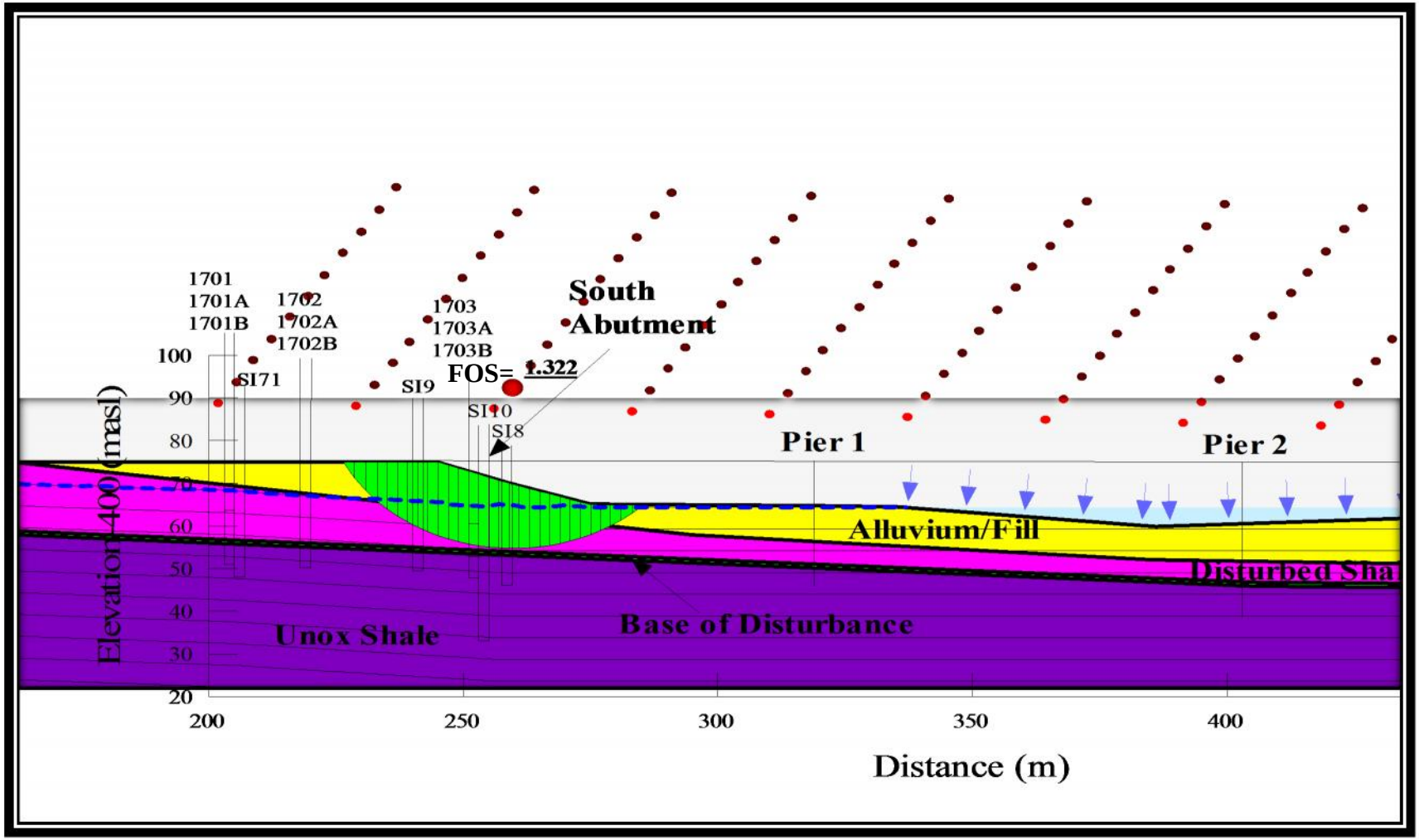

Figure 4.21: LE analysis of New Bridge - SR=1.5 - Circular failure

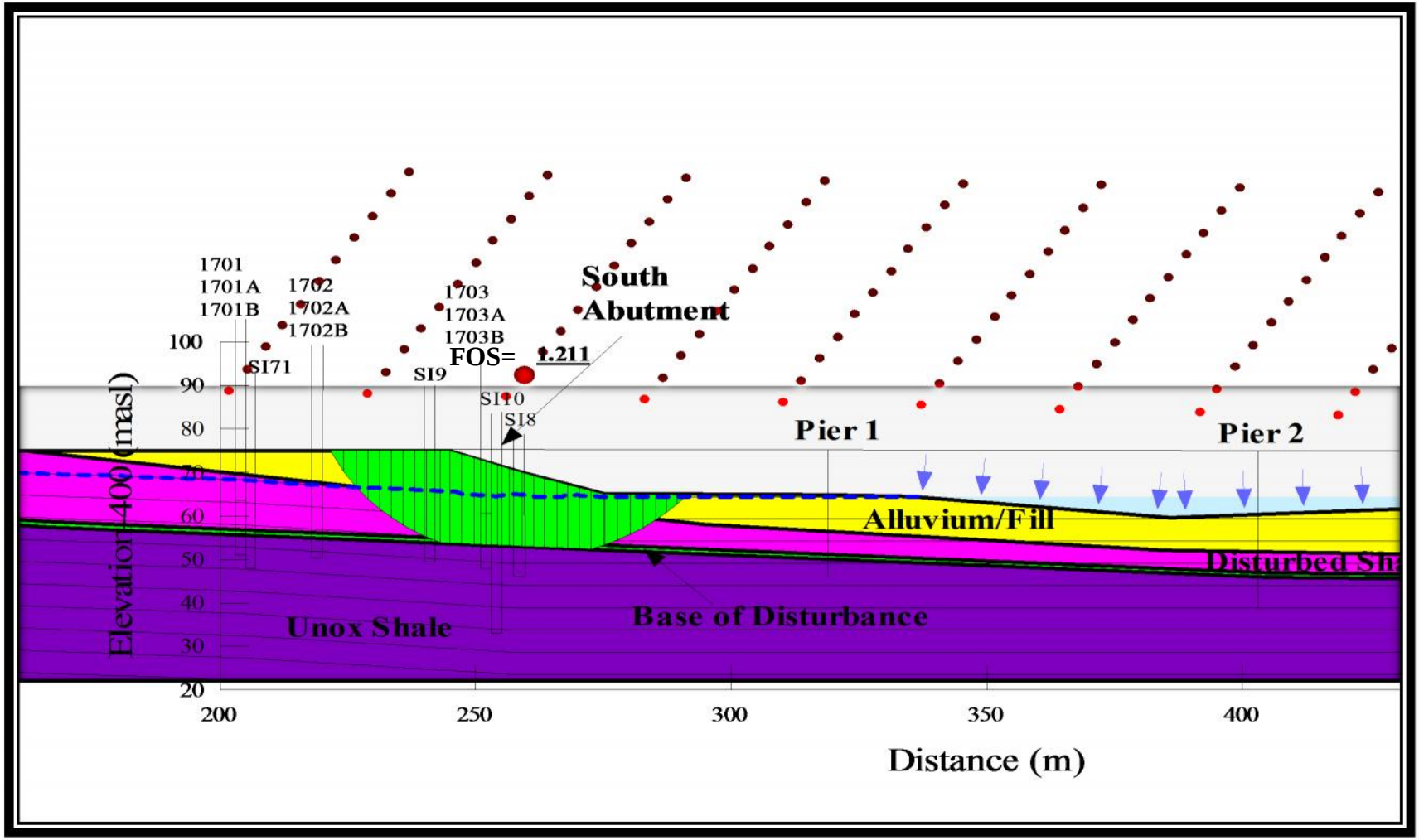

Figure 4.22: LE with FE stresses - SR=1.5 - Composite failure

4.4 Modeling Framework

To this point, Chapter 4 presented the modeling completed during this thesis work with the aim of developing a new framework for analysis of structures constructed on low factor of safety slopes. This framework for this analysis will be presented in point form for simplicity and practicality. The following 10 steps can be followed to complete an analysis within this framework:

1. Gather ALL existing field investigation data, survey data and previous reports related to the slope of interest. Synthesize site investigation data and monitoring data so that only relevant data is remaining. Develop an understanding of the failure type (circular, composite, etc.), mechanism and extents, if possible, by using the instrumentation plots and trends.
2. Determine the critical cross-section of the failure by the direction of movement and slope geometry. It would be most useful to have the cross-section directly through at least two SIs if possible.
3. Develop a limit equilibrium analysis to confirm and back analyze the strength parameters of the soil and confirm the initial FOS.
4. Gather triaxial test data to determine Young's modulus and find $\gamma_{M=2}$ for the materials in the model.
    - If no triaxial tests have been completed, make arrangements to gather additional samples for triaxial testing.
    - If additional sampling is not possible, follow the method set out by Vardanega and Bolton (2011) by using Equation [2.10]. Gather values of Young's modulus

from the literature or by following the methods set out by Anochikwa et al. (2012) and Smith et al. (2013) using pore pressure response to barometric loading.

5. Import the geometry from the LE analysis into a FE environment. Establish the in-situ stresses for the geometry being used. It is important to keep the geometry simple in this stage. Depending on the complexity of the slope, it may be necessary to start with a horizontal ground surface and "excavate" or "erode" the slope geometry in multiple load steps.
6. Apply the material properties needed to complete strength reduction analyses (SR=1.0 to SR-2.0). It is suggested to start with intervals of 0.2. Each strength reduction must be a child analysis of the previous.
7. Run the analysis for the correct mechanism (ie. one of the three scenarios used in this research – RSP, RP-RS or One Material).
8. Plot the SI's x-displacements in the FE program. Export the peak displacement vs. SR data to excel and plot the data to get a plot similar to that found in Figure 4.20.
9. Figure out the reduction factor required to match the field observed SI displacements and create an analysis with those material properties.
10. Extract the value of max shear strain at the slip surface, for the relevant SIs, from the FE program. Apply this value to Equation [2.2] to assess the percentage of shear strength that is being mobilized.

Chapter 5 Conclusion and Recommendations

5.1 Conclusions

The work completed for this thesis presents the development of a framework for analyzing the stability of low FOS slopes. This method is unique in that it allows for the analysis of the current state of the slope, without further field investigation, instead of just the safe/fail guidelines from traditional LE analysis. The importance of the observational method is evident throughout this process. Observations made in the field can be used to assess the current state of a slope and perhaps used to set serviceability triggers based on measured rates of movement.

Perhaps the most important key to this method is the initial field investigation. Triaxial testing must be completed in order to apply the MSD framework with minimal error. Bolton and Vardanega (2011) have presented a database of more than 100 triaxial tests on clay samples. This database can be used as a guideline, and added to, as new results are available.

The current state of practice in slope stability analyses is limit equilibrium analyses. Finite element analyses are more data intensive and are commonly ignored by most practicing engineers, mostly because they are unnecessary for the majority of slope stability analyses. The method presented at the end of Chapter 4 aims to simplify a seemingly complex problem for use in everyday practice. Even with minimal data, estimates of the state of a slope can be made as long as knowledge of the relative error is understood.

The Battlefords Bridges provides a case study site for calibration the proposed framework. Previous investigations completed by CAL and SMHI provided a solid understanding of the

failure mechanism and significant laboratory testing results. Triaxial tests were not available so estimations of the mobilized shear strength were made with the understanding of the accepted error. A range of M and 1/M values were presented in Chapter 4. This range could be narrowed significantly with even one trixial test. At this time, no correlation between M, 1/M and FOS could be made as only one case study site was completed.

5.2 Recommendations for further Research

The case study of the Battlefords Bridges is not unique in the Prairie Provinces. Many sites share similar geology and have similar problems with slope stability. The following are recommendations for further research to be completed in this area:

- Complete this analysis at more sites throughout the Prairie Provinces;
- Draw correlations between mobilized shear strength and FOS. This would lead to mobilized shear strength and FOS estimates using shear strain from SI observations;
- Complete triaxial testing of Late Cretaceous clay shales and add the results to the database created by Vardanega and Bolton (2011) (A portion of this database is attached in Appendix B);
- Analyze the impacts of pore water pressure generated from deformation of the soil structure using a effective stress with pore water pressure constitutive model (coupled analysis), and;
- Complete the FE analysis based on the results of a transient seepage analysis to assess the effects of pore pressure over time;

Works Cited

Abramson, L. W., Lee, T.S., Sharma, S., and Boyce, G.M. 2002. *Slope stability and stabilization methods.* Second Edition. New York: John Wiley & Sons Inc.

Anochikwa, C.I., van der Kamp, G and Barbour, S.L. 2012. Interpreting Pore-water Pressure Changes Induced by Water Table Fluctuations and Mechanical Loading Due to Soil Moisture Changes. *Canadian Geotechnical Journal*, 49(3), 357–366.

Bowles, J.E. 1997. *Foundation Analysis and Design.* Fifth Edition. New York: McGraw-Hill Companies Inc.

British Standards Institution. 1994. *Code of practice for earth retaining structures BS8002:1994*. London: British Standards Institution.

Christiansen, E. A. 1979. The Wisconsinan deglaciation of southern Saskatchewan and adjacent areas. *Canadian Journal of Earth Sciences*, 16(4), 913–938.

Christiansen, E. A. 1983. The Denholm landslide, Saskatchewan. Part I: Geology. *Canadian Geotechnical Journal*, 20(2), 197–207.

Christiansen, E. 1992. Pleistocene stratigraphy of the Saskatoon area, Saskatchewan, Canada: an update. *Canadian Journal of Earth Sciences*, 29(8), 1767–1778.

Christiansen, E. A., and Sauer, E. K. 2001. Stratigraphy and structure of a Late Wisconsinan salt collapse in the Saskatoon Low, south of Saskatoon, Saskatchewan, Canada: an update. *Canadian Journal of Earth Sciences*, 38(11), 1601–1613.

Clifton, A. W. and Kelly, A. J. 2001. *Regional Geology - Battlefords Bridge.* Geotechnical Engineering. Regina: Clifton Associates Ltd.

Clifton, A. W., Kelly, A. J., and Laboissiere, J. L. 1999. *Complilation and Preliminary Geotechnical Analysis - Battlefords Bridge.* Geotechnical Engineering. Regina: Clifton Associates Ltd.

Duncan, J.M. and Chang, C.Y. 1970, Nonlinear analysis of stress and strain in soil. *Journal of soil Mechanics and Foundations.* Div ASCE96, 1629-1653

Environment Canada. 1995, June 20. *The Ecological Framework of Canada*. Retrieved October 1, 2012, from Ecozone and Ecoregion Descriptions: http://ecozones.ca/english/zone/index.html

Government of Canada. 2012, May 29. *Weather Office*. Retrieved October 1, 2012, from National Climate Data and Information Archive: http://www.climate.weatheroffice.gc.ca/climate_normals/results_e.html?stnID=3244&lang=e&dCode=1&province=SASK&provBut=Search&month1=0&month2=12

Griffiths. D. V. and Lane, P.A. 1999. Slope stability analysis by finite elements. *Géotechnique,* 49(3), 387 - 403.

Hammah, R., Yacoub, T., Corkum, B., and Curran, J. 1999. A Comparison of Finite Element Slope Stability Analysis with Conventional Limit-Equilibrium Investigation. Unknown.

Kelly, A.J., Sauer, E.K., Barbour, S.L., Christiansen, E.A., and Widger, R.A. 1995. Deformation of the Deer Creek Bridge by an Active Landslide in Clay Shale. *Canadian Geotechnical Journal*, 32(4), 701–724.

Krahn, J. 2003. The 2001 R.M. Hardy Lecture: The limits of limit equilibrium analyses. *Canadian Geotechnical Journal*, 40(3), 643–660.

Krahn, J., and Barbour, S.L. 2004 Numerical Modelling – Prediction or Process? *Geotechnical News.* Richmond: Canadian Geotechnical Society.

Mollard, J.D. 1975. *Office airphoto study of slope stability in the Battlefords area.* J D Mollard and Associates Limited.

Merriam-Webster, I. 2005. *The Merriam-Webster dictionary.* Springfield, Mass.: Merriam-Webster.

Natural Resources Canada. 1974. Map. Atlas of Canada 4th edition, Sheet no 5-6, Physiographic Regions. Scale 1:15M.

Peck, R. B. 1969. Advantages and Limitations of the Observational Method In Applied Soil Mechanics. *Geotechnique*, *19*(2), 171–187.

Powderham, A. J. 1994. An overview of the observational method: development in cut and cover and bored tunnelling projects. *Géotechnique*, *44*(4), 619–636.

Powderham, A. J. 2002. The observational method—learning from projects. *Proceedings of the ICE - Geotechnical Engineering*, 155(1), 59–69.

RocScience. 2004. A New Era in Slope Stability Analysis: Shear Strength Reduction Finite Element Technique. *RocNews*, 1-10.

Sauer, E. K. 1983. The Denholm landslide, Saskatchewan Part II: analysis. *Canadian Geotechnical Journal*, *20*(2), 208–220.

Sauer, E. K. 1984. A landslide in clay shale in the North Saskatchewan River valley, canada. *Engineering Geology*, *20*(4), 279–300.

Shultz, L.G, 1978. Mixed-layer clay in the Pierre Shale and equivalent rocks, northern Great Plains region. United States Geological Survey, Professional Paper 1064-A

Skempton, A.W. 1955. Pore-Pressure Coefficients A and B. Géotechnique, 4(4): 143–147.

Smith, L.A., van der Kamp G., and Hendry M.J. 2013. A New Technique for Obtaining High-resolution Pore Pressure Records in Thick Claystone Aquitards and Its Use to Determine in Situ Compressibility. *Water Resources Research*, 49, 1-12.

Stauffer, M. R., Gendzwill, D. J., and Sauer, E. K. 1990. Ice-thrust features and the Maymont landslide in the North Saskatchewan River valley. *Canadian Journal of Earth Sciences*, *27*(2), 229–242.

Take, W. A. and Bolton, M. D. 2011. Seasonal ratcheting and softening in clay slopes, leading to first-time failure. *Géotechnique*, 61(9), 757–769.

Terzaghi, K., Peck, R. B., and Mesri, G. 1996. *Soil mechanics in engineering practice*. New York: Wiley.

van der Kamp, G. and Gale, J.E. 1983. Theory of Earth Tide and Barometric Effects in Porous Formations with Compressible Grains. *Water Resources Research*, 19(2), 538-544.

Vardanega, P. J., and Bolton, M. D. 2011. Strength mobilization in clays and silts. *Canadian Geotechnical Journal*, 48(10), 1485–1503.

Whittaker, S.G., Kyser, T.K., and Caldwell, W.G.E., 1988. Lithic geochemistry of the Claggett marine cyclothem in south-central Saskatchewan. *Canadian Journal of Earth Sciences* 25, 1554-1563.

Appendix A – Historical SI Plots

SI1/71

SI1 is located at the South abutment and between the two bridges. It was installed in January 1968. In 1985 the borehole was renamed SI71 with SMHI's switch to the metric system. Available monitoring data begins in July 1972.

Between July 1972 and August 1985, movement of 18.1 mm was observed in the A-axis and movement of -2.9 mm was observed in the B-axis. This movement shows that the primary direction of movement is towards the North and with a slight motion to the West. The average rate of movement over this time period was approximately 1 mm/yr. (Clifton et al., 1999).

Between August 1985 and March 1998 movement appeared to slow down with 9 mm of movement was observed in the A-axis and erratic in the B-axis. For this time period, the average rate of movement was observed to be 0.75 mm/yr. (Clifton et al., 1999)

Between December 2000 and April 2012 movement appeared to slow down even more with 4.9 mm of movement in the A-axis. The B-axis showed movement of 1.4 mm, which is likely, erroneous. For this time period, the average displacement was approximately 0.4 mm/yr. Movement in this inclinometer is taking place at an elevation of 455.8 m above sea level (masl). According to the borehole logs provided by SMHI, the movement is in the unoxidized shale.

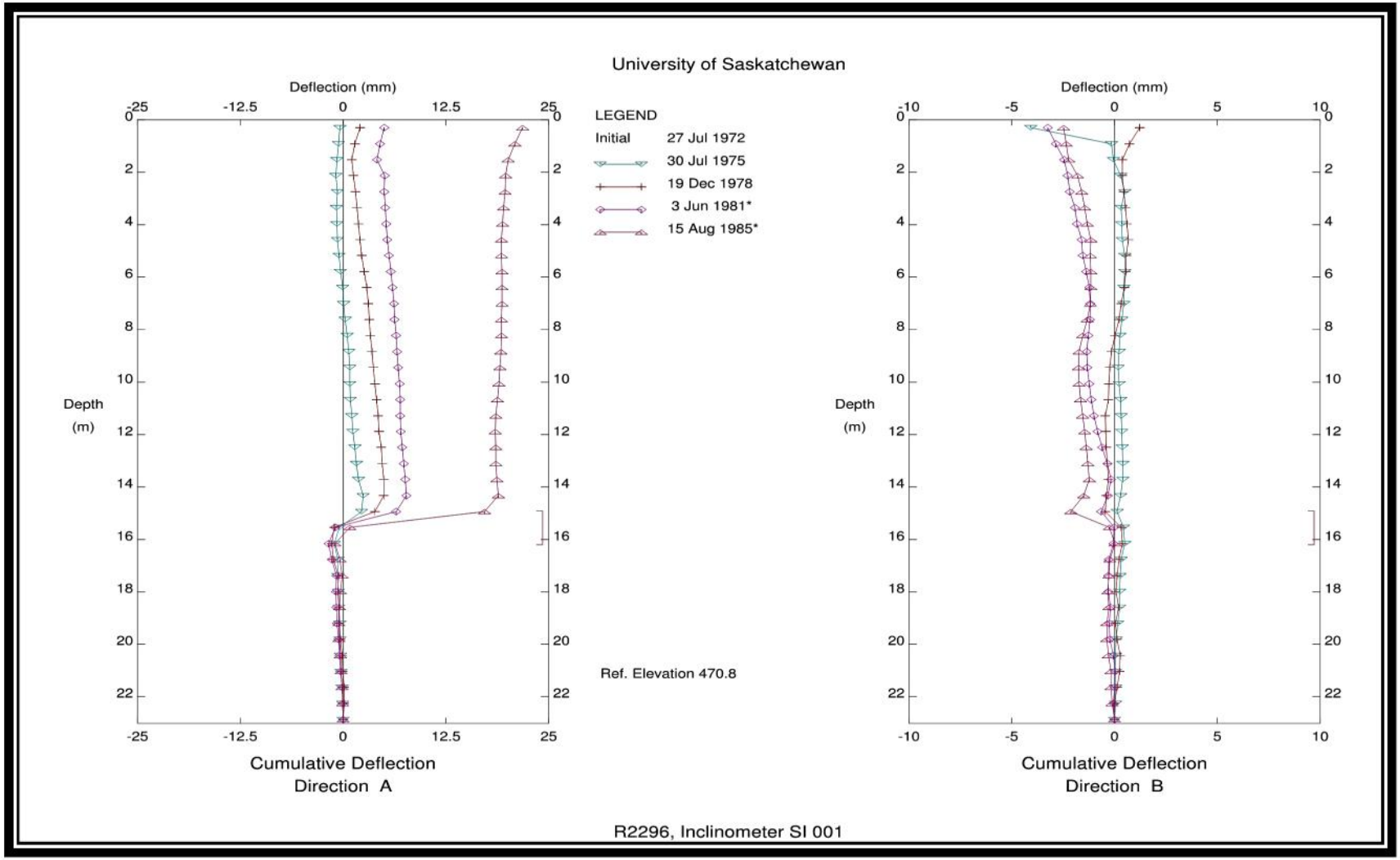

Figure A 1: SI1 cumulative displacement – A & B axis (1972-1985)

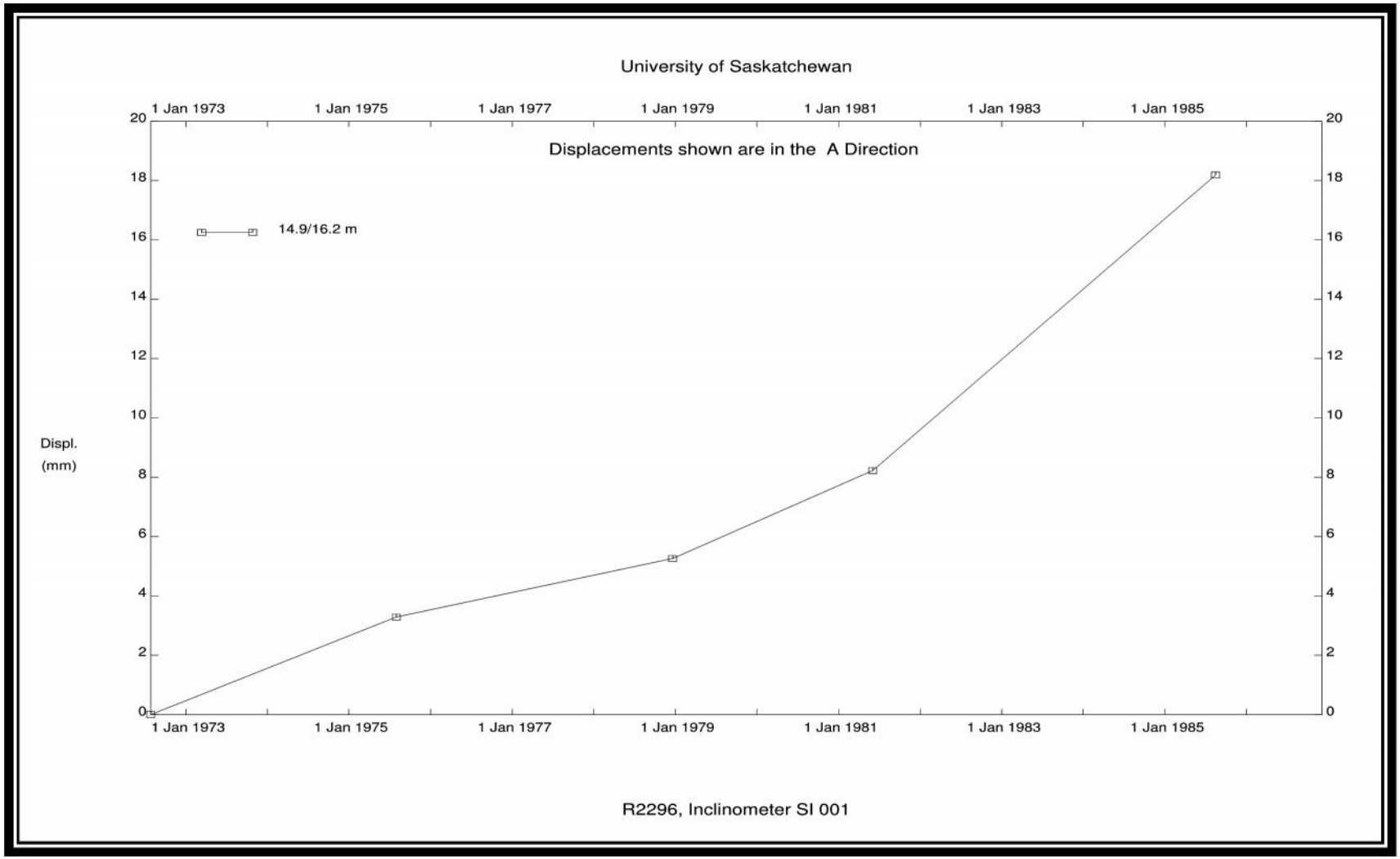

Figure A 2: SI1 displacement vs. time – A axis (1972-1985)

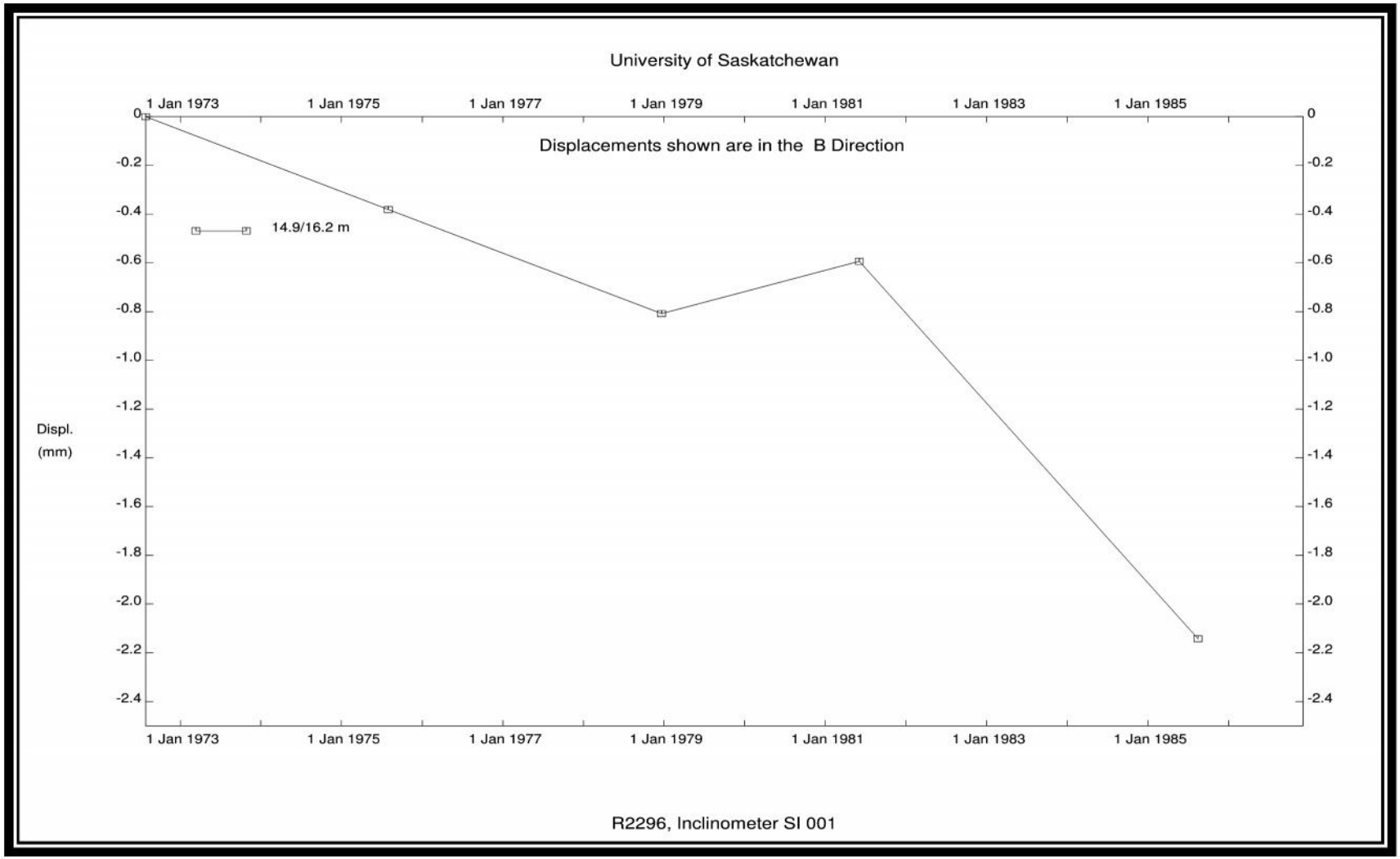

Figure A 3: SI1 displacement vs. time – B axis (1972-1985)

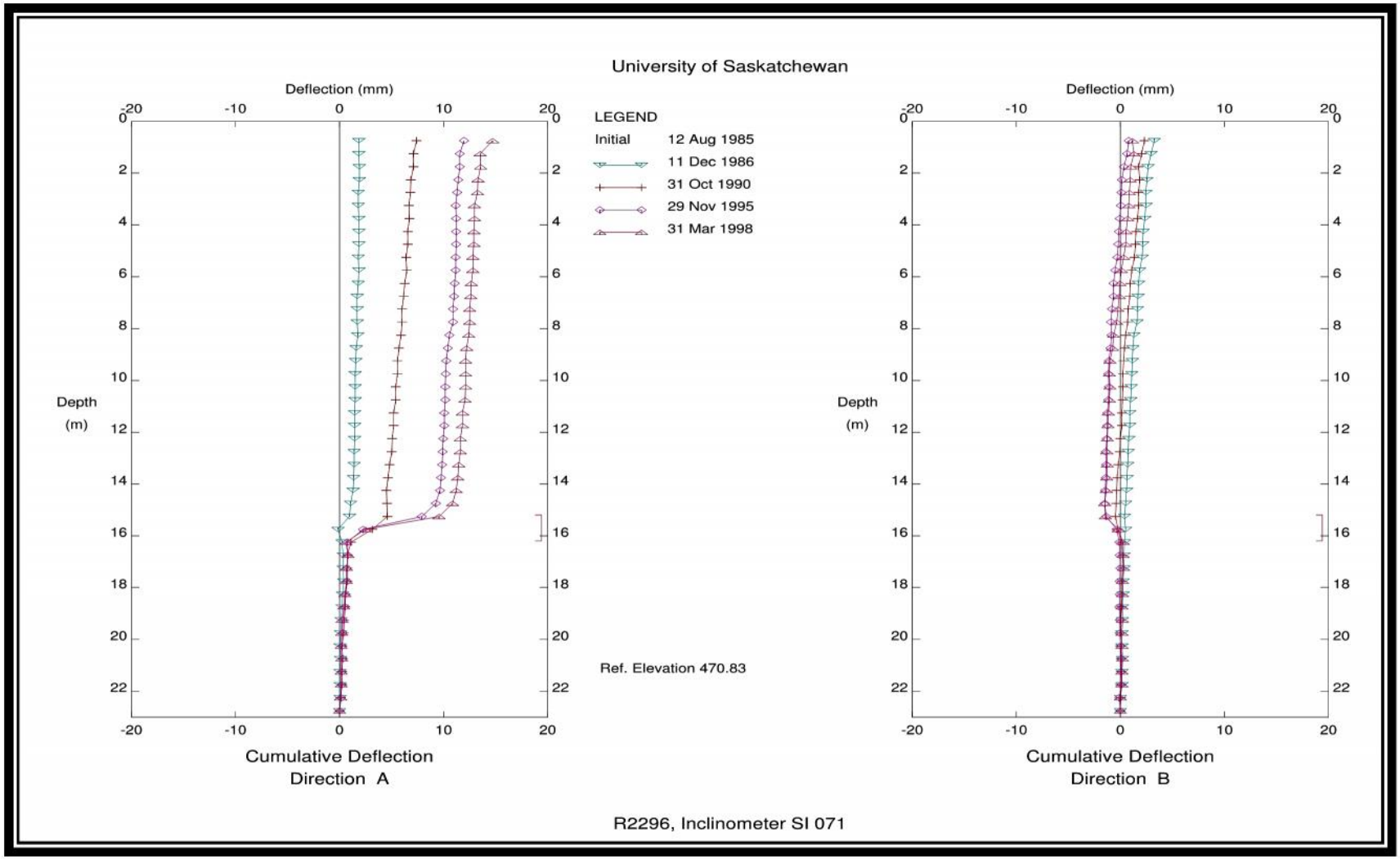

Figure A 4: SI71 cumulative displacement – A & B axis (1985-1998)

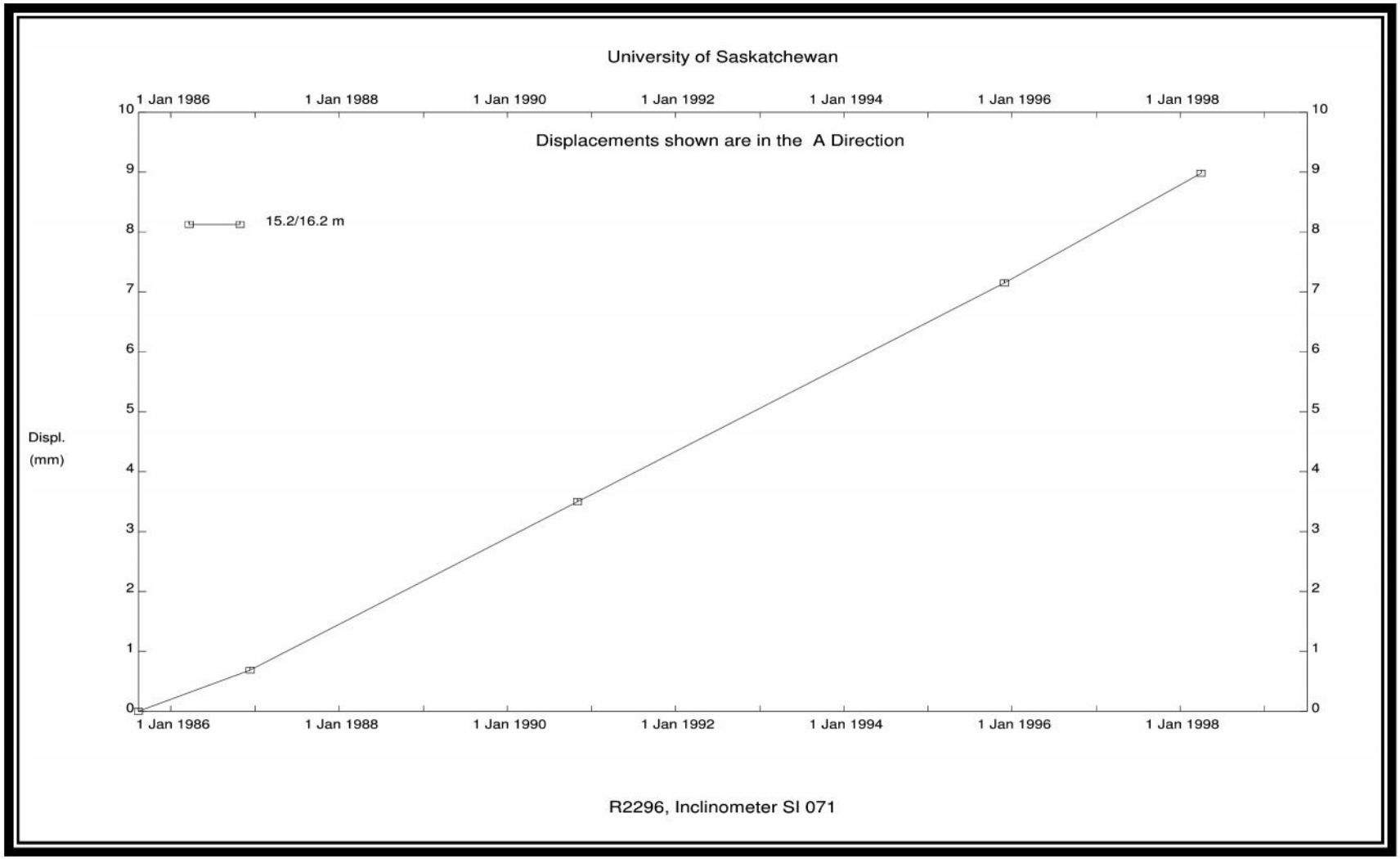

Figure A 5: SI71 displacement vs. time – A axis (1985-1998)

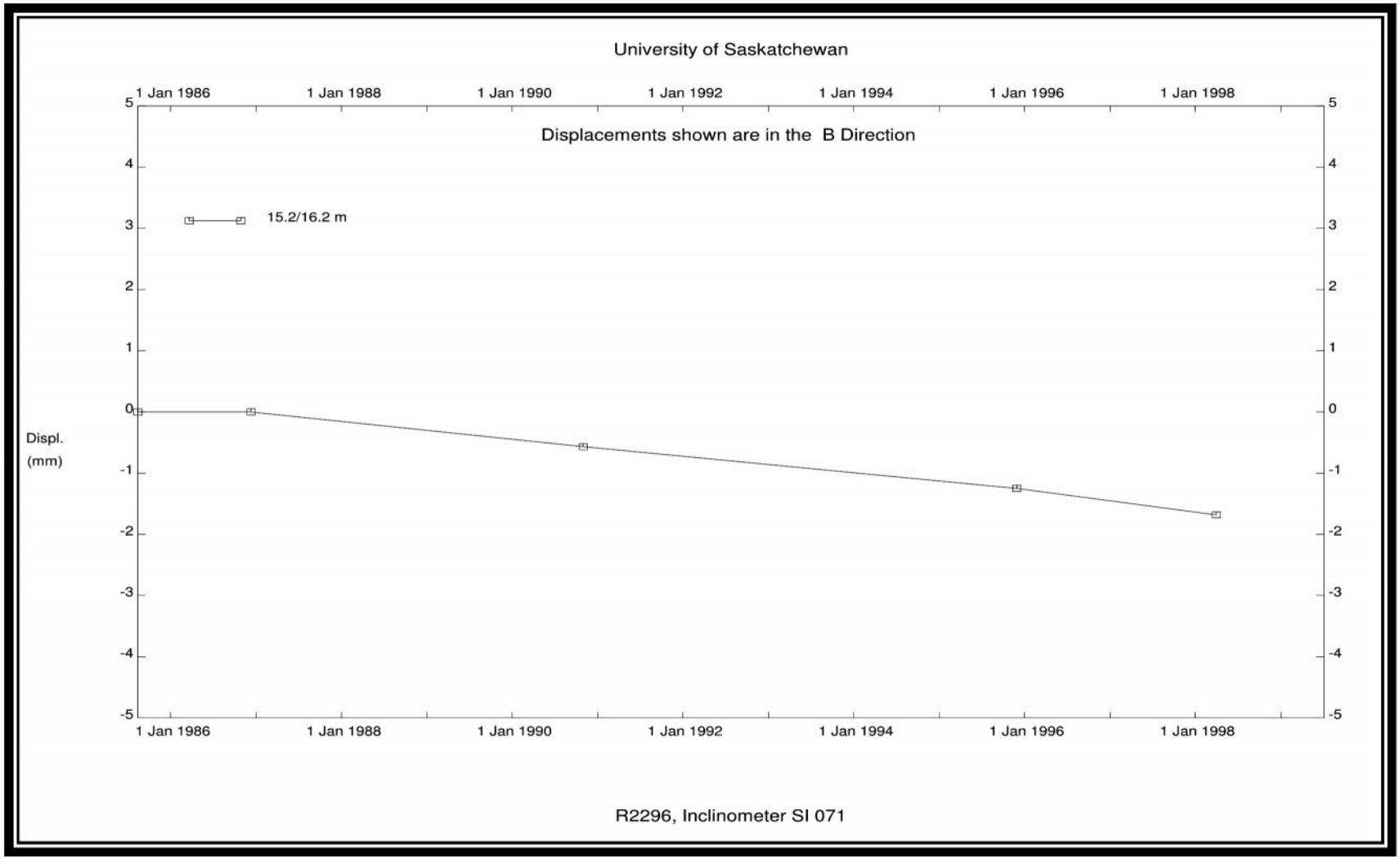

Figure A 6: SI71 displacement vs. time – B axis (1985-1998)

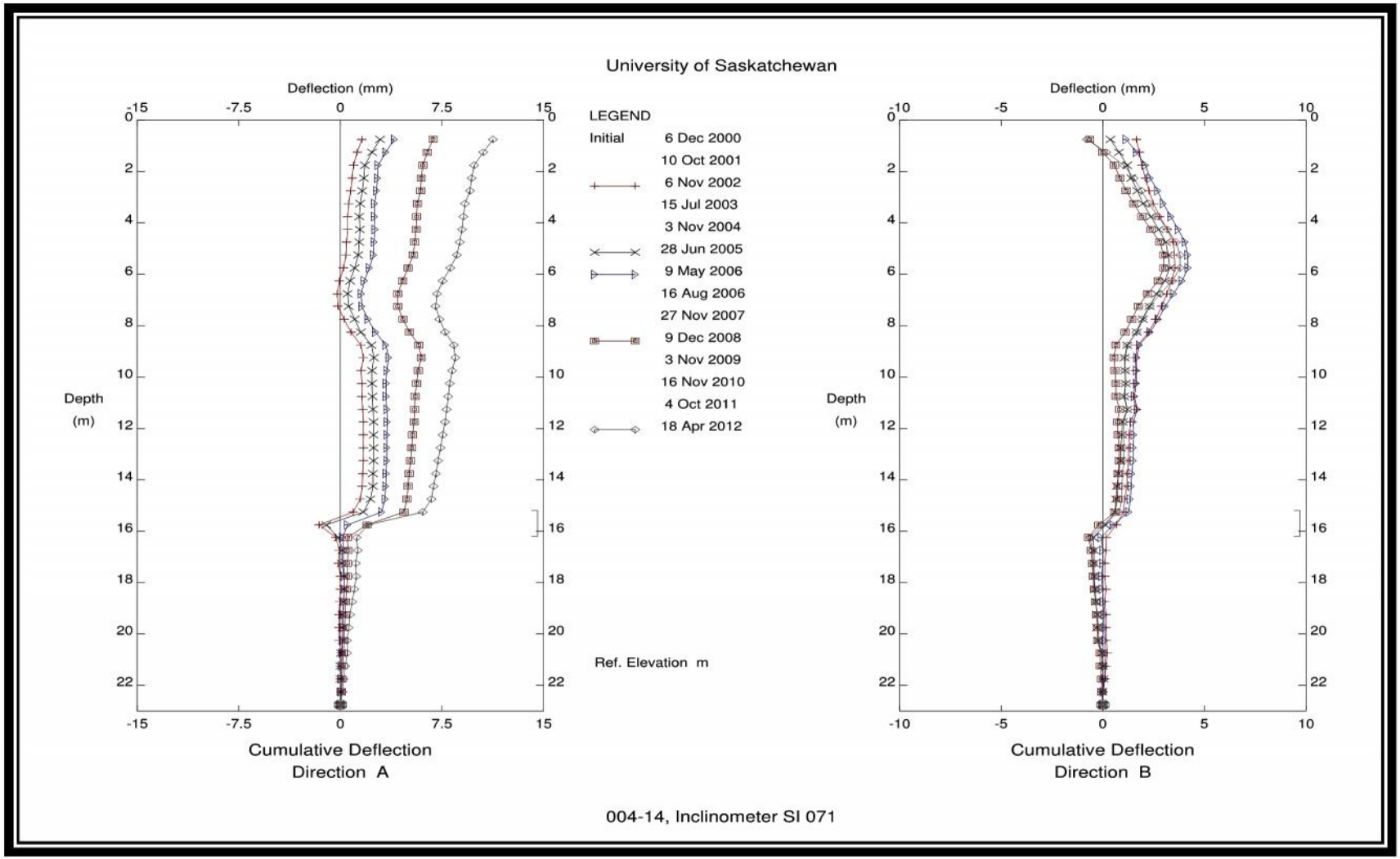

Figure A 7: SI71 cumulative displacement – A & B axis (2000-2012)

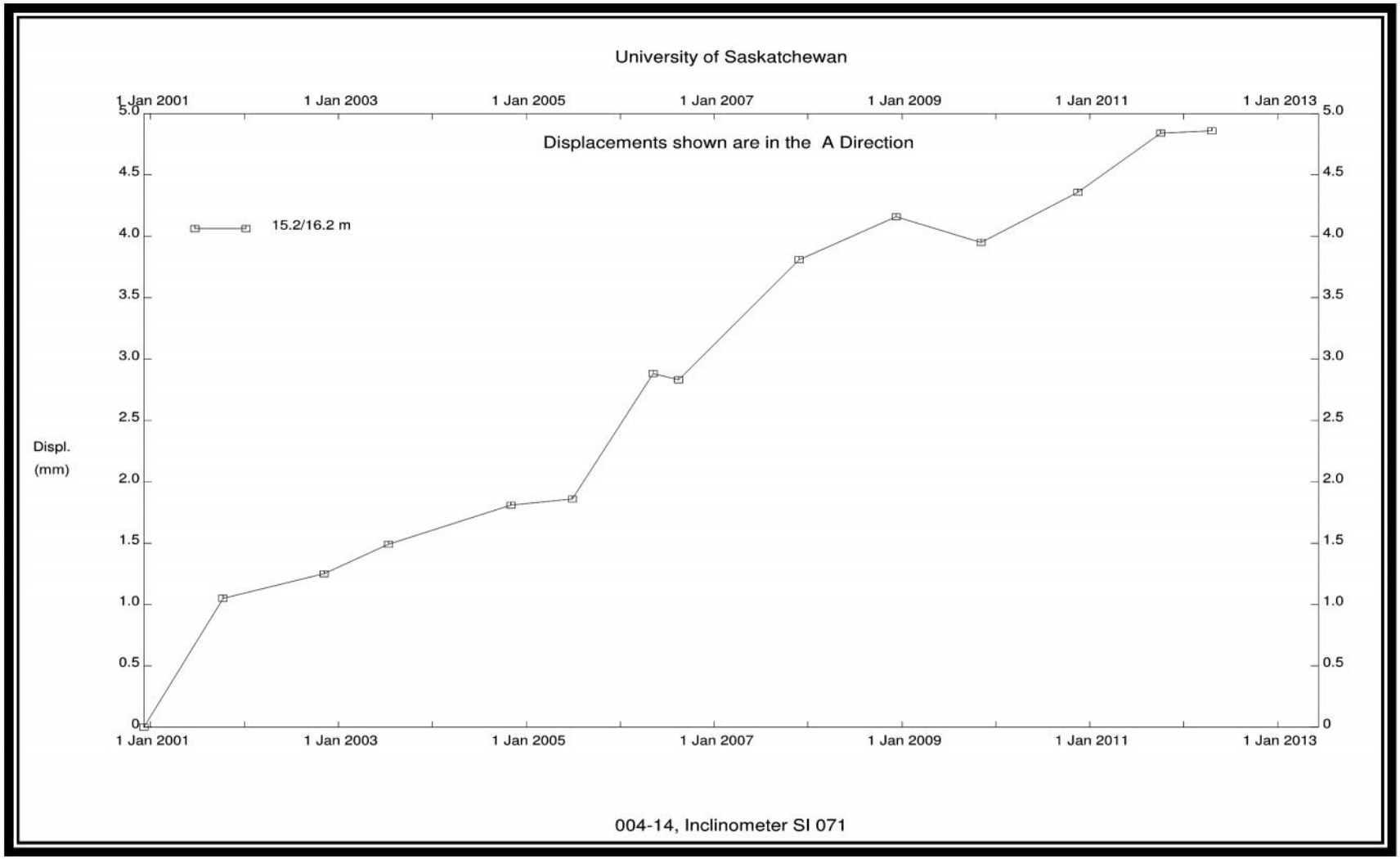

Figure A 8: SI71 displacement vs. time - A axis (2000-2012)

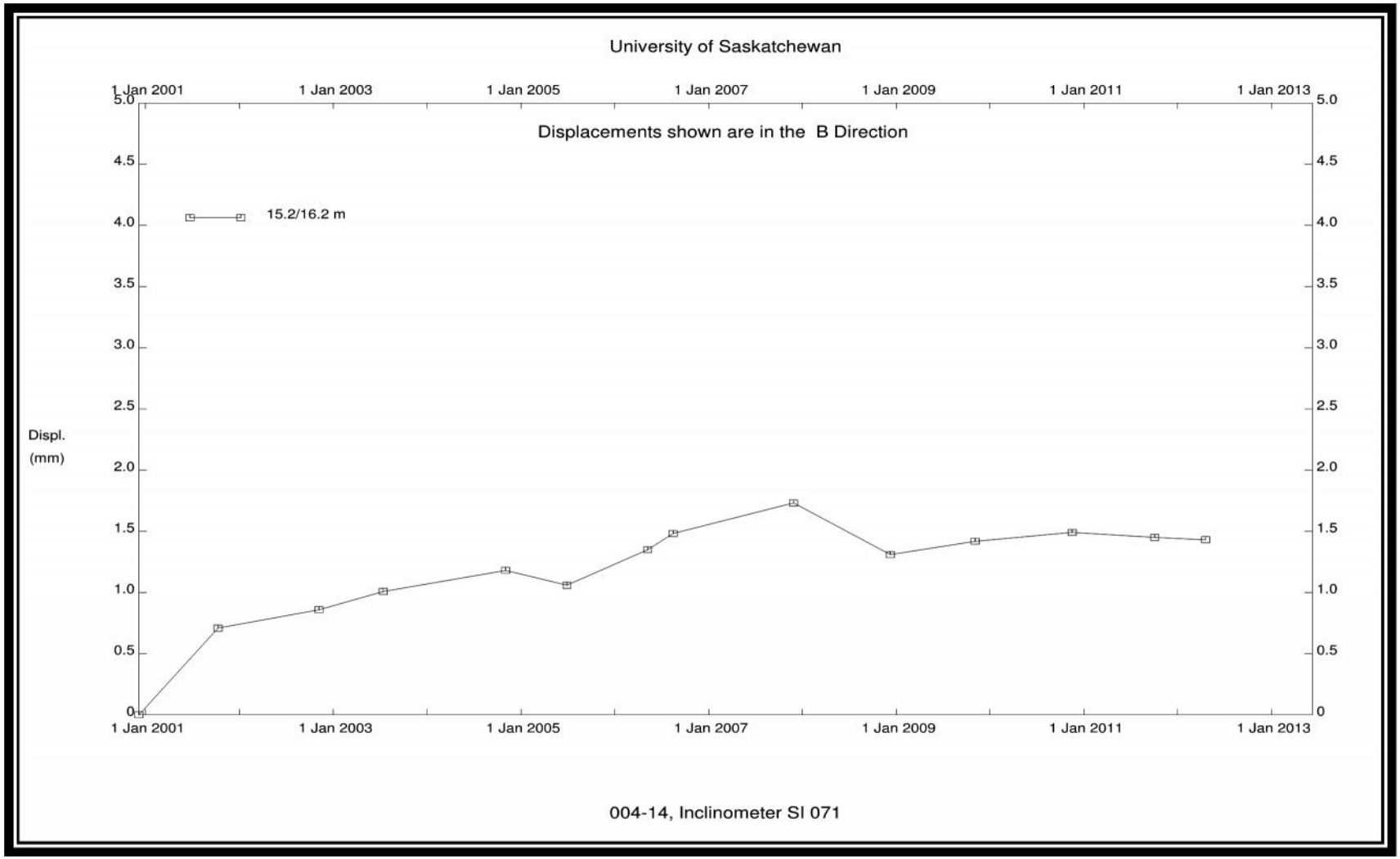

Figure A 9: SI71 displacement vs. time - B axis (2000-2012)

SI2/172

SI2 is located in the South abutment and was installed in January 1968 and was renamed SI72 with in 1985 with SMHI's switch to the metric system. The first available readings for this instrument were taken in July 1972. From July 1972 to March 1998 there was no movement observed in either axis of the slope inclinometer.

Between December 2000 and April 2012 there appeared to be approximately 2.9 mm of movement in the A-axis. It is likely that there was also movement in the B axis however, the readings were erratic and nothing meaningful could be salvaged from the data. Over this time period, the average movement with time was approximately 0.3 mm/yr. The movement is taking place on a shear plane located at 453.21 masl. According to the borehole logs provided by SMHI, the movement in the unoxidized shale.

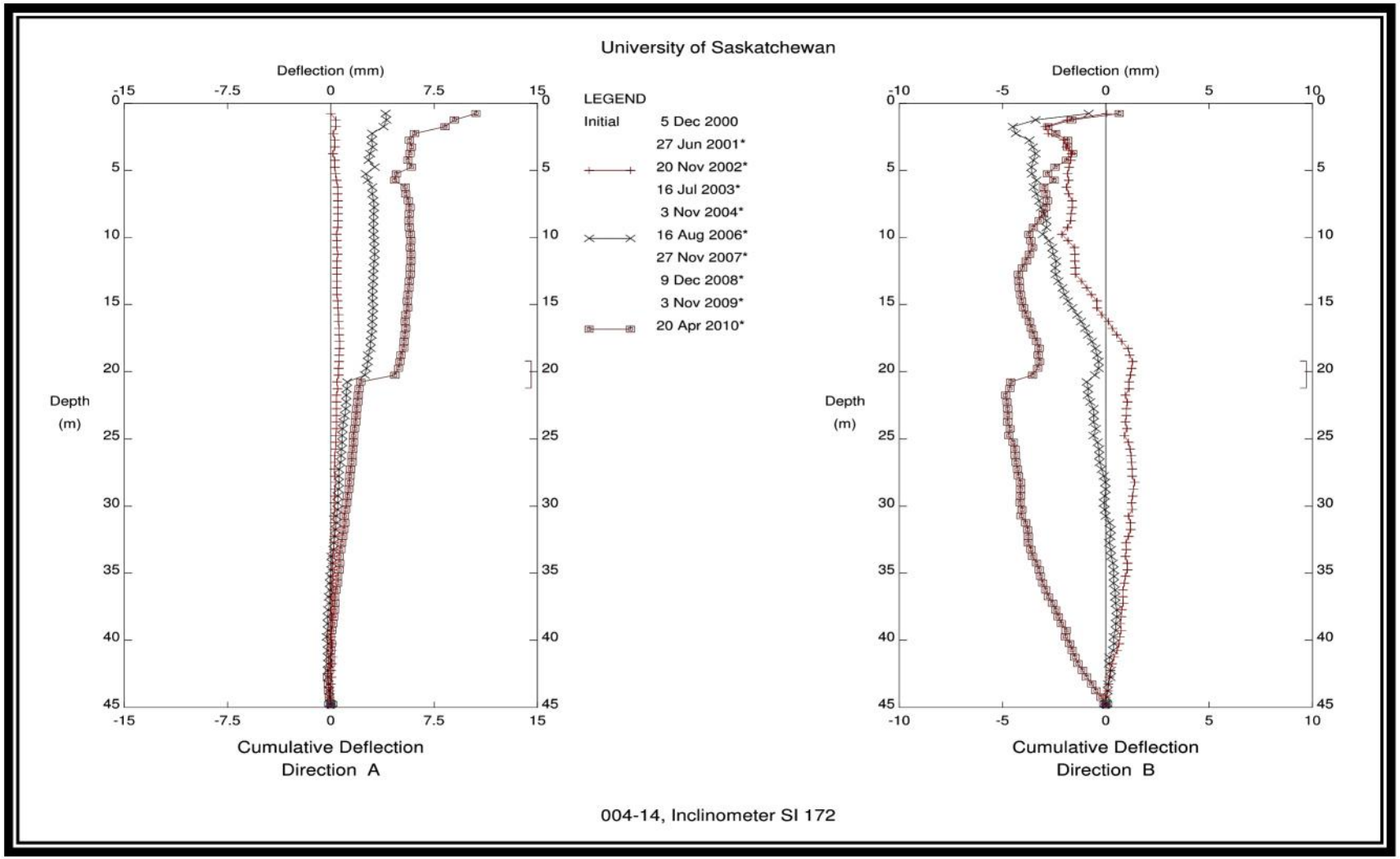

Figure A 10: SI172 cumulative displacement - A & B axis (2000-2010)

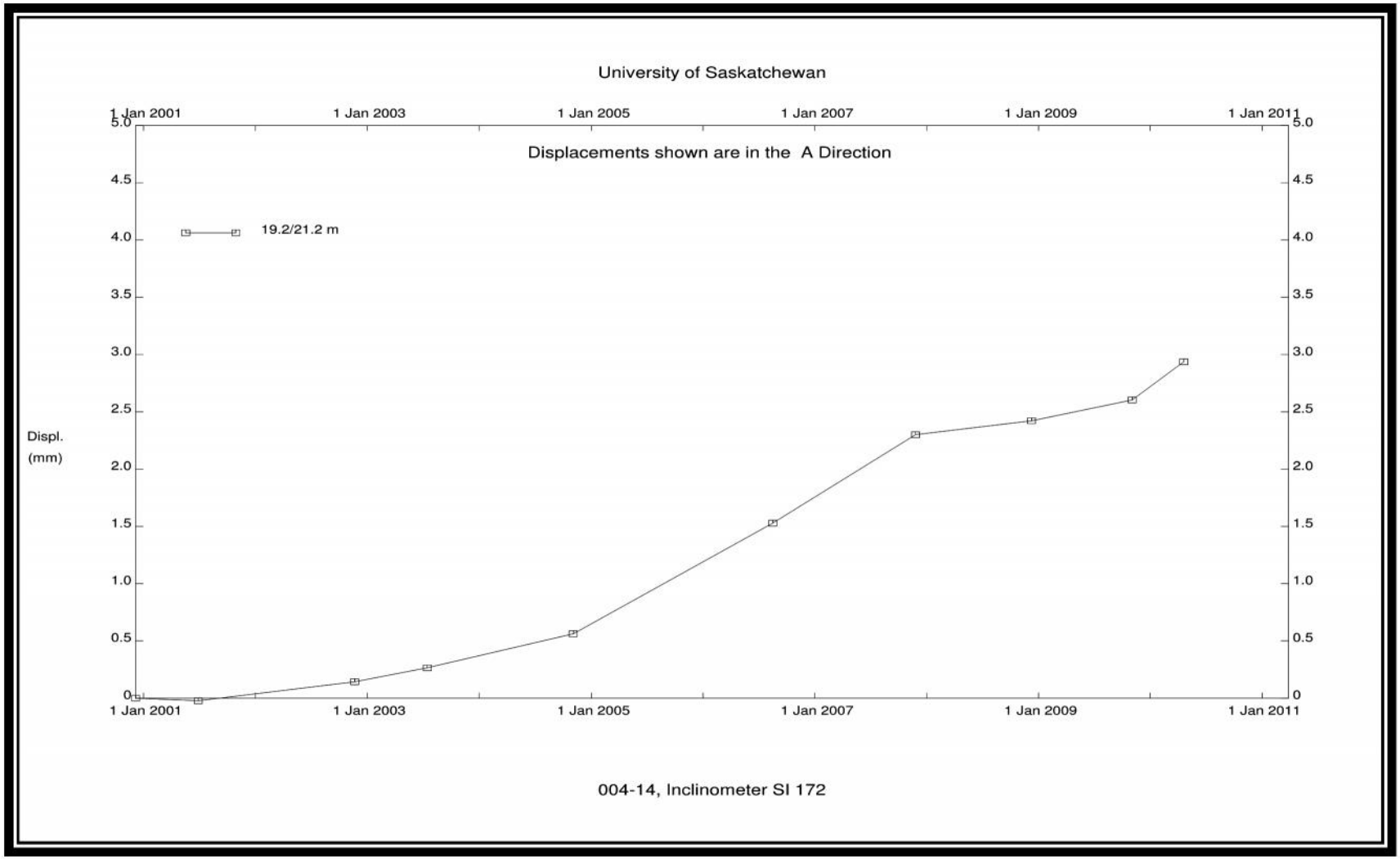

Figure A 11: SI172 displacement vs. time - A axis (2000-2010)

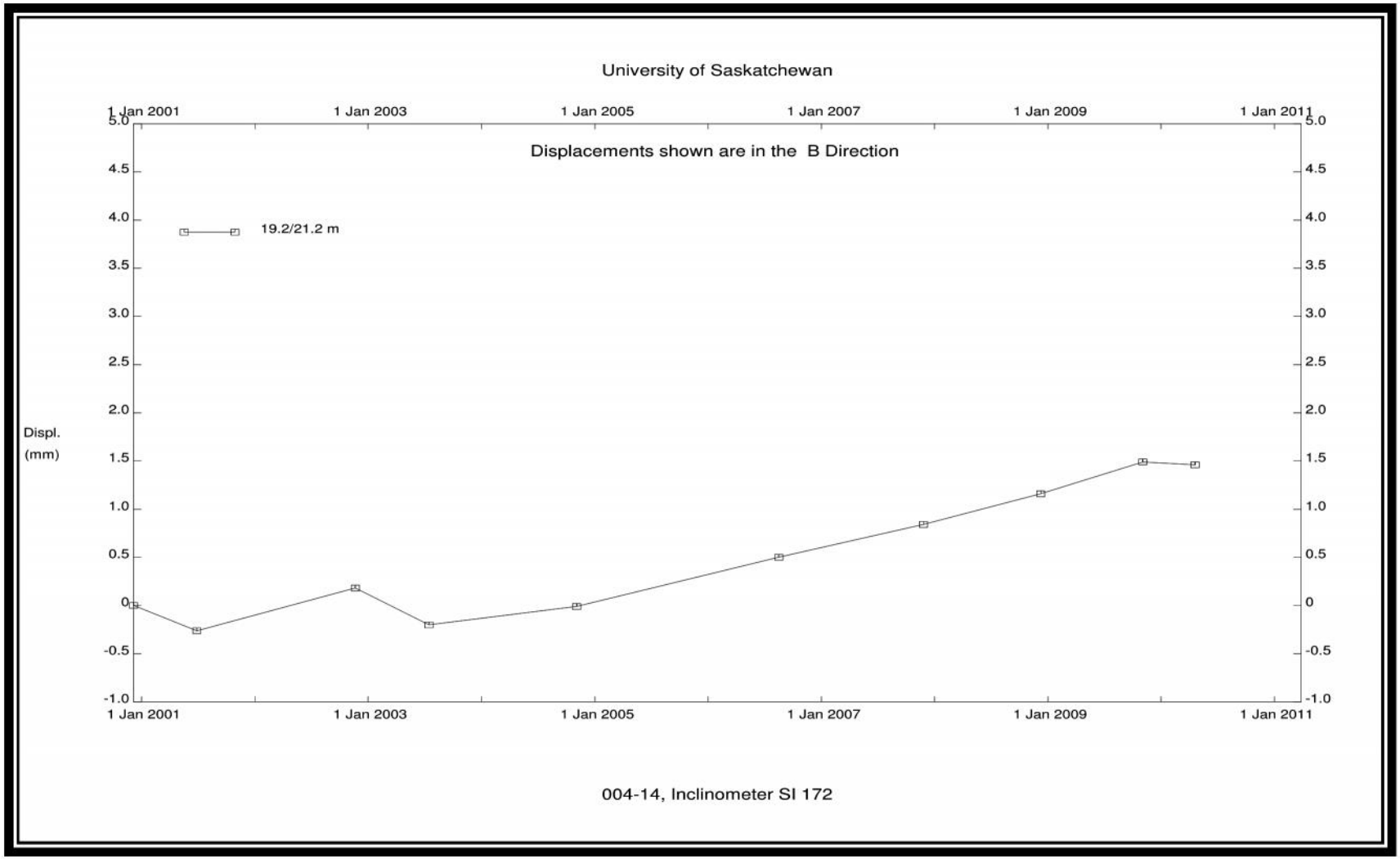

Figure A 12: SI172 displacement vs. time - B axis (2000-2010

SI3/73

SI3 is located at the South abutment of the Battlefords bridges and was installed in February 1968. The first available readings for this inclinometer were taken in August 1972 however no movement was observed in the SI until after July 1985. In 1985, SI3 was renamed SI73 with SMHI's switching to the metric system.

Between July 1985 and March 1998, there was approximately 2.1 mm of movement observed in the A-axis of SI73. According to CAL, 1999, the movement continued at average rate of 0.2 mm per year until 1995 when movement halted.

From April 2001 to July 2007 there was approximately 1.8 mm of cumulative displacement observed in the A-axis. This movement translates to an average annual displacement of 0.4 mm/yr. from 2003 to 2007. Movement in SI3/73 is taking place on a slip surface located at 455.2 masl. According to borehole logs provided by SMHI, this movement is taking place in unoxidized shale.

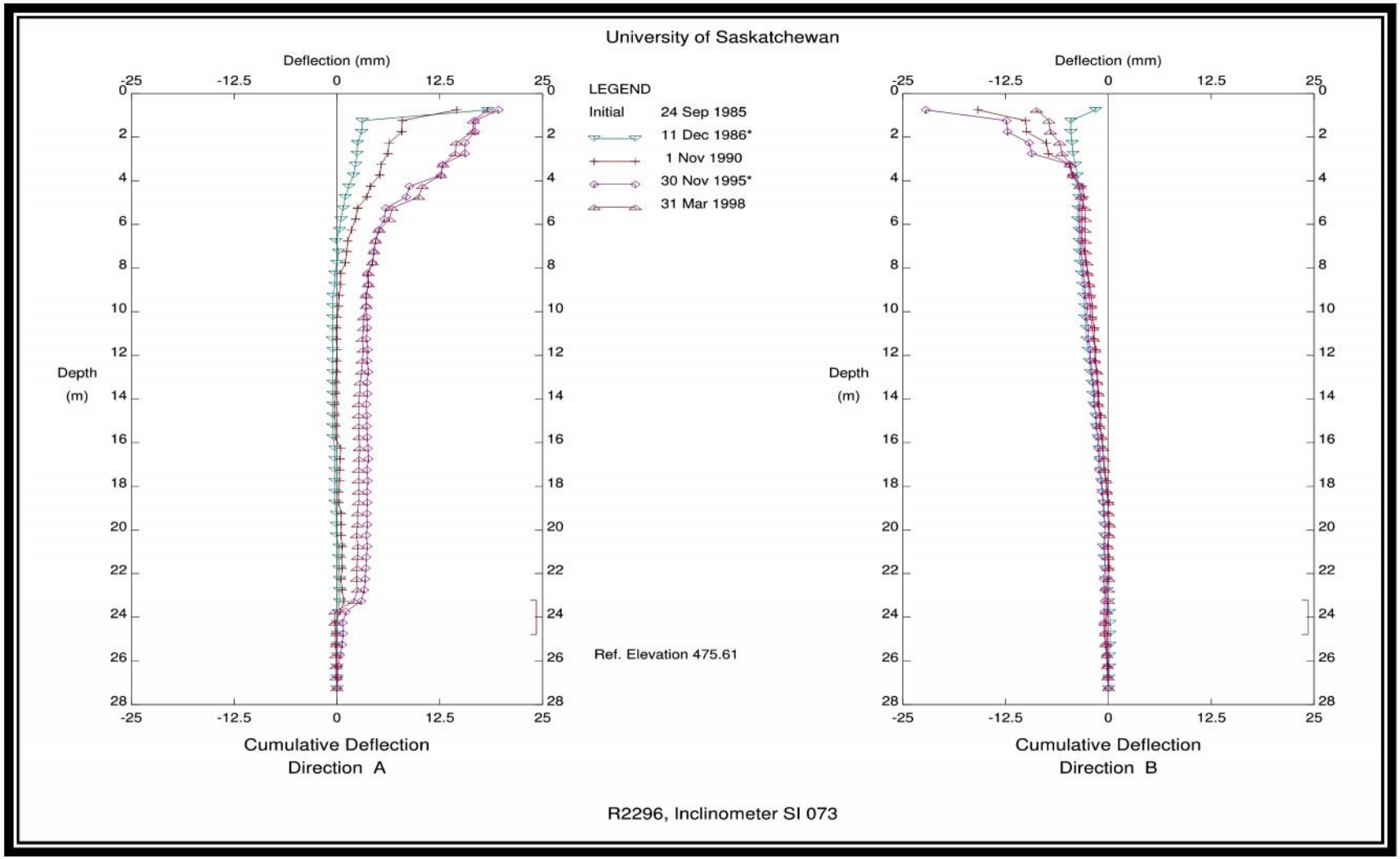

115

Figure A 13: SI73 cumulative displacement - A & B axis (1985-1998)

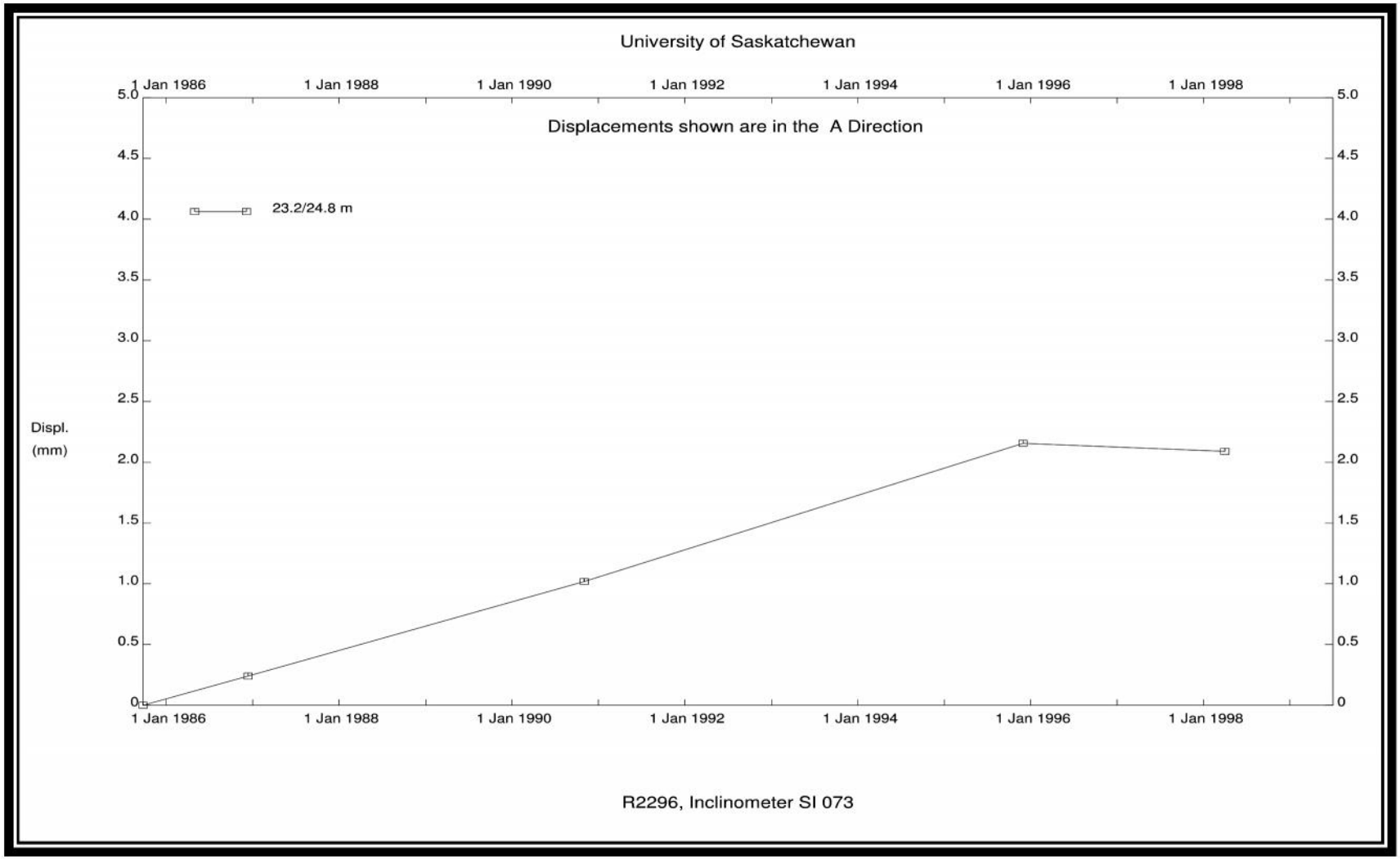

Figure A 14: SI73 displacement vs. time – A axis (1985-1998)

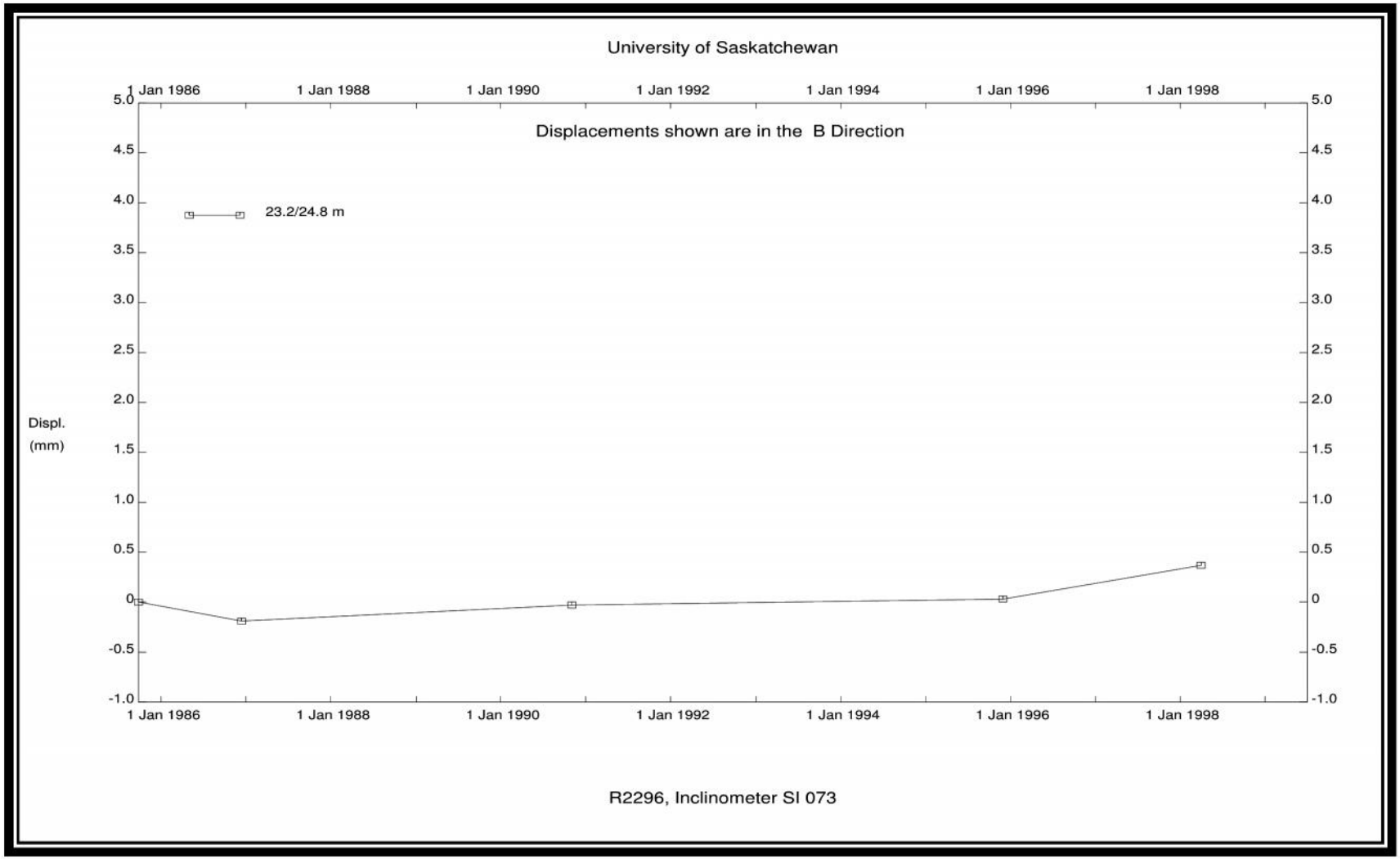

Figure A 15: SI73 displacement vs. time – B axis (1985-1998)

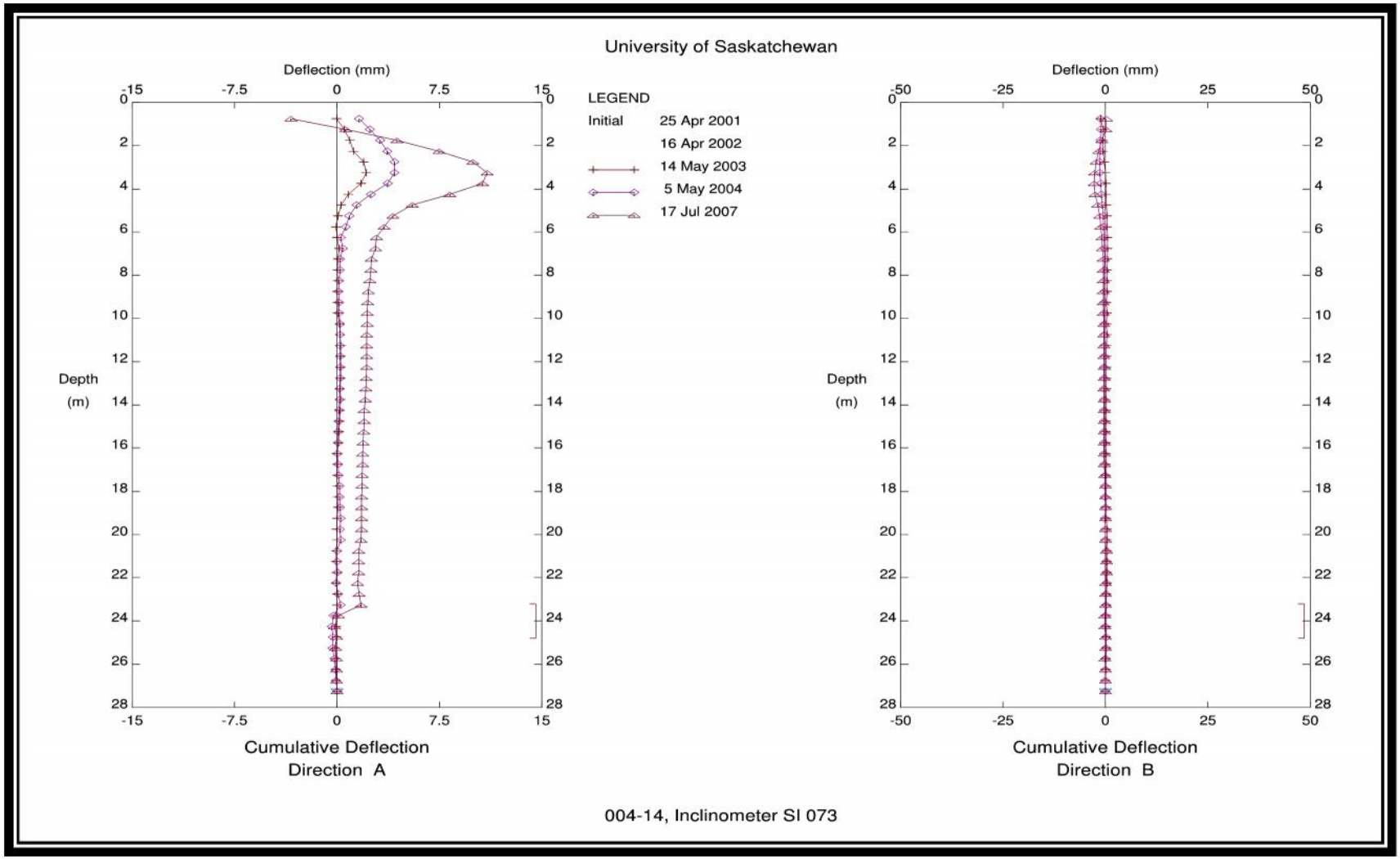

Figure A 16: SI73 cumulative displacement – A and B axis (2001-2007)

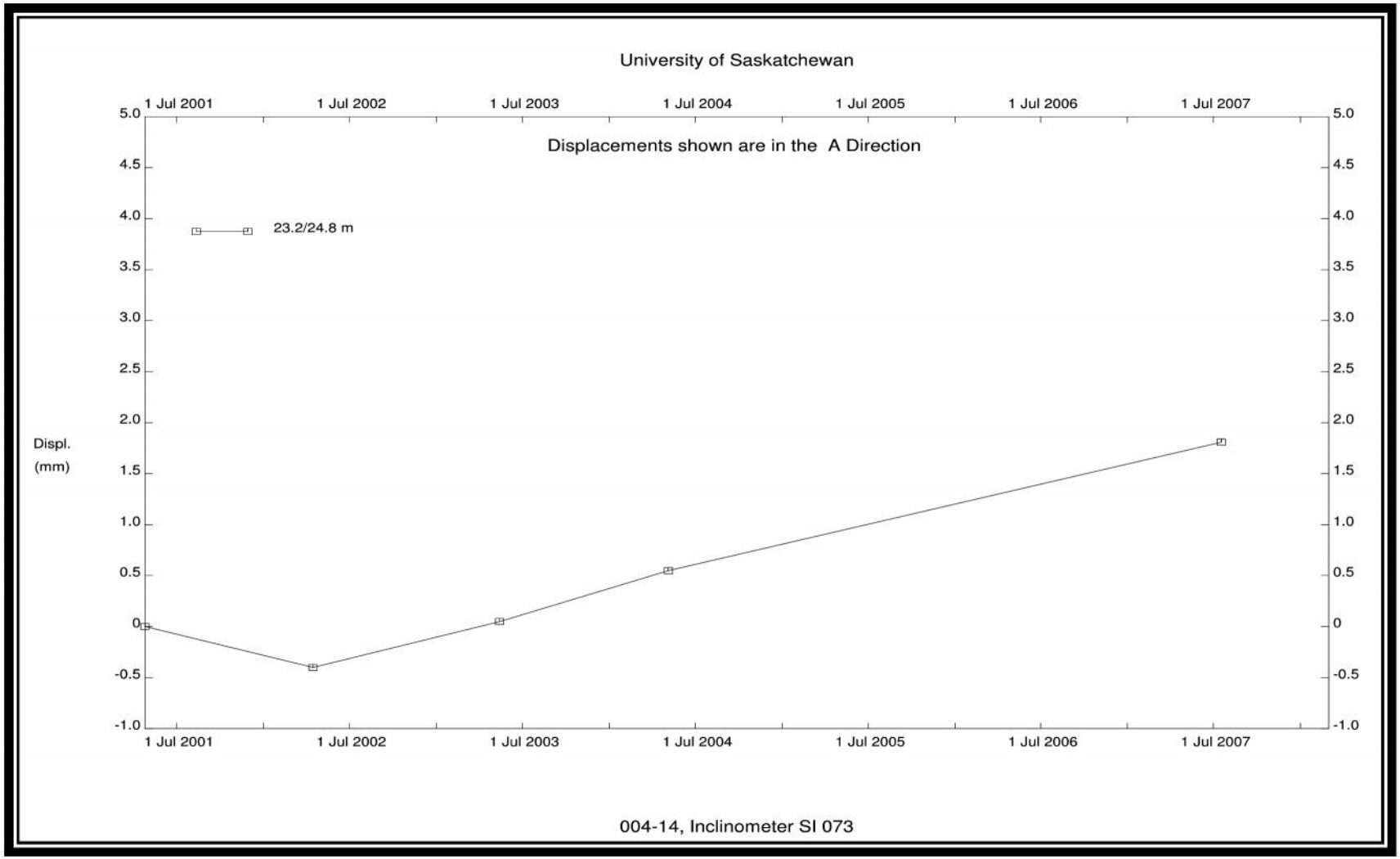

Figure A 17: SI73 displacement vs. time - A axis (2001-2007)

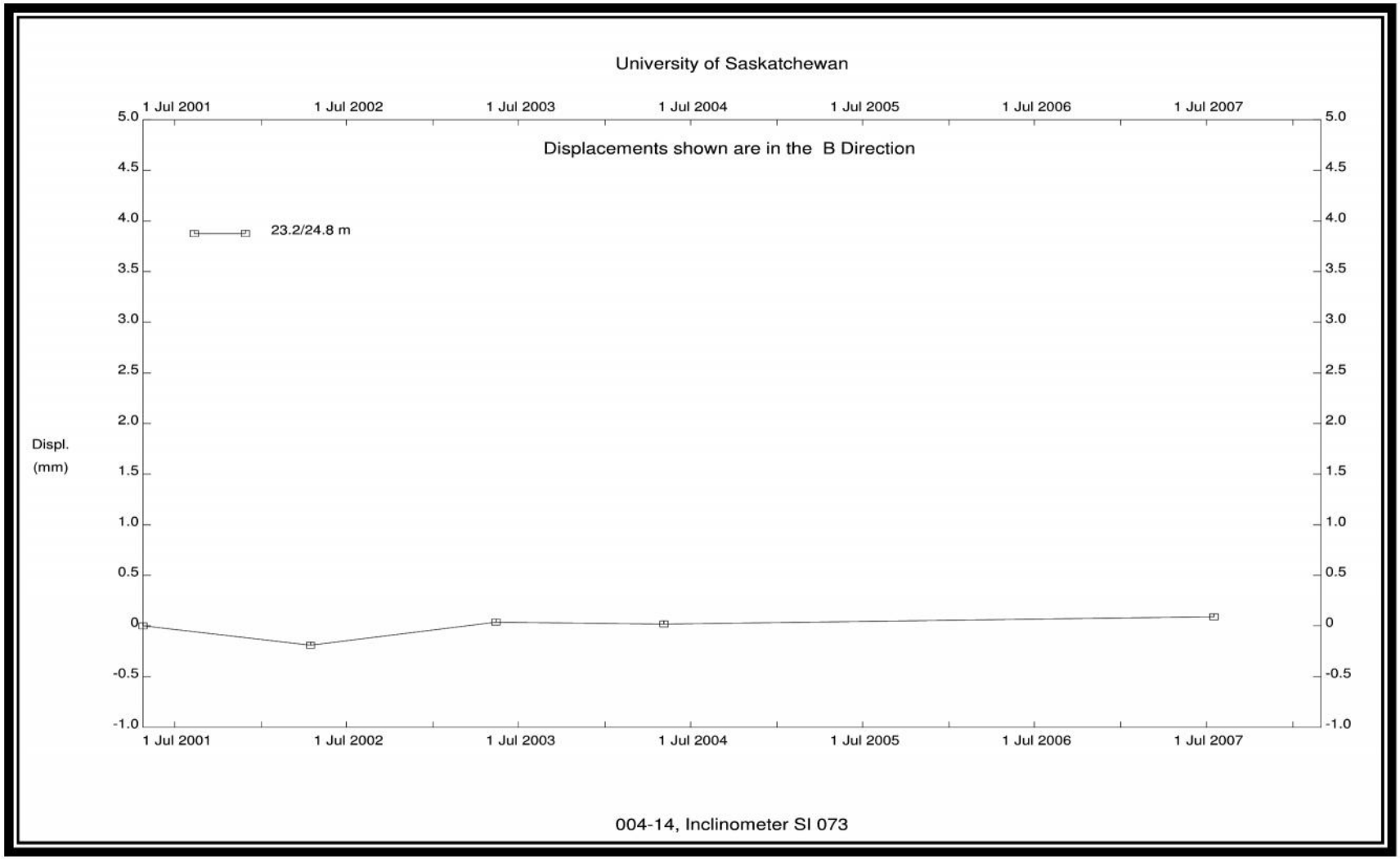

120

Figure A 18: SI73 displacement vs. time - B axis (2001-2007)

SI7/SI77

SI7 was installed East of the South abutment in August of 1968. Readings for this instrument are available starting in July 1972. In 1985 this instrument was renamed SI77 with SMHI's conversion to the metric system.

Between July 1972 and August 1985 3.4 mm of movement was observed in the A-axis. According to CAL, 1999 this movement works out to be approximately 0.2 mm/yr. until 1981 where the rate increased to 0.4 mm/yr.

Between August 1985 and March 1998 there was 3.7 mm of observed cumulative displacement in the A-axis. According to CAL, 1999 this movement averages to approximately 0.25 mm/yr.

Between December 2000 and April 2012 there was 4.2 mm of movement observed in the A-axis and 0.5 mm of movement observed in the B-axis. Throughout this time period, the rate of movement shows significant variation. in 2001, movement was approximately 0.5 mm/yr. and slowed to a halt by 2005. In 2006, movement continued at a rate of approximately 0.4 mm/yr. The maximum rate of movement observed occurred in 2006 at 0.8 mm/yr. Since 2008, movement has continued at a steady rate of approximately 0.5 mm/yr.

Movement in SI77 appears to be taking place along a shear plane located at 451.8 masl. According to the borehole log provided by SMHI, the stratum located at the depth of the slip surface is unoxidized shale. This shale is described to be extremely hard and brittle with well developed slicken sides.

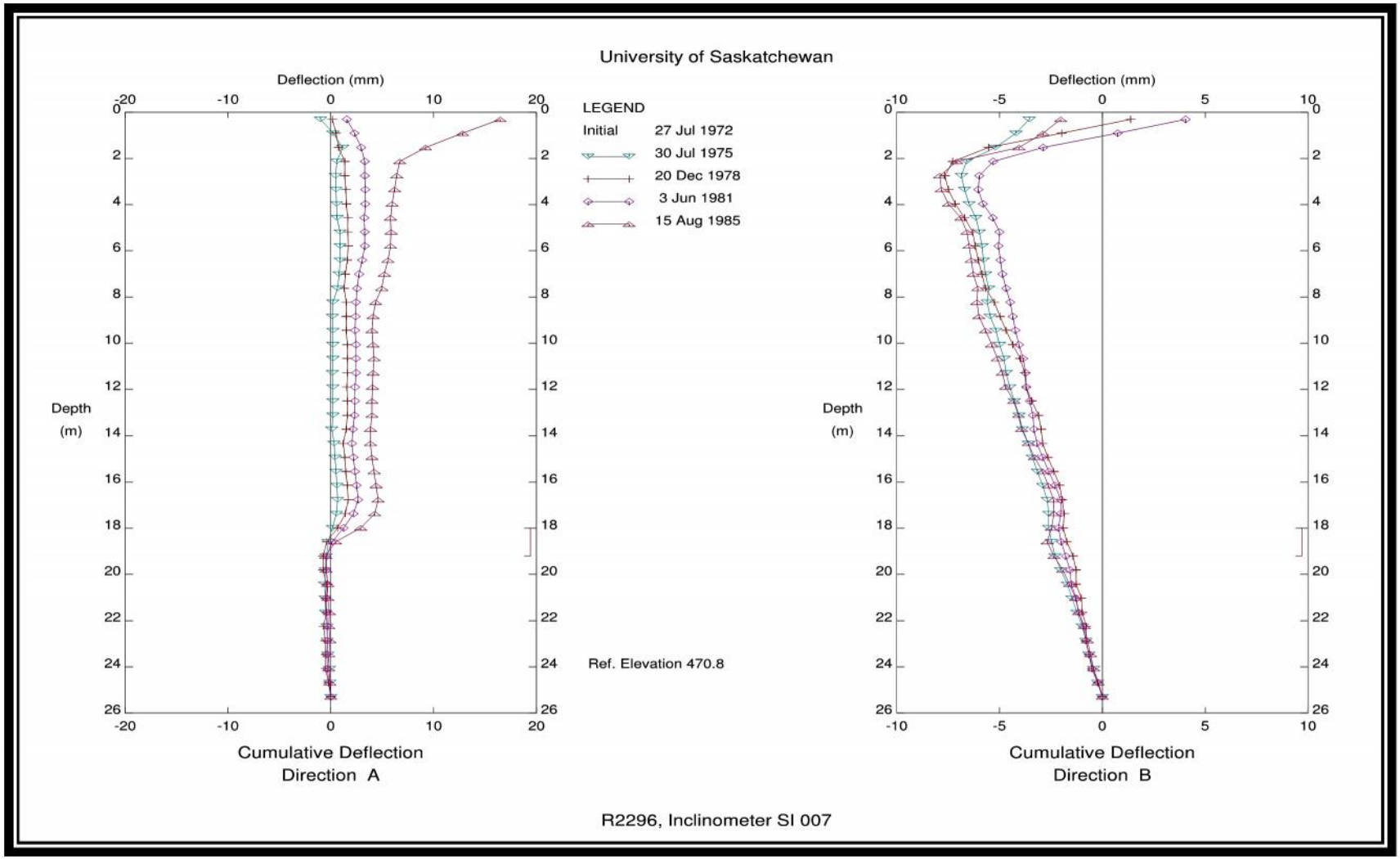

Figure A 19: SI7 cumulative displacement – A & B axis (1972-1985)

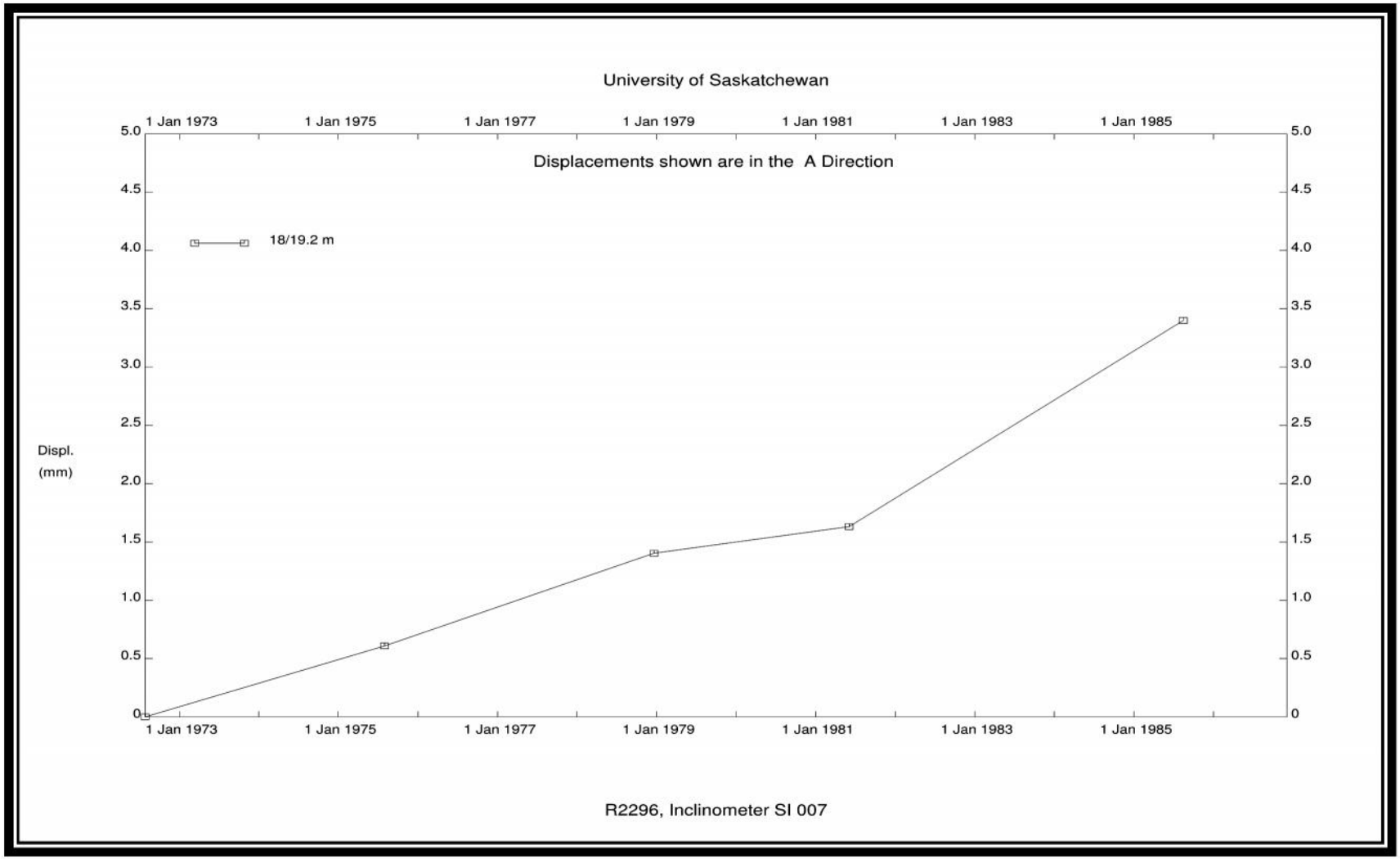

Figure A 20: SI7 displacement vs. time – A axis (1972-1985)

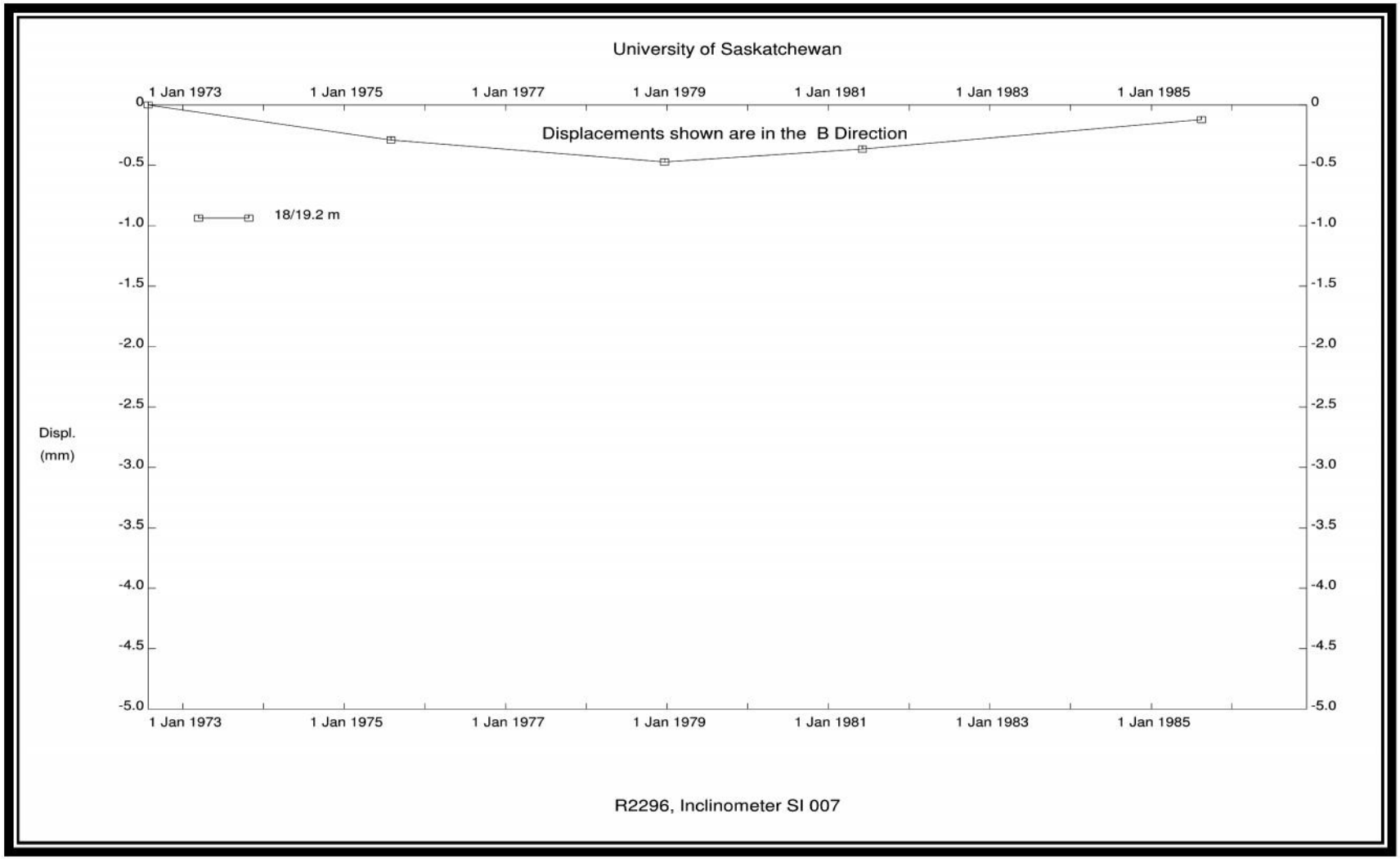

Figure A 21: SI7 displacement vs. time – B axis (1972-1985)

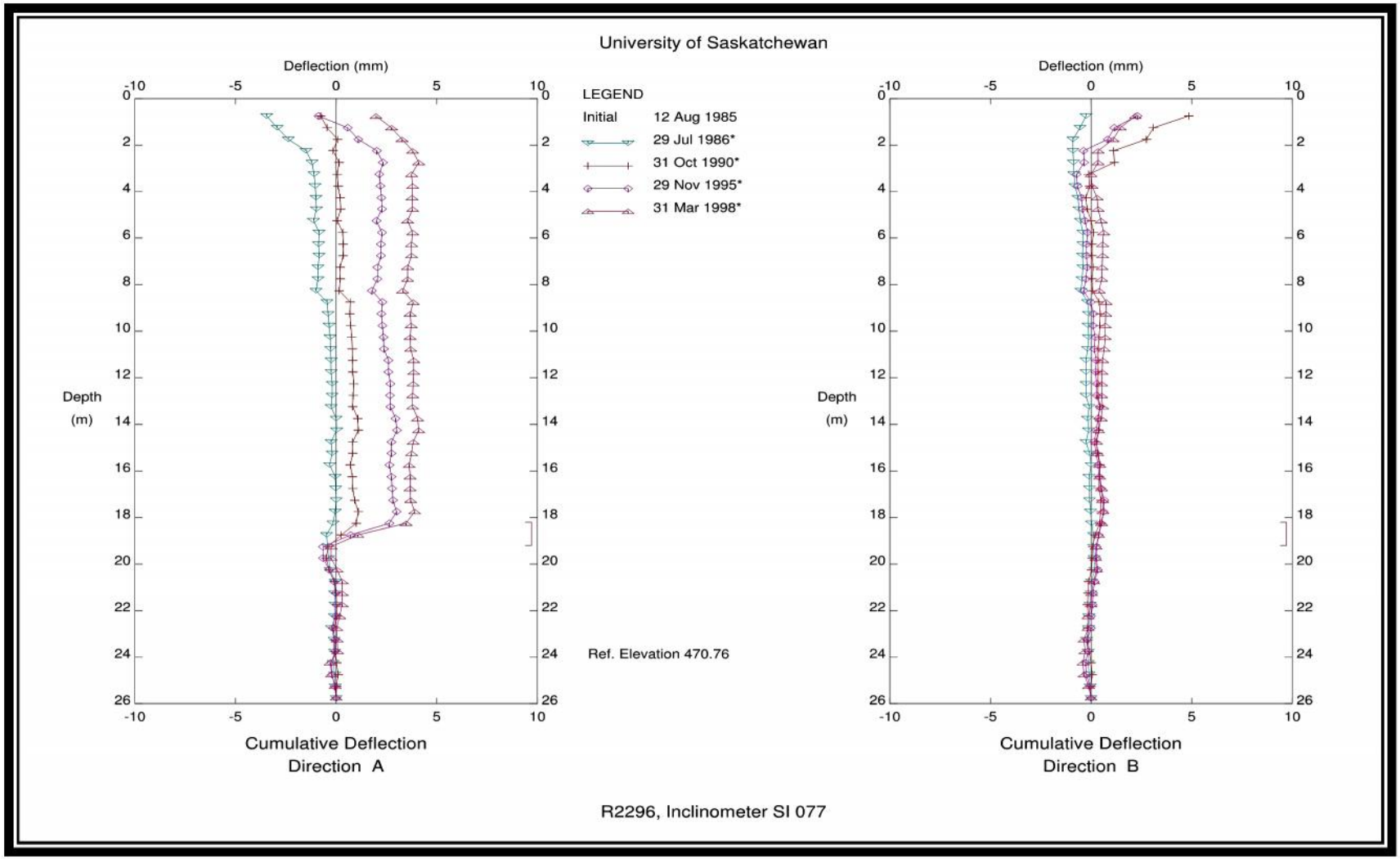

125

Figure A 22: SI77 cumulative displacement - A & B axis (1985-1998)

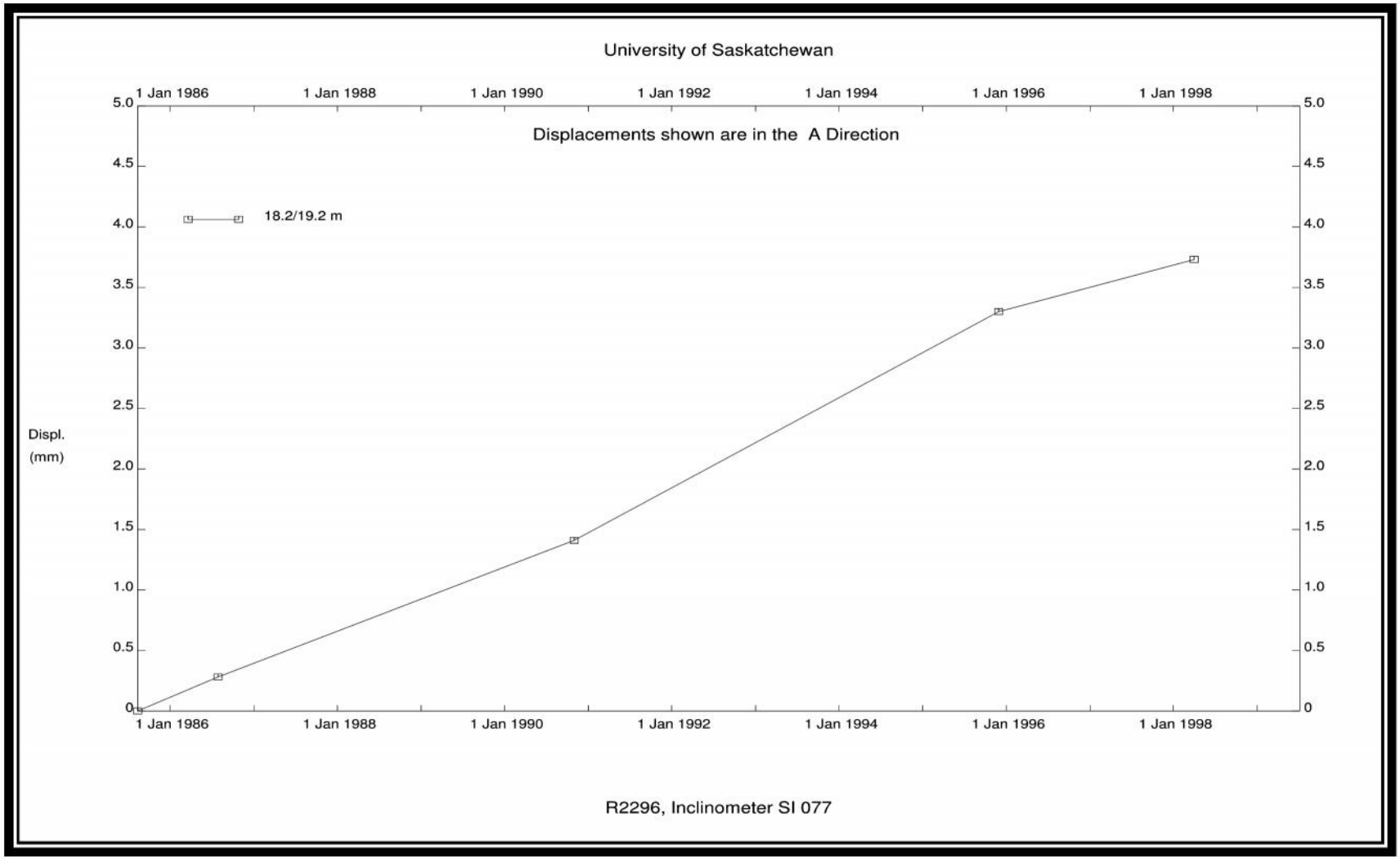

Figure A 23: SI77 displacement vs. time - A axis (1985-1998)

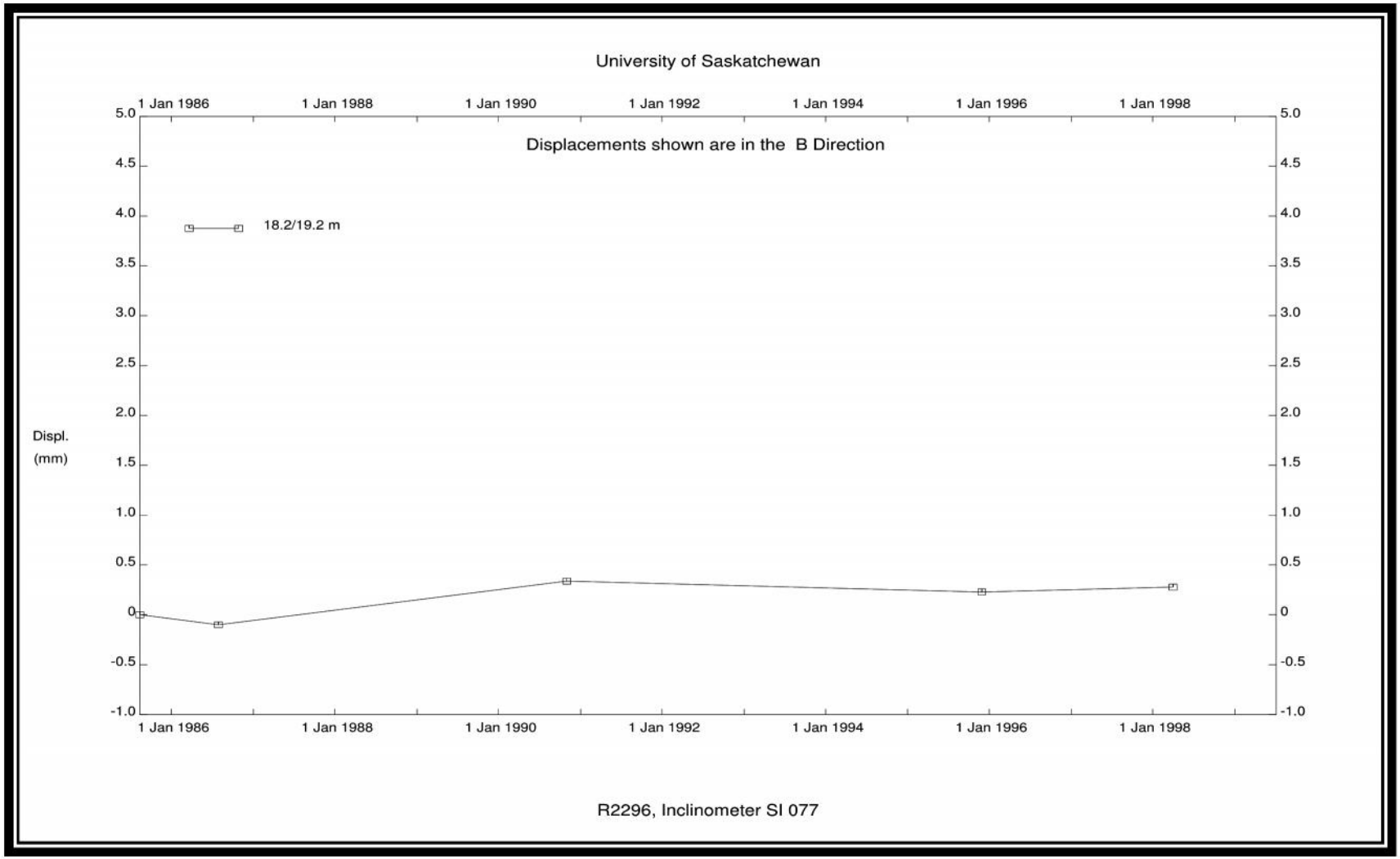

Figure A 24: SI77 displacement vs. time - B axis (1985-1998)

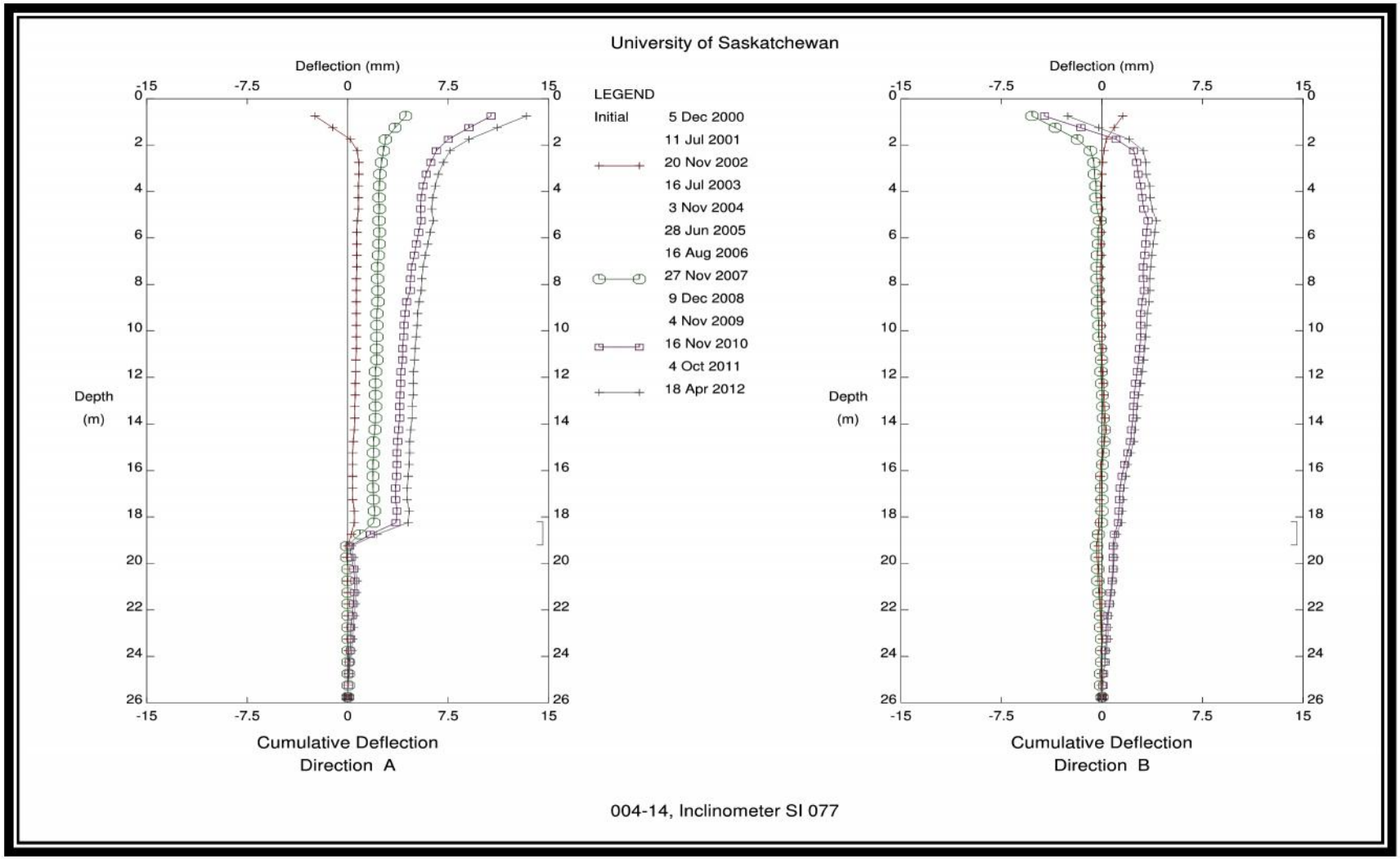

Figure A 25: SI77 cumulative displacement - A & B axis (2000-2012)

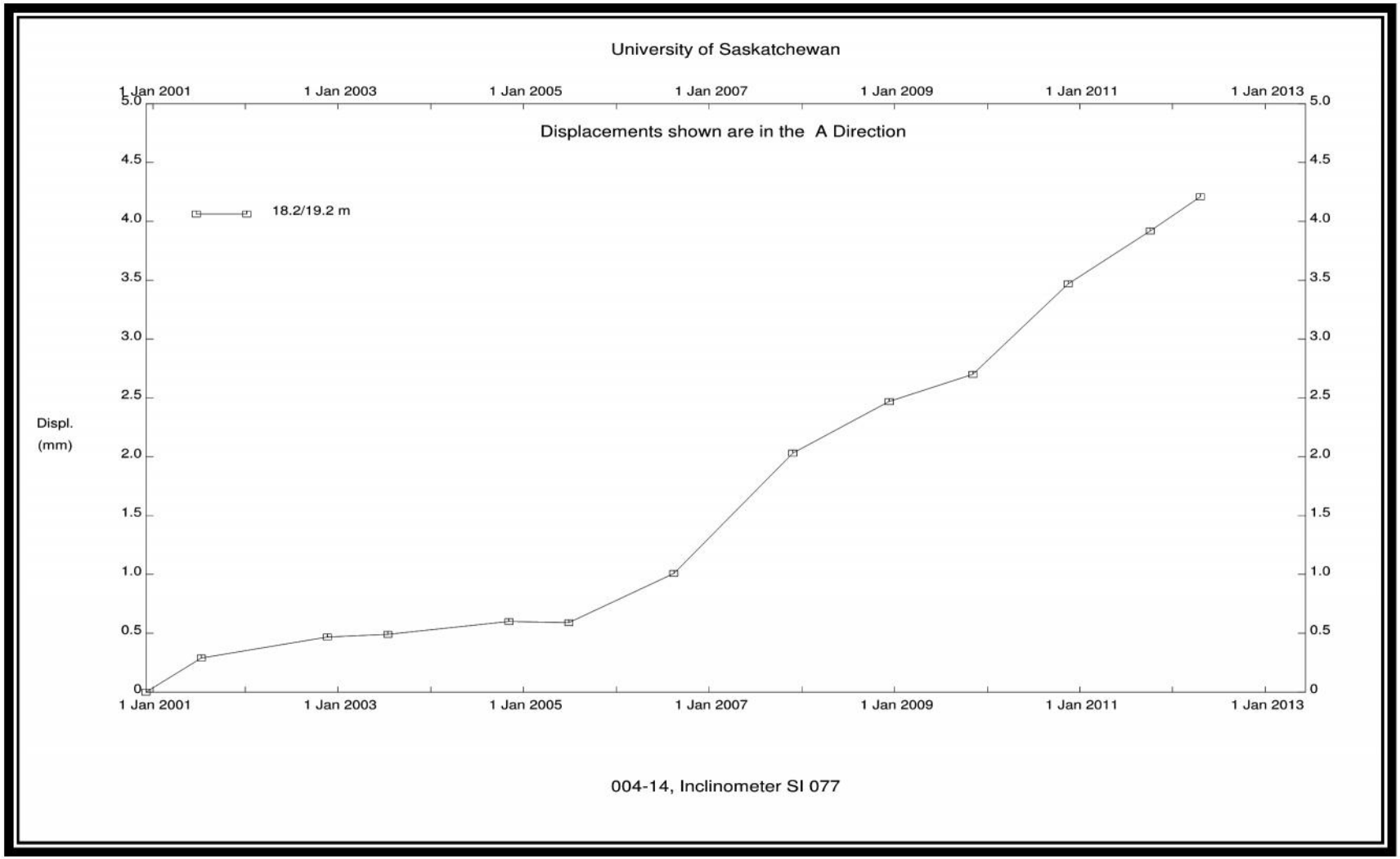

Figure A 26: SI77 displacement vs. time – A axis (2000-2012)

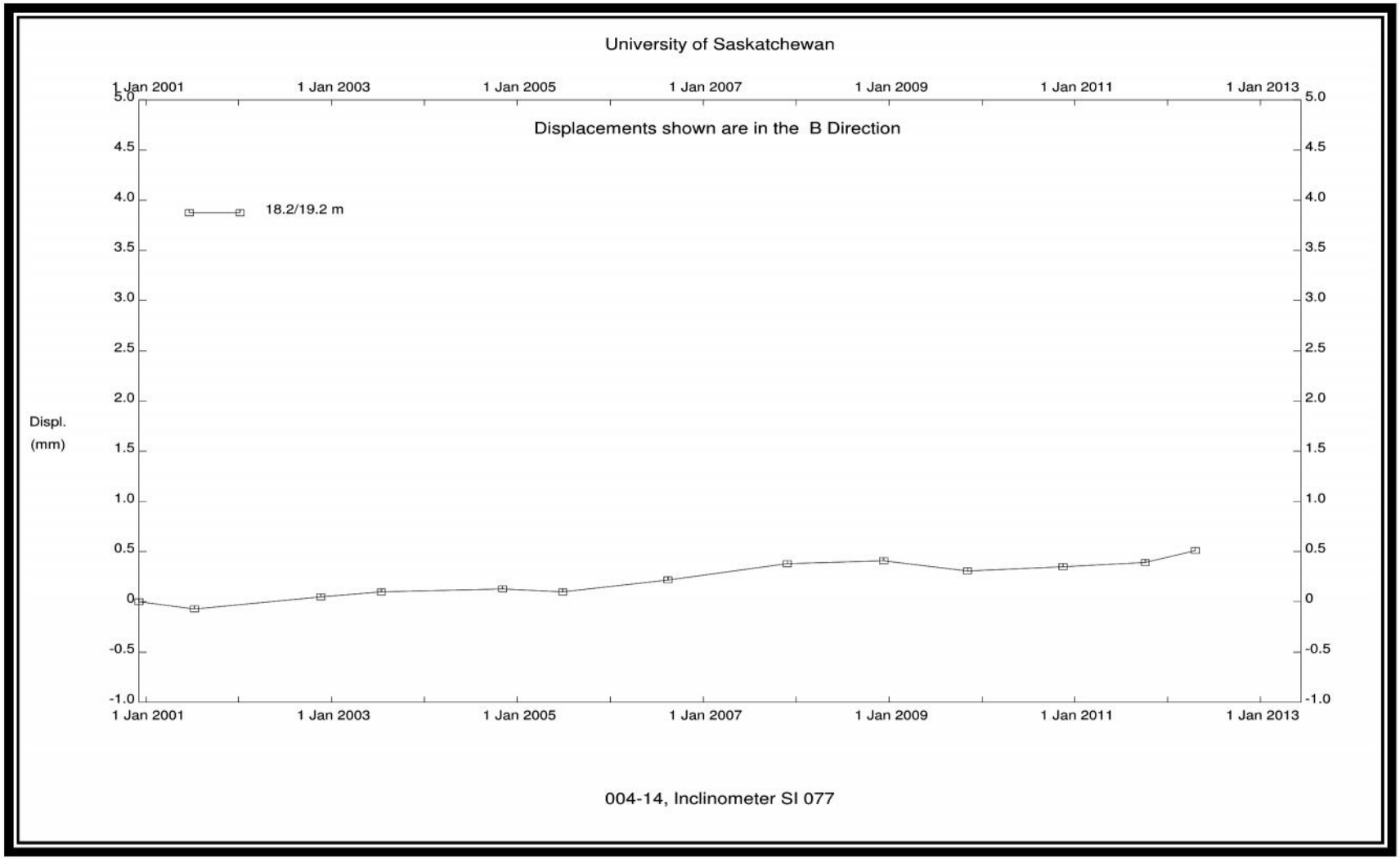

130

Figure A 27: SI77 displacement vs. time – B axis (2000-2012)

Appendix B – Triaxial Test Database

Table B 1:Triaxial test database for Cu>100 kPa - after Vardenaga & Bolton (2011)

Researcher	Clay	A	b	R2	n	Cu (kPa)	γM=2	IP	Wp	WL	w	Sample Depth (m)	OCR	P'o (kPa)
Burland et al. (1996)	Todi	5.15	0.52	1	27	2029	0.01147	0.28						3200
Burland et al. (1996)	Todi	8.06	0.66	1	25	1803	0.01469	0.28						2200
Burland et al. (1996)	Todi	8.46	0.66	1	16	1453	0.01405	0.28						1500
Burland et al. (1996)	Todi	11.62	0.77	1	14	1076	0.01650	0.28						600
Burland et al. (1996)	Todi	12.71	0.75	1	16	839	0.01329	0.28						443
Burland et al. (1996)	Todi	14.63	0.88	1	14	661	0.02159	0.28						200
Burland et al. (1996)	Todi	17.18	1.02	0.99	11	297	0.03083	0.28						50
Callisto and Rampello (2004)	Vallericca	3.93	0.39	0.98	9	876	0.00522	0.33	0.27	0.6	0.29			3200
Callisto and Rampello (2004)	Vallericca	4.25	0.38	0.98	7	313	0.00339	0.33	0.27	0.6	0.29			200
Callisto and Rampello (2004)	Vallericca	6.49	0.47	0.97	6	414	0.00418	0.33	0.27	0.6	0.29			428
Callisto and Rampello (2004)	Vallericca	6.9	0.53	0.98	7	205	0.00700	0.33	0.27	0.6	0.29			58

Callisto and Rampello (2004)	Vallericca	7.63	0.53	0.97	10	555	0.00572	0.33	0.27	0.6	0.29			1600
Callisto and Rampello (2004)	Vallericca	8.93	0.52	0.91	7	421	0.00373	0.33	0.27	0.6	0.29			412
Callisto and Rampello (2004)	Vallericca	10.18	0.61	0.95	13	697	0.00713	0.33	0.27	0.6	0.29			2400
Callisto and Rampello (2004)	Vallericca	11.69	0.59	0.88	8	436	0.00475	0.33	0.27	0.6	0.29			619
Callisto and Rampello (2004)	Vallericca	25.17	0.73	0.94	6	492	0.00477	0.33	0.27	0.6	0.29			817
Clifton et al. (1999)	Oxidized Lea Park				9	200	0.00948	0.65	0.24	0.89	0.26			310
Clifton et al. (1999)	Oxidized Lea Park				5	200	0.00993	0.72	0.25	0.97	0.26			310
Clifton et al. (1999)	Unoxidized Lea Park				66	487.5	0.01604	0.65	0.22	0.87	0.19			310
Clifton et al. (1999)	Unoxidized Lea Park				12	668.5	0.02169	0.84	0.25	1.09	0.26			310
Clough and Denby (1980)	San Fransisco Bay Mud	5.29	0.45	0.89	7	102	0.00536	0.35					1.3	
Díaz-Rodriguez et al. (2009)	Mexico City	5.9	0.55	0.97	18	116	0.01138	1.47	0.64	2.11	1.9	17.9		300

Díaz-Rodriguez et al. (2009)	Mexico City	7.2	0.59	0.96	15	114	0.01064	1.47	0.64	2.11	1.9	17.9	300
Díaz-Rodriguez et al. (2009)	Mexico City	7.71	0.65	0.99	22	108	0.01472	1.47	0.64	2.11	1.9	17.9	160
Díaz-Rodriguez et al. (2009)	Mexico City	11.06	0.7	0.98	21	173	0.01217	1.47	0.64	2.11	1.9	17.9	300
Díaz-Rodriguez et al. (2009)	Mexico City	14.01	0.73	0.99	19	158	0.01039	1.47	0.64	2.11	1.9	17.9	300
Futai et al. (2004)	Ouro Preto	2.98	0.48	0.97	11	251	0.02414	0.22	0.2	0.42	0.33	5	400
Futai et al. (2004)	Ouro Preto	4.22	0.52	0.96	9	253	0.01607	0.22	0.2	0.42	0.33	5	300
Futai et al. (2004)	Ouro Preto	4.92	0.54	0.99	7	116	0.01457	0.22	0.2	0.42	0.33	5	50
Futai et al. (2004)	Ouro Preto	4.98	0.53	0.89	6	149	0.01306	0.22	0.2	0.42	0.33	5	200
Futai et al. (2004)	Ouro Preto	5.11	0.58	0.99	6	125	0.01758	0.22	0.2	0.42	0.33	5	100
Futai et al. (2004)	Ouro Preto	6.43	0.66	0.99	14	401	0.02028	0.22	0.2	0.42	0.33	5	690
Futai et al. (2004)	Ouro Preto	7.34	0.62	0.98	9	292	0.01313	0.22	0.2	0.42	0.33	5	540
Gasparre (2005)	London	5.41	0.49	0.99	133	158	0.00782	0.37	0.29	0.66	0.26	7	260
Gasparre (2005)	London	3.69	0.45	0.99	85	290	0.01202	0.37	0.29	0.66	0.24	11	261

Gasparre (2005)	London	3.39	0.41	0.98	139	187	0.00915	0.37	0.28	0.65	0.26	13.4	257
Gasparre (2005)	London	5.86	0.47	1	92	220	0.00531	0.48	0.23	0.71	0.24	26.2	248
Gasparre (2005)	London	9.98	0.58	1	65	250	0.00568	0.33	0.26	0.59	0.25	38.8	502
Ladd (1964)	Amuay	4.34	0.4	0.98	7	249	0.00449	0.42	0.29	0.71	0.51		785
Ladd (1964)	Kawasaki	7.16	0.49	0.98	4	118	0.00415	0.34	0.36	0.7	0.67		294
SMHI (1967)	Oxidized Lea Park				158	172	0.00750	0.47	0.26	0.73	0.28		310
SMHI (1967)	Unoxidized Lea Park				140	201	0.01002	0.73	0.24	0.97	0.21		310
SMHI (1967)	Unoxidized Lea Park				236	192	0.00981	0.74	0.24	0.98	0.23		310
Moh et al. (1969)	Stiff Bangkok	5.69	0.52	0.99	7	103	0.00927	0.45	0.2	0.65	0.26	11	204
Moh et al. (1969)	Stiff Bangkok	6.37	0.55	1	5	288	0.01013	0.45	0.2	0.65	0.26	11	814
Moh et al. (1969)	Stiff Bangkok	9.55	0.64	0.99	5	158	0.01016	0.45	0.2	0.65	0.26	11	407
Yimsiri (2002)	London II	7.17	0.5	1	111	199	0.00481	0.45			0.26	13.6	270
Yimsiri (2002)	London II	7.39	0.53	1	219	202	0.00645	0.45	0.28	0.6	0.26	13.6	270
Yimsiri (2002)	London II	7.18	0.54	1	78	336	0.00727	0.42			0.22	16.4	310
Yimsiri (2002)	London II	8.33	0.6	1	87	365	0.00934	0.42			0.22	16.4	310
Yimsiri (2002)	London II	11.05	0.64	1	125	407	0.00769	0.33			0.21	22.9	410
Yimsiri (2002)	London II	14.69	0.62	0.99	112	348	0.00425	0.33			0.22	22.9	410